

# Quantifying numerical diffusion and dispersion produced by D-Flow Flexible Mesh when modelling a lock-exchange experiment

D. Koetsenruijter

**Bachelor Thesis**

Delft University of Technology  
Department of Hydraulic Engineering





# Abstract

This research aims to quantify the numerical diffusion and -dispersion produced by D-Flow FM while modelling salinity transport, using a lock-exchange experiment. This is done by investigating the model's sensitivity to important numerical parameters such as time step size and grid resolution by means of a sensitivity analysis.

For the lock-exchange experiment the following configurations are set; the initial conditions define a salinity difference of 10 ppt, ranging from 15 to 25 ppt over a single cell in the horizontal (i.e.  $\Delta x$ ), at  $x = 5000$ . The boundary conditions set a zero-discharge condition and are free slip, except for the bottom of the domain which induces a Manning's type friction. The domain is defined to be 100 meters wide, 10 kilometers long, has a depth of 10 meters and every simulation spans a period of 5 hours. The geometry is discretized by a computational grid with 100 cells of 100 meters, 3 cells of 100 meters and 10 cells of 1 meter in x-, y- and z-direction.

In order to perform the sensitivity analysis a number of simulations have to be performed. Four sets of parameter ranges are simulated. First, for a range of values of the  $Courant_{max}$  parameter are simulated, then the same is done for  $\Delta t$ ,  $\Delta x$  and  $\Delta z$  is done. For the latter two the reference model is further developed, in which a constant time step size ( $\Delta x$ ) and a constant spatial resolution in the x-direction ( $\Delta t$ ) is set.

Numerical diffusion is first quantified using the ratio between observed- and theoretical frontal propagation speed of both fronts [Pietrzak, 1998]. Then four types of numerical errors are distinguished; global diffusion, local diffusion, over-/undershoot and spurious oscillations. These errors are quantified by plotting the salinity of a single cell over time, at a depth and point in the domain where maximum dispersive errors are expected. These are determined by inspection of the reference model, where the depths and locations are at  $d = 2.5m$  and  $x = 2500m$  for the low density front,  $d = 4.5$  and  $x = 5000m$  for the location of the initial salinity difference and  $d = 6.5$  and  $x = 7500$  for the high density front. The salinity differences per parameter are thus relative to the respective reference model. The standard deviation of these relative differences over the range of the parameter serve as a measure for the model's sensitivity to the four error types. Yet, before they are compared they are first normalized by the coefficient of variation.

First, no direct relation between the Courant number at the fronts and diffusion of the frontal propagation speeds could be found. Nonetheless, it is clear that when the  $\Delta t$  and  $\Delta x$  are sufficiently small, diffusion across the domain can very effectively be minimized by decreasing  $\Delta z$ . With respect to the numerical diffusion produced by the model a plain observation is that it reduces especially if a constant time step size is set. The resolution in z-direction shows a high mean relative difference throughout the sensitivity analysis. This indicates a high amount of standard deviation thus a large influence on the model's accuracy. Therefore it seems that when the limiting values of  $\Delta x$  and  $\Delta t$  are known  $\Delta z$  can serve to fit the model to produce as little diffusion as possible.

Further, it is noted that extreme values were observed as the model reached its limits in terms of Courant numbers and vertical velocities. Such a limit of the Courant number is beautifully visualized by a seemingly lack of viscosity when  $\Delta t = 250s$ , if  $\Delta t$  is then increased to 300 seconds the model fails.

Based on these results it is recommended to start modelling with either a varying  $\Delta x$  or  $\Delta t$ , depending on which is considered limiting (start with the limiting parameter). Increase the resolution of the parameter until the results show similar diffusion as in a model using an automatic time step setting with  $Courant_{max} = 0.7$ . Finally, decrease  $\Delta z$  in order to get rid of the last diffusive errors.

Concluding, the sensitivity of the model's most important type of errors to different parameters were quantified in terms of global diffusion, local diffusion, over-/undershoot and spurious oscillations. Global diffusion are most sensitive to  $\Delta z$  and generally have a range of influence of 2 ppt. Local diffusion is mostly sensitive to  $\Delta z$  and  $\Delta x$  and can change salinity values up to 5 ppt. at the fronts. Over-/undershoot is most sensitive to the  $Courant_{max}$  parameter but occurs very little and only up to 1 ppt. Both parameters  $\Delta t$  and  $Courant_{max}$  have a significant influence on the dispersive oscillatory type of error; for the middle of the domain spurious oscillations are sensitive to  $\Delta t$  up to a value of 1 ppt. For the low density front both  $\Delta t$  and  $Courant_{max}$  can influence salinity values up to 2 ppt.



# Contents

<b>Abstract</b>	<b>iii</b>
<b>1 Introduction</b>	<b>1</b>
<b>2 Method</b>	<b>5</b>
2.1 Definition of a baseline model . . . . .	5
2.2 Parameter variation and sensitivity analysis . . . . .	7
2.3 Quantification of errors and sensitivity. . . . .	9
<b>3 Results</b>	<b>11</b>
3.1 Reference model . . . . .	11
3.2 Maximum Courant number. . . . .	15
3.3 Time step size . . . . .	16
3.4 Resolution x-direction . . . . .	17
3.5 Resolution z-direction . . . . .	18
3.6 Sensitivity analysis . . . . .	19
3.6.1 Classification of errors . . . . .	19
3.6.2 Observations and analysis . . . . .	19
<b>4 Discussion and conclusion</b>	<b>25</b>
4.1 Discussion . . . . .	26
<b>Bibliography</b>	<b>27</b>
<b>A Simulation results</b>	<b>29</b>
A.1 Courant numbers reference model . . . . .	29
A.2 Relative salinity differences per parameter . . . . .	30
A.2.1 Max. Courant. . . . .	30
A.2.2 Time step size . . . . .	31
A.2.3 Resolution x-direction . . . . .	32
A.2.4 Resolution z-direction . . . . .	33
A.3 Table of simulations . . . . .	34
A.4 Example explorative model . . . . .	39
A.5 Limits of D-Flow FM . . . . .	39
A.5.1 Limits of time step size . . . . .	39
A.5.2 Limits of resolution x-direction . . . . .	41
A.5.3 Limits of resolution z-direction . . . . .	42
A.6 Salinity contour plots of simulations used for analysis . . . . .	44
A.6.1 Max. Courant. . . . .	45
A.6.2 Time step size . . . . .	54
A.6.3 Resolution x-direction . . . . .	61
A.6.4 Resolution z-direction . . . . .	66



# 1

## Introduction

The salinity of water systems is caused by salification of a fresh water body. Often fresh water is to remain fresh in order to extract drinking water, for use in agriculture or because of its importance to an ecological system. However, in coastal water systems such as the Rhine-Meuse delta, mixing of fresh and salt water is inevitable. Salinity differences cause for density driven currents to occur (see figure 1.1). Because important water infrastructure in the Netherlands, such as the drinking water supply, is strongly influenced by these currents, it is important to understand, model and predict these phenomena. Moreover, because of smaller river discharges and a growing demand for fresh water, due to the effects of a changing climate, salinity in surface waters in the whole European delta is a growing problem. [Friocourt et al., 2014]. This increases the need to accurately model density driven currents caused by salinity differences. With the use of D-Flow Flexible Mesh, a software package by Deltares, such density driven flows can be numerically approximated using 2D and 3D flow modelling. However, a side effect of these numerical flow models is the occurrence of numerical errors caused by characteristics of the discretization scheme that is used and the type of flow that is modelled. Two types of numerical errors that typically occur are numerical diffusion and -dispersion.

This research aims to quantify the numerical diffusion and -dispersion produced by D-Flow FM while modelling salinity transport, using a lock-exchange experiment. This is done by investigating the models' sensitivity to important numerical parameters such as time step size and grid resolution by means of a sensitivity analysis.

First, in chapter one, this report describes the methodology used to attain the models' sensitivity. In chapter two the results of the simulations with different parameters and the models sensitivity are presented. Finally, in chapter four, conclusions with respect to sensitivity of the model's accuracy to certain parameters are presented and the obtained results are discussed.

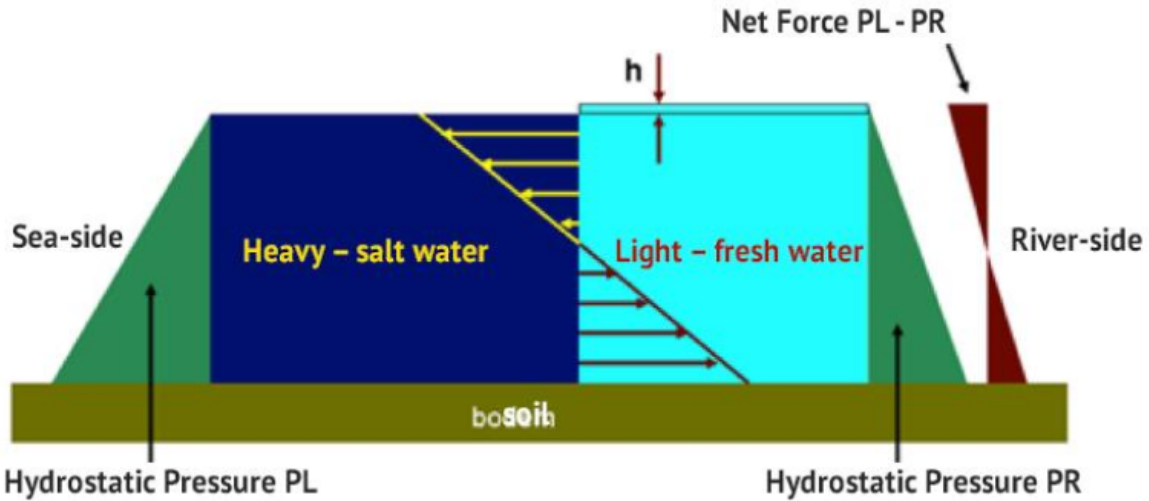


Figure 1.1: Physical model of a density driven current - Source: Friocourt et al. [2014]

### Numerical diffusion and -dispersion

Numerical diffusion is sometimes referred to as “numerical viscosity” since the associated approximation errors mimic the effect of an increase in viscosity, i.e. the solution is overdamped. For numerical methods that apply finite-differences in combination with an explicit time integration scheme often artificial damping is introduced to keep the scheme stable Zijlema [2015, Chapter 3]. For an example see the right side of figure 1.2 and notice where the approximation is cut off. Such damping is called a flux limiter and ensures monotonicity, an example of which is the monotone central limiter introduced by Van Leer [1977]. This flux limiter is implemented by D-Flow FM and used for modelling the salinity transport in this study.

The first order upwind scheme implemented by D-Flow FM is a (partially) explicit scheme in time which makes it conditionally stable as explained in Zijlema [2015, p. 76]. This condition, which follows from analysis using the Von Neumann method, is called the Courant-Fredrich-Lowy condition (or Courant number) and sets a limit on the ratio  $\frac{\Delta t}{\Delta x}$  (which can be interpreted as a domain of influence). The limit states that the domain of influence of a model has to be larger than the velocity of the disturbance it is modelling otherwise stability of the scheme is not guaranteed. Based upon this D-Flow FM also implements a time step size limiter that automatically sets  $\Delta t$  based on the value of a parameter called  $Courant_{max}$ . This automatic time step setting always tries to maximize  $\Delta t$ , given the modelled velocity and  $\Delta x$ , such that the Courant number can not exceed the value set in  $Courant_{max}$ . Thus, the definition of the Courant number is as follows:

$$C = \frac{\Delta t}{\Delta x} \cdot u_{flow} \leq 1$$

Consequently to not meeting the Courant-Fredrich-Lowy condition numerical dispersion could arise. Numerical dispersion is related to unrealistic oscillations in an approximation of an advection-diffusion problem that may occur when modelling steep gradients. Such steep gradients force the model to oscillate at locations away from the discontinuity in order to maintain a smooth solution and approximate the sudden steep gradient at the same time. For a clear example of numerical dispersion see the left side of figure 1.2, notice where it models values higher and lower than the maximum values of the exact solution.

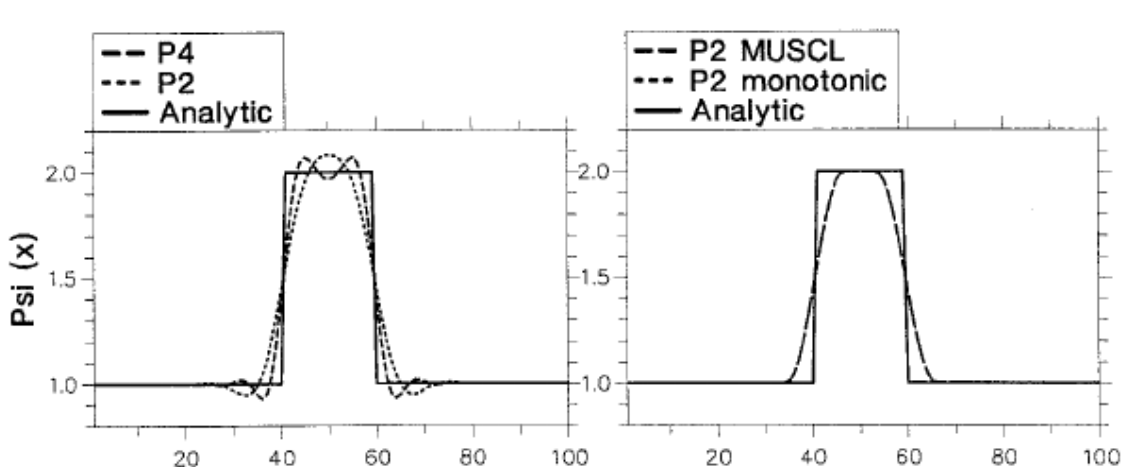


Figure 1.2: Typical examples of numerical diffusion (left) and dispersion (right) in approximating steep gradients - Source: Pietrzak [1998]

Because avoiding errors related to numerical diffusion and -dispersion requires contrasting measures [O'Brien et al., 1950] with respect to settings of the numerical model a quantification of their responses to certain modelling parameters is desirable.

A challenge in quantifying these errors arises when modelling flow in which large vertical velocities occur, i.e. in non-laminar flow. If for this sort of flow, which possibly occurs in the lock-exchange experiment, the shallow water equations are used, which is the case in the D-Flow Flexible Mesh flow model, flow related errors can be expected. Thus, because the flow model used by D-Flow FM also produces errors that are an effect of the assumptions made in the flow model and not of the numerical model used, a clear distinction between these two origins of error should be made.

## Lock-exchange experiment

To be able to refer the sensitivity of numerical errors produced by D-Flow FM to specific settings and parameters of the model a lock-exchange experiment is set up. In a lock-exchange the initial situation consists of a rectangular tank with a horizontal free water surface, it is split vertically in half containing fluids with different densities on each side. In this research the density difference is caused by an initial salinity difference. At the start of the experiment ( $t = 0$ ) the fluids set in motion and form two fronts, a low- and high density front, as a result of the gravitational and buoyant forces (see figure 1.3). The numerical errors produced during such an experiment have been investigated before in which similar physics are produced compared to the results of this report [Adduce et al., 2012, Cenedese et al., 2018, Shin et al., 2004].

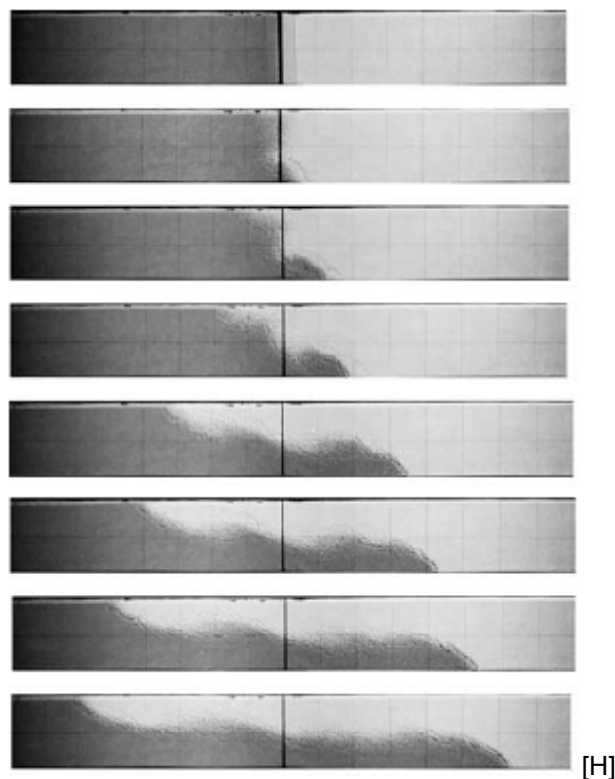


Figure 1.3: Example of a lock-exchange experiment depicting two current fronts flow opposite directions over time - Source Shin et al. [2004]

# 2

## Method

In modelling flow and transport phenomena, and numerical modelling in general, two variables have a major effect on the stability and accuracy of the solution; the spatial resolution and time step size. Additionally there are many other parameters in D-Flow FM that can be configurated and might have influence on the numerical errors. For further reference see the D-Flow FM user manual (Deltarees [2020]). In this study four parameters are varied within relevant ranges during the simulation phase of this research;  $Courant_{max}$ ,  $\Delta t$ ,  $\Delta x$  and  $\Delta z$ . Finally the observed sensitivity of the numerical errors to each parameter is analyzed. Where the sensitivity of a parameter is defined as the normalized standard deviation of the errors produced with different values of this parameter, per change of this parameter. The origin of the errors is deduced from plots depicting the salinity differences of each parameter relative to its respective version of the reference model. The salinity differences are quantified by comparing the salinity of a single cell over time at the location of the initial disturbance and at locations where each front is fully developed. Finally, the magnitude of the errors is determined through plots depicting the mean and standard deviation of this relative salinity difference over the whole range of values over which each parameter is changed. Besides, the standard deviation of the relative salinity difference is normalized by the coefficient of variation, which is considered a measure for the change in the parameter. Additionally, the observed numerical diffusion is quantified as the ratio of the theoretically approximated propagation speed of the front and the observed frontal propagation speed (FPS), for both the high density front (HDF) and low density front (LDF). This ratio is then plotted against the observed Courant numbers at the front.

### 2.1. Definition of a baseline model

First, a reference model is defined in order to have a physically realistic baseline for comparison of the errors produced in the sensitiviy analysis. After close inspection of the results produced by this model it becomes clear where and when to look for the maximum numerical errors. The results are inspected through salinity profiles over time, for the whole domain and for a single cell. Additionally through a detailed plot of the density fronts as they are fully developed at  $t = 2.5h$ . Thus realistic modelling of physical processes in the model can be confirmed and the type and location of possible errors can be identified. Whether they are related to the flow model or a result of the numerical approximation becomes evident during the parameter variations.

Based on this inspection of the refence model the model's settings and parameters that will remain constant throughout the analysis are defined. Because a constant  $\Delta t$  is desired for variations of  $\Delta x$  and  $\Delta z$  this reference model is further developed as  $Courant_{max}$  and  $\Delta t$  are varied. Thus the reference model is configured with  $\Delta t = 10s$  such that errors in the frame of reference are minimized. Moreover, the reference model is configured with  $\Delta x = 20m$  in order for the variations in  $\Delta x$  and  $\Delta z$  to be comparable. By doing so, the errors observed in the subsequent sensitivity analysis are clearly recognizable.

For the initial reference model most default settings are used to set up the lock-exchange model. The initial conditions define a salinity difference of 10 ppt, ranging from 15 to 25 ppt over a single cell in the horizontal (i.e.  $\Delta x$ ), at  $x = 5000$ . The boundary conditions are determined to be free-slip for all

sides of the watertank and prescribe a zero-discharge condition. The bottom of the watertank does provide resistance in the form of Manning's equation with a friction coefficient of 0.023. The water tank is defined to be 100 meters wide, 10 kilometers long, has a depth of 10 meters and every simulation spans a period of 5 hours. The geometry is discretized by a computational grid with 100 cells of 100 meters, 3 cells of 100 meters and 10 cells of 1 meter in x-, y- and z-direction respectively. The background temperature is set to be 10 degrees Celsius, which is not default but more conventional than the default 6 degrees Celsius. The size of  $\Delta t$  follows from the  $Courant_{max}$  parameter and the automatic time step setting implemented by D-Flow FM, which calculates the maximum  $\Delta t$  given the modelled velocities and spatial resolution (for a short explanation see chapter 1, for further reference consult Deltares [2020]). The value for  $Courant_{max}$  is kept at its default value of 0.7. It only accounts for salinity transport processes and uses a monotonized central limiter type as proposed by Van Leer [1977]. For the relevant settings of this reference model see table 2.1.

Parameters	Unit	Value
<b>Geometry</b>		
# Grids - M	-	100
# Grids - N	-	3
Delta x	m	100
Delta y	m	100
<b>General</b>		
# Layers	-	10
<b>Timeframe</b>		
Period	s	18000
Courant number	-	0.7
max. time step	s	1200
Initial time step	s	1
<b>Processes</b>		
Salinity	ppt	TRUE
<b>Initial conditions</b>		
Waterlevel	m	10
Salinity delta	ppt	25-15
Temperature	degC	10
<b>Boundary conditions</b>		
Discharge	m3/s	TRUE
Velocity	m/s	FALSE
Type	-	Free-slip

Table 2.1: Settings of the reference model *Note: Max. time step & Initial time step are set to  $\Delta t = 10s$  after the temporal variations are done. See chapter 3.3*

## 2.2. Parameter variation and sensitivity analysis

In order to perform the sensitivity analysis a number of simulations have to be performed. By varying the different parameters the associated numerical errors can be computed. Because this is done over a realistic and relevant range of values, the numerical diffusion and -dispersion errors generally produced by D-Flow FM in the context of the Rhine-Meuse delta can be quantified. Further, because the Courant number plays an important role in computational fluid dynamics it serves as an the primary measure in the subsequent variations. Therefore, a requirement for these ranges is that they should allow the subsequent parameter variations to be varied over a comparable range of Courant numbers. This range of Courant numbers is defined as follows:  $C \in [0.1, 2]$ , however also extreme values ( $C = 0.01$  or  $C = 5$ ) are of interest, since herewith the limits of the model's accuracy become evident.

Four sets of parameter ranges are configured and used to simulate the lock-exchange experiment. First, the temporal variations consisting of  $\Delta t$  and the  $Courant_{max}$  are performed and compared to the primary reference model. Second, the spatial variations consisting of  $\Delta x$ ,  $\Delta z$  are performed and compared to the reference model. For the latter two the reference model to which the simulations are compared maintains a constant  $\Delta t$  and a constant  $\Delta x$ . All variations can be found in table 2.2 in which the models used for reference are colored green and the simulations that were excluded from the sensitivity analysis (and thus from coefficient of variation) are depicted red.

For the parameter variations the sequential order matters as it is desirable to compare models with a constant  $\Delta t$  concerning the spatial variations. Therefore it is important to investigate the effect of the automatic time step setting (as implemented by D-Flow FM, based on the  $Courant_{max}$  parameter) and a range of values for  $\Delta t$  before continuing with a reference model that maintains a constant  $\Delta t$ . Consequently, first, simulations with a varying Courant number are performed while using the automatic time step setting in D-Flow FM. These first results are examined and compared to the reference model. Second,  $\Delta t$  defined explicitly for the given range of values (see 2.2). This is only possible if the  $Courant_{max}$  parameter is set sufficiently high so that the automatic time step size setting of D-Flow FM does not take effect. Third, based on the outcome of the results of the temporal variations the  $\Delta t$  of the reference model is set to be  $\Delta t = 10s$  and  $\Delta x$  is varied. Fourth,  $\Delta z$  is varied after the reference model has been set with a constant resolution of  $\Delta x = 20m$ . Both spatial variations are compared to the reference model set with  $\Delta x = 20m$  and  $\Delta z = 1m$ . For all four parameters the range of values used to simulate the lock-exchange are depicted in table 2.2, along with the run ID of the simulation (also see table A.1 for the results per simulation). Some of the simulations are excluded from further analysis because of the extreme erroneous results, for the salinity profiles of some of these extremes see section A.5.

<b>Max. Courant</b>	<b>[ - ]</b>	<b>Δt</b>	<b>[ s ]</b>	<b>Δx</b>	<b>[ m ]</b>	<b>Δz</b>	<b>[ m ]</b>		
<b>Run ID</b>	<b>Value</b>	<b>Run ID</b>	<b>value</b>	<b>Run ID</b>	<b>value</b>	<b>Run ID</b>	<b>value</b>		
0106-8	0,1	0606-17	0,1	1006-1	5	1006-13	0,22		
0106-9	0,2	0606-16	1	1006-2	10	1006-12	0,30		
0106-10	0,3	0606-15	5	1006-3	16	1006-11	0,37		
0106-11	0,4	0606-1	10	1006-4	20	1006-10	0,43		
0106-1	0,5	0606-2	20	1006-5	25	1006-9	0,50		
0106-2	0,6	0606-3	30	1006-6	31,25	1006-8	0,59		
<b>2605-1</b>	<b>0,7</b>	0606-4	40	1006-7	36,5	1006-7	0,67		
0106-3	0,8	0606-5	50	1006-8	40	1006-6	0,77		
0106-4	0,9	0606-6	60	1006-9	50	1006-5	0,83		
0106-5	1	0606-7	70	1006-10	62,5	1006-4	0,91		
0106-6	1,1	0606-8	80	1006-11	100	1006-2	1,00		
0106-7	1,2	0606-9	90	1006-12	200	1006-1	2,00		
0106-12	1,3	0606-10	100	1006-13	400				
0106-13	1,4	0606-21	120						
0106-14	1,5	0606-22	140						
0106-15	1,6	0606-23	160						
0106-16	1,7	0606-24	180						
0106-17	1,8	0606-11	200						
0106-18	1,9	0606-18	250						
0106-19	2	0606-12	300						
		0606-19	350						
		0606-20	400						
		0606-13	500						
		0606-14	1000						
<b>Coefficient of Variation</b>	<b>0,563</b>			<b>1,081</b>		<b>0,956</b>			
							<b>0,493</b>		

Table 2.2: Range of values for temporal and spatial parameter variations and their coefficient of variation. Red colored simulations are excluded from the sensitivity analysis because of extreme erroneous results, green colored simulations have served as a reference in the sensitivity analysis.

## 2.3. Quantification of errors and sensitivity

The simulations are compared according to the quantification of the observed numerical diffusion and dispersion. Numerical diffusion is quantified using the ratio between observed- and theoretical frontal propagation speed of both fronts. Where the theoretical frontal propagation speed is estimated by the following formulas, as used by Pietrzak [1998] and confirmed through experiment by Simpson and Manga [1998], based on the energy conserving nature of gravity induced currents in long prismatic channels.

$$U = C_{front} \cdot \sqrt{(g' \cdot d)}$$

With:

$$g' = g(\rho_2 - \rho_1)/\rho_2$$

Given that:

$$\rho_1 < \rho_2$$

And:

$$\begin{cases} C_{front} = 0.44, & \text{for the high density front} \\ C_{front} = 0.56, & \text{for the low density front} \end{cases}$$

The numerical dispersion is quantified by plotting the salinity of a single cell over time, at a depth and points where maximum dispersion errors are expected, which is inferred from inspection of the reference model. These depths are at 2.5 meter and 6.5 meter for the low density front and the high density front, respectively. In order to observe the effect of both the fully developed fronts (travelling in opposite directions) and to get insight in what happens after  $t = 0$  at the location of the initial disturbance, these points are set at  $x = 5000$ ,  $x = 2500$  and  $x = 7500$ . At the location of the initial salinity difference (at  $x = 5000$ ) the depth of maximum dispersion equals 4.5 meters. The salinity at the before-mentioned locations are then plotted and compared to the appropriate reference model from which a salinity difference can be calculated. This salinity difference is thus relative to the respective reference model and its normalized standard deviation serves as the measure the sensitivity of numerical errors to the respective parameter.

The relative salinity difference  $S$  of a simulation configured with  $p_i$  as a value for the parameter concerned at a location  $x, d$  in the spatial domain over the complete period of the simulation is defined as:

$$\text{Relative salinity difference}_{p_i} = S_{p_i}^{x,d} = \text{Salinity}_{p_i}^{x,d} - \text{Salinity}_{reference}^{x,d}$$

Where  $p_i$  is a value for the parameter that is varied and  $x, d$  is the location and depth where maximum numerical errors are expected.

Therewith the normalized standard deviation  $\sigma_{norm} - S_{p_n}^{x,d}$  of these salinity differences taken over a range of values  $p_n$  becomes:

$$\text{Normalized standard deviation} = \sigma_{norm} - S_{p_n}^{x,d} = \frac{\sigma - S_{p_n}^{x,d}}{C_{v,p_n}}$$

With,

$$\text{Coefficient of variation}_{p_n} = C_{v,p_n} = \frac{\sigma_{p_n}}{\mu_{p_n}}$$

and,

$\sigma - S_{p_n}^{x,d}$  = Standard deviation of the relative salinity difference at  $x, d$  over all simulated values  $p_n$  for the parameter

$\sigma_{p_n}$  = Standard deviation of the range of values used for the parameter in the sensitivity analysis

$\mu_{p_n}$  = Mean of the range of values used for the parameter in the sensitivity analysis

After quantifying the numerical diffusion and -dispersion per simulation the produced errors are compared over the range of the parameter. Firstly, at the low- and high density front the Courant numbers are plotted against the diffusion rates of these fronts. Regression on these diffusion rates point out the effect of a parameter on the diffusive errors of the model. Secondly, the standard deviation of the quantified numerical dispersion for each parameter range is normalized with the coefficient of variation of that range. Herewith the relative change of the numerical errors per parameter variation can be visualized and quantified. This is considered to be a measure for the sensitivity of the model's numerical errors to the parameter concerned.

# 3

## Results

As expected the D-Flow FM shows spurious oscillations for large values of  $Courant_{max}$ , nonetheless this only starts to develop at values higher than 1.6. For  $\Delta t$  the limit of accuracy seems to be around  $\Delta t = 50s$ , given  $\Delta x = 100m$  and  $\Delta z = 1m$ . For both  $Courant_{max}$  and  $\Delta t$  the diffusion rate of the frontal propagation speeds stays approximately constant around 0.6. With respect to  $\Delta x$  and  $\Delta z$  the diffusion rates are very close to 1.0, meaning almost no diffusion of the frontal propagation speeds is observed. However these simulations were run with a reference model with a reasonably accurate  $\Delta t$  of 10 seconds. Lastly, the limits of the model are not observed for  $Courant_{max} \leq 2.0$  but show clearly for estimated Courant numbers between 0.7 and 1.5 in the horizontal. Whereas the model only fails at Courant numbers of 10 in the vertical (see section A.5).

First the results of the reference model are presented in which the physical characteristics of the lock-exchange experiment can be observed. This serves as a confirmation for the model's physical similarity such that it can be used for further reference. Second, the results of the temporal variations ( $\Delta t$  and  $Courant_{max}$ ) are described. Third the results of the spatial variations ( $\Delta x$ ,  $\Delta z$  are presented. Finally conclusions with respect to the model's sensitivity for different parameters can be drawn based on the comparison of the different parameter variations.

The results are analysed by means of the salinity profiles over time of a single cell at specific depths and locations for all values of the parameter, for brevity called the single cell salinity. These single cell salinities are subtracted from the appropriate reference model after which a relative difference is obtained. This difference is subsequently used to quantify the numerical dispersion for the range of parameter values, which along with the computed numerical diffusion is presented in section 3.6. The analysis of single cell salinities of all simulations are presented in appendix A and the salinity contours for all simulations are presented in appendix A.6.

### 3.1. Reference model

The reference model serves as a first indication and quantification for the type and order of the numerical errors of interest. Therefore, by post processing the results of the reference model into different type of plots better insight in the produced approximation and thus the produced errors is obtained. This is initially done by looking at three basic plots of the computed salinity. Thereafter, based on these insights, initial conclusions with respect to the type of error are described. For the settings used in this model see Table 2.1. The frontal propagation speed of both fronts are always linear over time. This indicates an energy conserving approximation as assumed in the theoretical estimation of the frontal propagation speed for both the low- and high density fronts is valid, which also coincides with [Cenedese et al., 2018]. The frontal propagation speed in the high density wave is lower than in the low density front which coincides with experiments performed by [Simpson and Manga, 1998]. Both the frontal propagation speeds are smaller than the proposed theoretically estimated value which suggests the occurrence of numerical diffusion, the corresponding computed diffusion rate is 0.6. At the trailing edge of the front naturally looking oscillations can be observed which may be dedicated to the formation of internal waves typically seen as shear stresses in the mixing layer of a stratified flow regime develop Rafferty. However, the choppy angles of these oscillations can indicate some form of numerical over-

/undershoot is present (see figures 3.2 and 3.3). This would make sense given the large  $\Delta x$ , thus a small Courant number which indicates a large propagation speed of the approximation compared to the propagation of the physical disturbance, causing it to overshoot.

In figure 3.1 a plot of the width averaged salinity over time is shown, for the complete spatial domain of the experiment ( $x \in [0, 10000]m$ ). It depicts the theoretically defined and observed frontal propagation speeds for both fronts. With the goal of getting an overview of the experiment and its global numerical diffusive and -dispersive characteristics. As a first observation the development of the front can clearly be seen, a linear propagation speed of both fronts and an increase of the mixing layer over time are also observed. Besides a perfectly physically realistic reflection can be observed at the low density front (at  $t = 5h$ ); the height of the reflected wave is twice the height of the incoming wave and its propagation speed is equal but in opposite direction. Further no value significantly (defined as  $10^{-3}$ ) outside the initial salinity range of  $[15, 25]ppt$ . is produced by the model otherwise these would have been plotted as a red or a blue dot. However, the contour lines that indicate the 15 and 25 ppt. salinity contour do show large areas where the salinity thus slightly exceeds these limits. This is expected to be an effect of the monotone central limiter type used as a flux limiter on the salinity transport approximation [Van Leer, 1977].

Further the theoretically estimated and observed locations of the front are plotted as a normal-and dashed line respectively. The location of the fronts are determined by looking at the lowest and highest value of  $x$ , for the low- and high density respectively, for which the absolute the salinity gradient maximized over the depth exceeds  $0.01$  ppt./m. The mixing layer of the front can be seen to expand as time increases up to a width of around 200 meters at  $t = 2.5h$ . Because of this the velocity observed within 200 meters of the location of the front, extending towards the tail of the density gradient, is used to calculate the Courant number at the front which is finally used while plotting the diffusion.

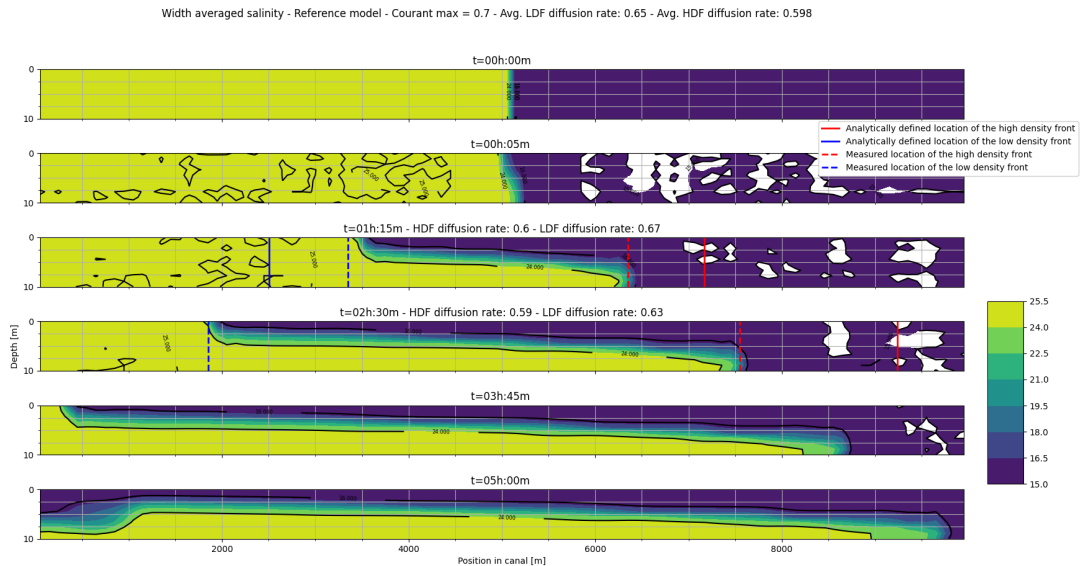


Figure 3.1: Contour plot of the salinity over time for the primary reference model

In figure 3.2 a detailed plot of both fronts and the observed Courant numbers at the front are presented. The plot depicts the situation at  $t = 2.5h$  such that the fronts are fully developed, aimed at gaining insight in how oscillations in the salinity profile close to the propagating disturbance develop. The oscillations at the trailing part of the front seem to be natural and no direct dispersion errors (e.g. in the form of clearly spurious oscillations or extreme values) are observed in front of the large density gradient. Further, as a confirmation that the characteristics of the front are captured within a range of 200m behind the front, the maximum Courant numbers indeed occur within this range. This can be deduced from figure A.1 in which the maximum velocity over the depth is used to calculated the Courant number for the complete spatial domain over time. Moreover the maximum Courant numbers can be observed at  $t = 2.5h$  thus being a justification for choosing this timestep to inspect in further detail.

Finally, a first estimation of the Courant number validates the models accuracy since it corresponds with the observed Courant numbers;  $C = \frac{\Delta t}{\Delta x} \cdot u = \frac{65}{100} \cdot [0.46, 0.58] \approx 0.35$ . Where  $\Delta t$  is the average time step size of the reference model while using the automatic time step setting of D-Flow FM and the flow velocity is the theoretically estimated velocity of the fronts. It should be noted that the Courant numbers are surprisingly low for  $Courant_{max} = 0.7$ . However, the Courant number increases as the time step size increases thus using the average time step gives an underestimate of the Courant number.

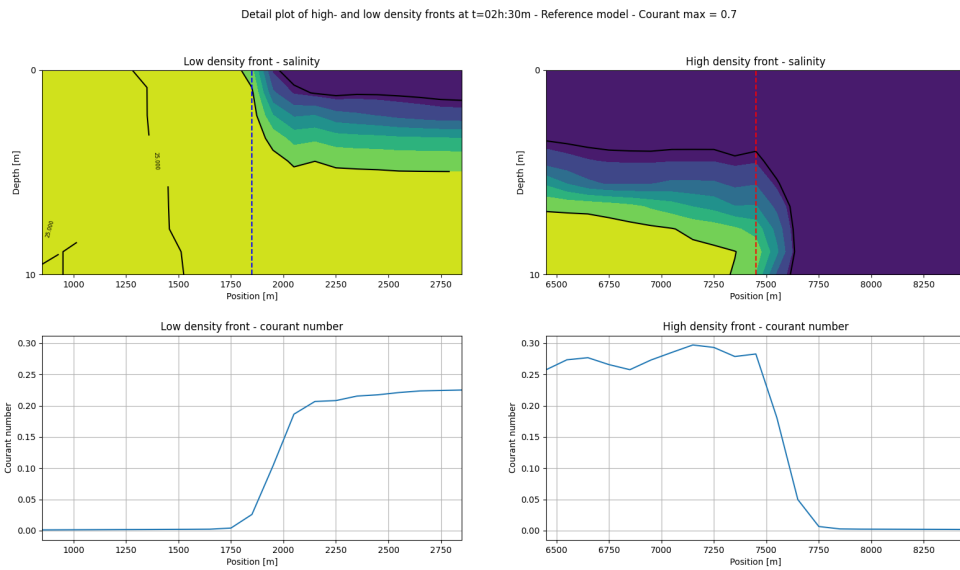


Figure 3.2: Detailed plot of the density fronts produced by the primary reference model. Natural oscillations at the trailing edge of the front can be observed.

Finally, in figure 3.3 a plot is presented that depicts the salinity at a single cell at three locations, being  $x = 2550$ ,  $x = 5050$  and  $x = 7650$ , used to get an indication of the behaviour of the approximated salinity over time as the front passes. The data that is plotted here is also used to quantify the observed dispersion compared to the reference model. The most important observation is that the maximum gradient occurs at different depths per front. Because at these large gradients the highest numerical errors are expected these are maintained as the depths at which numerical dispersion is quantified, being; at a depth of 4.5 meter for the middle of domain, 2.5 meter for the low density front and 6.5 meter for the high density front. Further the oscillations can be seen to be choppy which indicates overshoot possibly due to a lack of resolution.

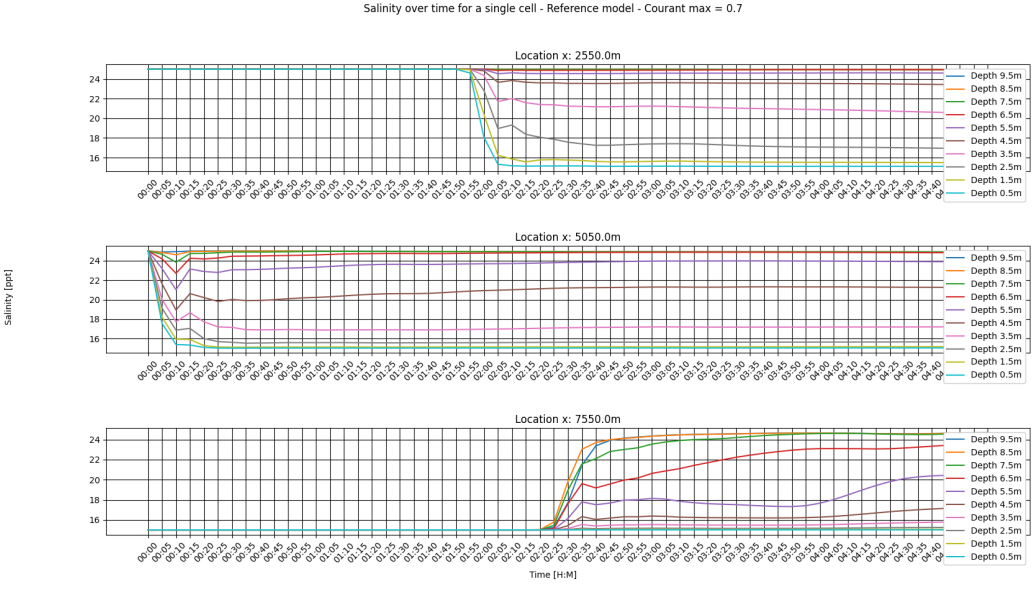


Figure 3.3: Salinity of a single cell at different depths and three locations over time. The maximum amplitude of oscillation in the salinity profile occur at 2.5 meter depth for the low density front, 4.5 meter depth for the middle of the domain and 6.5 meter for the high density front.

Thus obtaining results that coincide with the expected physics and results from previous studies (Cenedese et al. [2018], Simpson and Manga [1998] and Pietrzak [1998]), both numerical diffusion and dispersion are identified. However, to obtain better insight in what causes the observed phenomena and how these relate to the numerical accuracy of the model more information is required. To this end the results per parameter variation with respect to the produced errors and their sensitivity to each parameter are presented hereafter.

## 3.2. Maximum Courant number

As expected the model shows spurious oscillations for large values of  $Courant_{max}$ , nonetheless this only starts occurring at values higher than 1.6. At values between 1.0 and 1.6 and for values lower than 0.1 only minor over- and undershoot can be observed. An abrupt oscillation at  $x = 5000m$  is modelled at all variations of the  $Courant_{max}$  parameter and can also be observed in the reference mode. This is probably a result of the choppy spike on top of the front (see figure 3.2). The steep low density front causes obvious spurious oscillations at a  $Courant_{max}$  of 1.6 up to 2.0 with an amplitude of approximately 1 ppt. At the low density front the errors observed are significantly larger, especially at  $Courant_{max}$  values of 1.6 to 2.0. Generally the absolute order of the errors is up to 2 ppt. for  $Courant_{max}$  values higher than 1.6 but remain below 0.5 ppt. for  $Courant_{max}$  values lower than 0.7. Until  $Courant_{max}$  equals 0.1, then the model seems to become quite diffusive  $\Delta t$ , which causes the front to arrive slightly later.

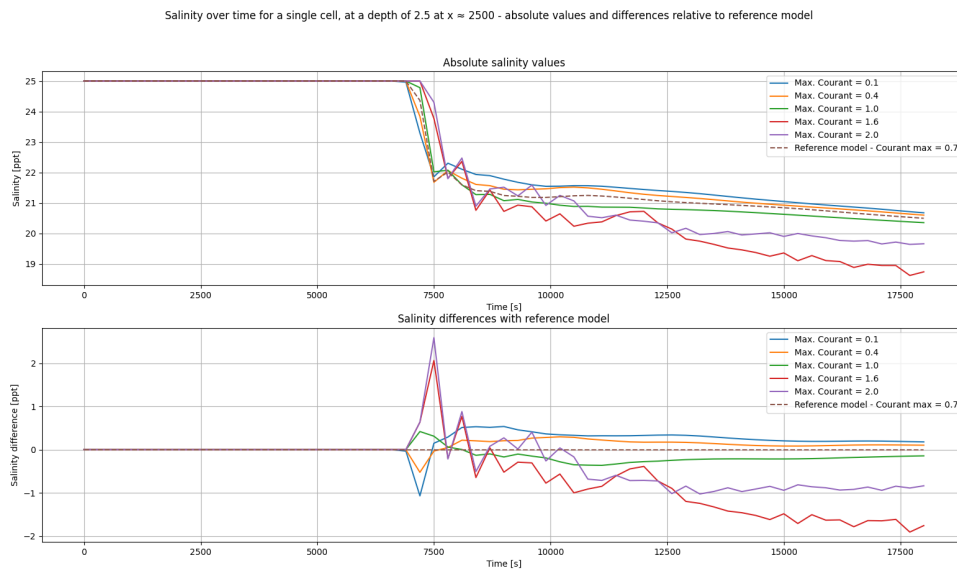


Figure 3.4: Salinity of a single cell at  $d = 2.5m$  showing the low density front passing. The effect of the  $Courant_{max}$  on the salinity differences, which are of quite large scale, can be observed. Especially for  $Courant_{max}$  numbers between 1.6 and 2.0 the effect of the parameter on errors in the salinity profile can be seen in the large oscillation after the front has passed.

In figure A.3 the initial disturbance at  $x = 5000$  can clearly be seen to decrease almost immediately (after approximately 600 seconds) to a salinity value of 18 ppt., then after a small oscillation it soon decreases to its steady state value of approximately 17 ppt. The origin of this oscillation can be explained by figure 3.2 where a steep spike at the top of the front can be seen, also for all values of  $Courant_{max}$  the model produces such a spike which indicates it could find its origin in the resolution of the model. The salinity differences produced at  $x = 5000$  after  $t = 2500$  (figure A.3) are of relatively small scale compared to those observed at the low density front in figure 3.4.

Further it is important to notice the oscillations at  $Courant_{max} \geq 1.6$  observed in all figures depicting the variations of  $Courant_{max}$  (figures 3.4, A.3 and A.2). These are possibly related to shear induced internal waves causing vertical velocities that can not be accounted for in the flow model Rafferty. Next, passing of the low density front in figure 3.4 can clearly be observed and the salinity differences are of quite large values. Especially for  $Courant_{max}$  numbers between 1.6 and 2.0 the effect of the parameter on errors in the salinity profile can clearly be observed. This can possibly be explained as follows; as the  $Courant_{max}$  number increases the model can increase  $\Delta t$  further and thus increases the temporal range over which possible errors truncate. When such an error truncates over a part of the model where in space and time a large gradient has to be modelled it causes the model to overshoot. This can be observed in the red and purple salinity profiles that continue far longer at a value of 25 ppt. than the other profiles. Since the Courant number can be seen as the ratio between the update speed of the approximation and the speed at which disturbances travel, the model simply updates faster than the

density gradient travels and thus overshoots more as the  $Courant_{max}$  number increases above 1.0. Oscillations of a large scale short after the large gradient then occur as the approximation converges back to exact solution. Further it can be noted that for very small values of  $Courant_{max}$  the solution does not change much compared to the reference model, it merely responds a little faster which can be dedicated to  $Courant_{max}$  forcing  $\Delta t$  to be small (see figure 3.4). Lastly in figure A.2 a large continuous error develops for  $Courant_{max} \geq 1.6$ , the maximum dissipation depth (as proposed by Shin et al. [2004, p. 14]) seems to be approached sooner.

### 3.3. Time step size

At larger values of the time step size ( $\Delta t \geq 50s$ ) clear oscillations start to develop as the front has passed, up to an amplitude of approximately 1.5 ppt. For  $\Delta t \leq 50s$  (giving an approximate Courant number of 0.25, with  $\Delta x = 100$  and a velocity of 0.5 m/s) the amplitude of these oscillations drops below 0.5 ppt. The oscillations observed have an amplitude of approximately 2 ppt. at the location of the initial disturbance and at the low density front. At the low density front the oscillations also continue to exist for a longer period of time. The constant salinity difference for  $\Delta t \leq 50s$  of approximately 0.5 ppt. can not be described as a numerical error due its smooth and constant form. However, the observed differences can be explained by the fact that the reference model's average time step size equals 65 seconds, which is automatically determined and kept as large as possible as long as the Courant number does not exceed the  $Courant_{max}$  parameter. Therefore solutions with a smaller time step size can be more accurate yet differ from the reference model across the domain. Lastly the same steep and choppy high density front can be seen to develop for an estimated Courant number higher than 1.25 as was observed in the variations of  $Courant_{max}$ .

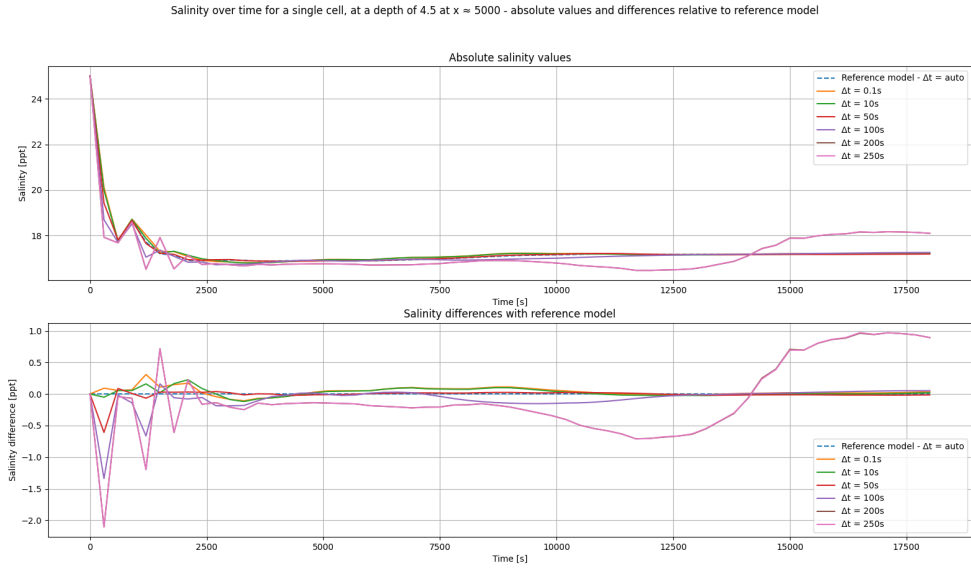


Figure 3.5: Salinity of a single cell at  $d = 4.5m$  at the location of the initial salinity difference. Clear oscillations can be seen as  $\Delta t$  increases to 250 seconds of the same type and scale as in the variations of  $Courant_{max}$  which coincides with the expected behaviour at large Courant numbers.

In figure 3.5 clear oscillations can be seen as  $\Delta t$  increases to 250 seconds. Although the absolute error is of a smaller value than at high values of  $Courant_{max}$  the characteristics of the oscillation indicate that at steep gradients and a large enough  $\Delta t$  spurious oscillations occur in between the fronts when they are still relatively close to each other. These oscillations can be seen to develop for  $\Delta t \geq 50s$ , given a maximum observed velocity 0.5 m/s (see table A.1) and a  $\Delta x$  of 100m this gives a Courant number of 0.25 which is much lower than expected yet coincides with values found in the reference model (see figure A.1). In figure A.4, depicting the low density front, the same sort of oscillations are observed up to an error of 2.5 ppt., yet only for  $\Delta t = 250s$ . Further, figure A.4 shows the same kind and magnitude of errors as observed in the variations of  $Courant_{max}$  as  $\Delta t$  increases. Next, spurious

oscillations on a smaller scale can be seen to develop at large time step sizes after the low density front has long passed. As no steep gradient is to be approximated no numerical oscillations are expected. This indicates that possibly small scale vertical velocities the hydrostatic model can not deal with, are the cause of the erroneous small scale oscillations for  $t \geq \pm 10000s$ . The same was observed in figure A.3 depicting relative salinity differences at  $x = 5000$  for the variations of  $Courant_{max}$ . Lastly, in figure A.5 also the same choppy top of the high density front can be seen to develop for  $t = 250s$  as for  $Courant_{max} = 2.0$ . Again this can be related to the amount of time it takes to reach the maximum dissipation depth as used in Shin et al. [2004], but this requires further research.

### 3.4. Resolution x-direction

A first observation is that the whole domain is less oscillatory probably due to the small time step size that is configured ( $\Delta t = 10s$ ). Increasing relative salinity differences are observed as  $\Delta x$  increases, some of which caused by a diffusive error but is possibly also part due to an increasing error in placement of the measurement location. Although the order of errors observed is of 2 ppt. this is not used to quantify the global numerical diffusion of the model because of its time dependency and possible measurement error. The fact that the model is mainly diffusive might be explained by the fact that the time step size is chosen to be quite small ( $\Delta t = 10s$ ) which, for larger  $\Delta x$  causes the Courant number to decrease significantly. Since the domain of influence then becomes much larger than the discretized domain the local approximation becomes overly damped. Lastly, a little over and undershoot can be seen to develop for all values of  $\Delta x$ . But because the shape of the profile does not change this is attributed to the backlog of the more diffused approximations.

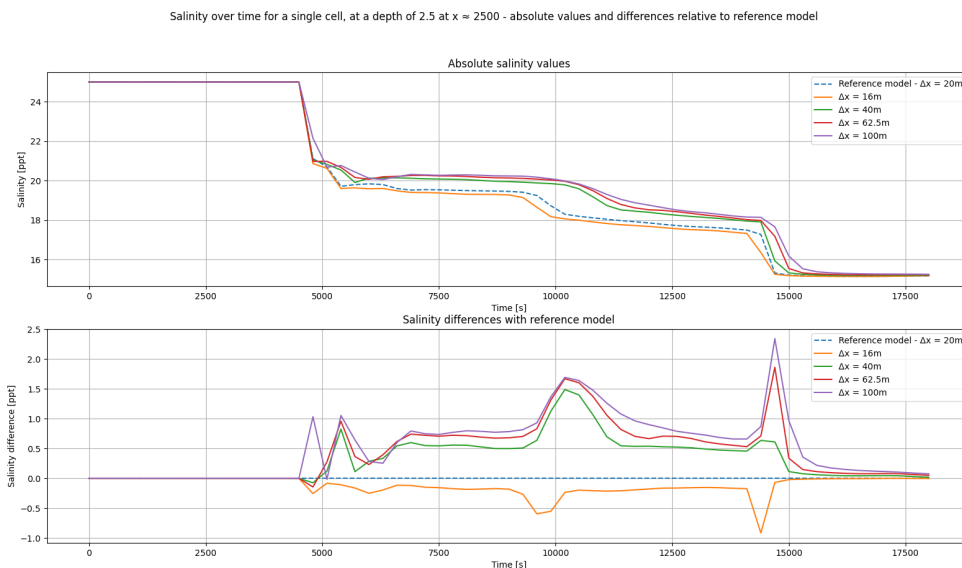


Figure 3.6: Salinity of a single cell at  $d = 2.5m$  showing the low density front passing. Clear diffusion over time can be observed at larger values of  $\Delta x$ . At  $t = 15000$  also the effects of the reflected wave can be observed in the final salinity drop.

In general the origin of the errors observed in the variations of  $\Delta x$  appear to be mostly of a diffusive kind, looking at the increasing error over time, as seen in figure 3.6. This diffusion becomes clearly visible with larger values of  $\Delta x$  and is most recognizable at  $t = 10000$ , where the front experiences another small drop in salinity. However a larger  $\Delta x$  could also cause a larger measurement error due to larger displacement of the measurement location, figure A.6 possibly indicates this. Which also partly explains the fact that at smaller values of  $\Delta x$  the high density front arrives earlier (see figure A.7). Yet this delay can not completely be explained by misplacement of the measurement since at, for example,  $\Delta x = 100m$  the front has a backlog larger than 100 meters. At the location of the initial disturbance (figure A.6) it seems the shape and or location of the mixing layer changes with an increasing  $\Delta x$ , since the salinities do not convert to the same value even after the steep salinity gradient has passed. However, this can also indicate an error in measurement placement. For the location of the low density

front the same is true, in figure 3.6 the front can be seen passing at  $t = 5000$ s and here for values of  $\Delta z \geq 40m$  diffusive characteristics start to develop. Next, at both fronts peaks in the relative salinity difference can be observed which are caused by the backlog of the more diffused fronts. This is best seen in A.7 where the relative differences reaches up to 6 ppt., solely caused by diffusion of the frontal propagation speed as the Courant number increases with larger values of  $\Delta z$ . Finally the reflected wave can be observed to cause the salinity in the cell to drop to 15 ppt.

### 3.5. Resolution z-direction

The numerical diffusion in the model decreases as  $\Delta z$  decreases which coincides with section 3.6. For the high density front the same goes. This is also confirmed by the sensitivity analysis (see section 3.6). Although in this same section it becomes clear that for the current  $\Delta t$  and  $\Delta x$  the diffusive error on a global scale is minimized, the variations of  $\Delta z$  show that locally salinity differences are extremely sensitive to changes in  $\Delta z$ . These errors, which reach up to values of 8 ppt., are caused by the large backlog of the front and indeed indicate, yet are not used to quantify, the (large) numerical diffusion. The quantification of this kind of diffusion in section 3.6 (diffusion of the frontal propagation speed) shows that the large backlog disappears at  $\Delta z \leq 0.91m$ .

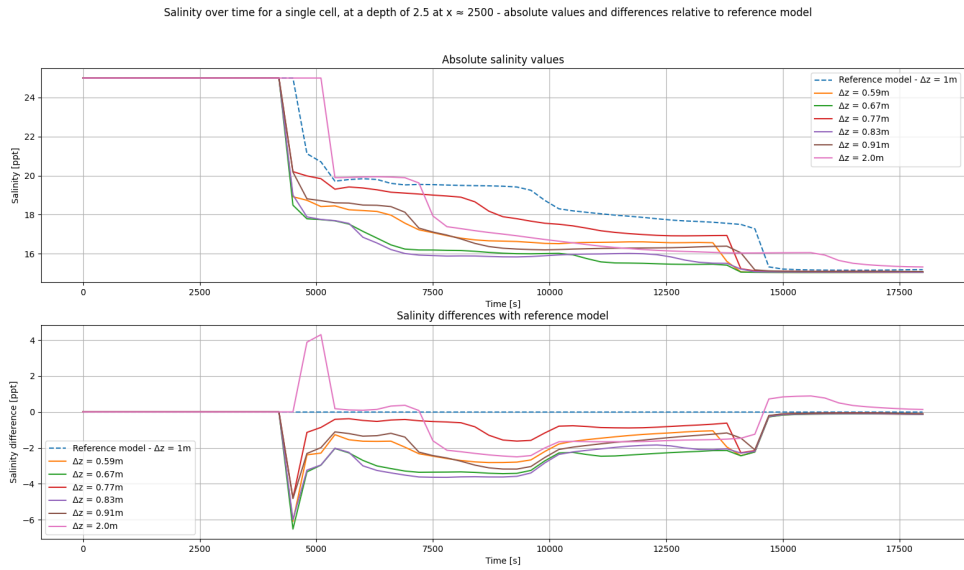


Figure 3.7: Salinity of a single cell at  $d = 2.5m$  showing the low density front passing. A large diffusion of the frontal frontal propagation speed is visualized by the backlog of the front at  $\Delta z = 2m$ . Further most diffusion of the frontal propagation speed is minimized for  $\Delta z \leq 0.91$ .

In figure 3.7 the frontal propagation speed for the low density front seems to increase as  $\Delta z$  decreases through which it approximates the theoretically calculated propagation speed of 0.46 m/s (as shown in 3.6). The figure thus indicates that for smaller  $\Delta z$  values the numerical diffusion significantly decreases. In figure A.8 it can be observed the salinity at a depth of 4.5 meters increases as  $\Delta z$  decreases, this happens because the vertical location of the boundary layer moves upward (this can be inferred from close inspection of the salinity profiles for the variation of  $\Delta z$  in section A.6). But part is also due to the measurement location being placed closer to a depth of 4.5 as  $\Delta z$  decreases. The fact that the boundary layer moves upward with a decreasing  $\Delta z$  can possibly be due to the model approximating the maximum dissipation depth as used in Shin et al. [2004]. Additionally, it could be attributed to the fact that the continuity equation of the flow model in the z-direction can better account for vertical velocity gradients and thus movement of the mixing layer. Further, the decreasing diffusivity can be observed very well for the low density front depicted in figure 3.7 where the maximum diffusion is observed at  $\Delta z = 2m$  and for all values where  $\Delta z \leq 0.91$  the diffusion has reached its minimum. In the sensitivity analysis figure 3.8 confirms this, here the separated blue dot at the bottom of the regression line is the diffusion rate for  $\Delta z = 2m$ . Finally, in figure A.7 it should be noted that although

the lowest vertical resolution shows the smallest amount of diffusive effects, the other resolutions are not proportionally spread in terms of backlog. Where  $\Delta z = 0.59m$  and  $\Delta z = 0.77m$  show only a with the reference model, the in between value of  $\Delta z = 0.67$  shows a small discrepancy increasing the error to approximately 3 ppt. This could indicate that the ratio of  $\Delta z$  to  $\Delta x$  has an influence on the accuracy of the model, this requires further research. Moreover the shape of the front changes for all values of  $\Delta z$  which causes peaks in the relative differences. With the exception of the approximation where  $\Delta z = 2m$ , here the cause is diffusion of the frontal propagation speed.

## 3.6. Sensitivity analysis

In order to analyze sensitivity of the model's accuracy to different parameters a distinction between four types of error is made. This is done based on how each type of error affects the profile of the relative salinity differences, in terms of the mean and the spread. Thereafter the model's sensitivity to each parameter is analysed; first based on the diffusion of the frontal propagation speeds, second based on the mean relative salinity difference per parameter and third based on the normalized standard deviation of the relative salinity differences.

### 3.6.1. Classification of errors

With respect to the sensitivity of the model's error to different parameters, a distinction is made between the type of error observed. First two types of observed numerical diffusion are distinguished; *the global* and *local diffusive error*. Second a distinction is made between two types of numerical dispersion; *over-/undershoot* and *spurious oscillations*.

The global diffusion error can be recognized by a constant mean of the relative salinity difference throughout the period of the simulation. Global diffusion is often caused by diffusion of the frontal propagation speed or the total salinity difference across the front, resulting in a constant error throughout the subsequent period of the simulation. Therewith, a large influence on the global diffusion is recognized by a large standard deviation from this mean for the complete period of the simulation. A possible example of a variation heavily affecting global diffusion can be seen in figure 3.7, where a constant relative salinity difference of approximately 3 ppt. is present until the reflected wave affects the observed cell.

On the contrary, local numerical diffusion spans a short period of time and only occurs at locations of steep gradients. However, it can cause for large relative differences ( $\pm 1 - 5\text{ppt.}$ ) that influence the accuracy of the model significantly. Local diffusive errors occur if only the shape of the front differs over the change of a parameter. An example of which can be seen in figure A.9 where multiple salinity fronts take on a different shapes yet model the same front. Such diffusion causes a single spike in the relative differences.

Similarly over-/undershoot causes spikes in the relative differences but of a much smaller magnitude than local diffusion ( $\pm 0.5 - 1\text{ppt.}$ ) yet also occurs at locations of steep gradients. For an example of over-/undershoot see the green salinity profile in figure 3.4 (where  $Courant_{max} = 1.0$ ). Here it can be seen that the profile overshoots at the front causing a relative difference of approximately 0.5 ppt. after which it approaches the reference model again. Over-/undershoots cause a small single spike in the relative differences at the precise location of a steep gradient.

Lastly, spurious oscillations are distinguished by their repeating pattern and only differ from a single over-/undershoot insofar they are repeatedly over- and undershooting (again see figure 3.4 but then the profile for  $Courant_{max} = 1.6$  or 2.0).

### 3.6.2. Observations and analysis

First, the model's sensitivity to global diffusion is analyzed by means of the diffusion rates of the frontal propagation speed and their possible trends (see figure 3.8). These trends, attained through linear regression of the diffusion rate data, show that no direct link between the Courant number and global diffusion can be made. With the exception that if  $\Delta t$  and  $\Delta x$  are sufficiently small almost no diffusion can be expected for reasonable Courant numbers ( $\geq \pm 0.05$ ).

Although  $\Delta z$  appears to follow a trend, given the high value of  $R^2$  and seemingly random residual errors, contradictive results have been computed in the beginning of this study. During a few first explorative simulations  $\Delta z$  was significantly small while maintaining a  $\Delta x$  of 100m and still the diffusion rate was around 0.7 (for this particular example see figure A.10).

In line with this the diffusion rates where  $\Delta x = 100m$  (for the variations of  $Courant_{max}$  and  $\Delta t$ ) are all around 0.6 and hardly undergo change for different observed Courant numbers. In general the model is less diffused for the spatial variations of  $\Delta x$  and  $\Delta z$  where  $\Delta t = 10s$ . Which makes sense given the partially explicit time integration, which becomes less diffusive as  $\Delta t$  decreases.

Additionally, for the variations of  $\Delta x$ , the diffusion of the high density front appears to increase and approach an asymptote around 1.0 as the Courant number increases from 0.01 to 0.4. Since the residuals show a somewhat parabolic shape. Whether this asymptote exists for other values of  $\Delta t$  could be further investigated by varying  $\Delta x$  at different  $\Delta t$ .

In general it becomes clear that when  $\Delta t$  and  $\Delta x$  are sufficiently small global diffusion can very effectively be minimized by decreasing  $\Delta z$ . Further research studying the variations of  $\Delta z$  in the range 1.0-2.0 meter and at different  $\Delta t$  and  $\Delta x$  in this context would have to show for what range of values of  $\Delta z$ ,  $\Delta x$  and  $\Delta t$  such global diffusion can best be tackled.

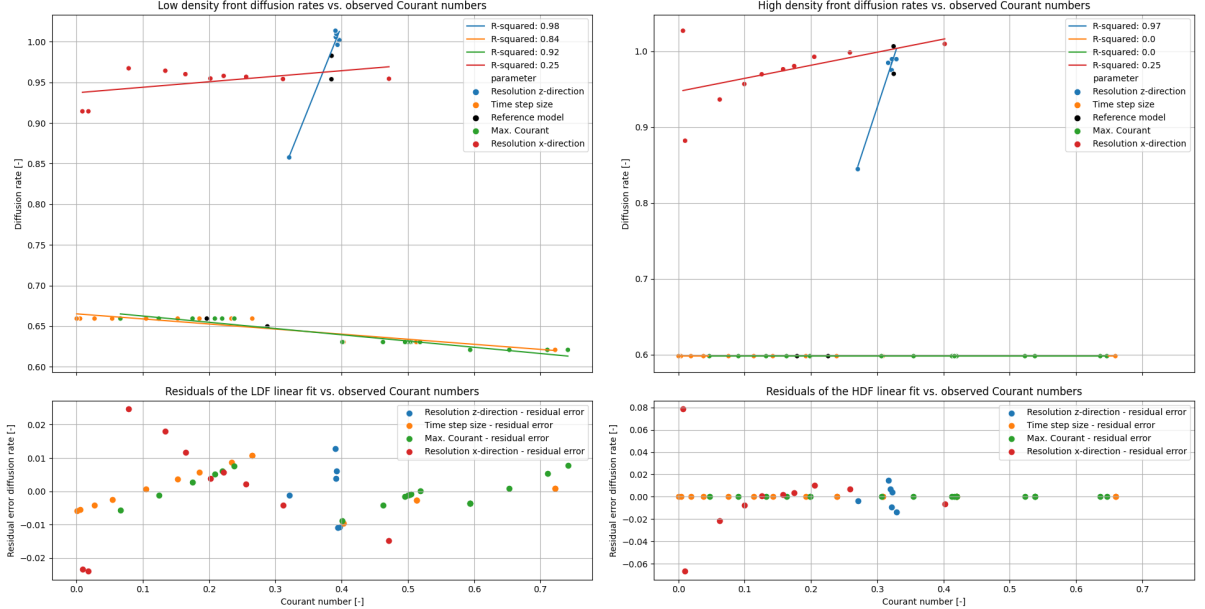


Figure 3.8: Diffusion rates as defined in chapter 2 for different parameters and their respective ranges of variation vs. the Courant numbers observed at the density fronts. The regression trends show no direct link between the Courant number and global diffusion but the diffusive error can be minimized by decreasing  $\Delta z$  in case  $\Delta x$  and  $\Delta t$  are already sufficiently small.

Next the model's sensitivity to each parameter is determined through analyzing the mean and spread of their relative salinity differences at all three observation locations (see figures 3.9, 3.10 and 3.11). These figures depict the mean and the standard deviation of the relative differences by means of a fat line and slightly transparent area, respectively. In these relative differences the four types of numerical errors, as listed in section 3.6.1, can be identified. In order to compare the standard deviation of the results for the different parameters, the spread of the relative salinity differences are normalized by the appropriate coefficient of variation. These normalized standard deviations are depicted in figure 3.12 (for coefficients of variations see table 2.2). Subsequently the sensitivity of the model's accuracy is quantified according to the errors identified in this normalized standard deviation.

In figure 3.9  $\Delta z$  shows a high mean relative difference and moreover a high amount of standard deviation too. This indicates that  $\Delta z$  has a large influence on the salinity in the middle of the domain, where the boundary layer is most developed. With an influence range of approximately 2ppt. Additionally this spans most of the domain which suggests that global diffusion errors are sensitive to variations in  $\Delta z$  which actually coincides results from figure 3.8. A possible explanation could be that the interface between the two density currents across the domain can only be accurately thin when  $\Delta z$  is small enough. If  $\Delta z$  is too big the salinity gradient has to be bridged by a mixing layer that is erroneously large. These differences cause a large spread of the approximated salinity at a single cell and thus indicate a large sensitivity. The above figure also depicts a large influence on the local diffusion by  $\Delta x$  of approximately 1 ppt., in the form of a peak in the beginning of the simulation. However, the origin of this peak is possibly due to a measurement error (see figure A.6). Besides it shows  $\Delta x$  has an influ-

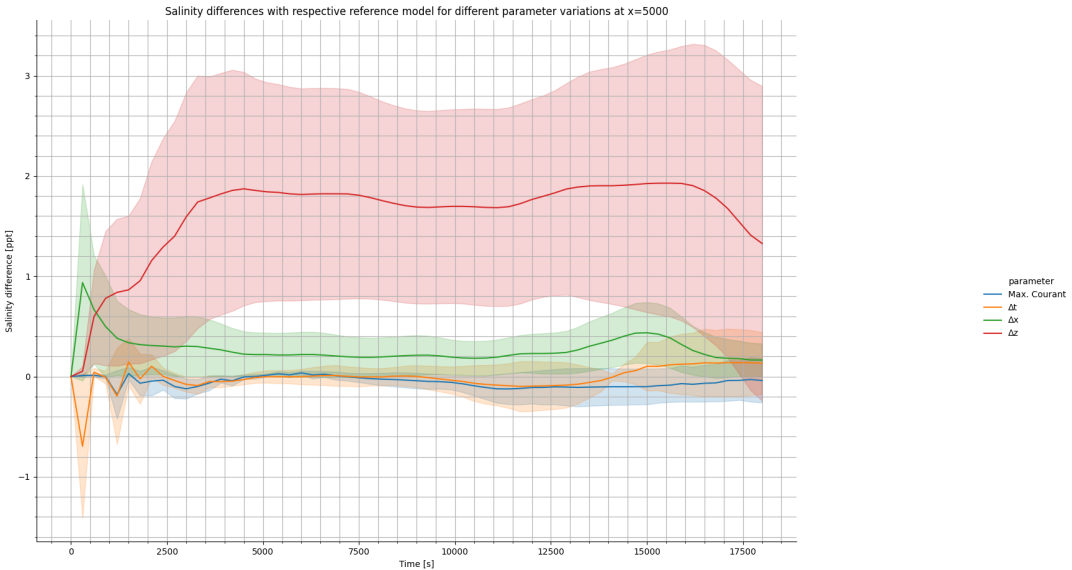


Figure 3.9: Mean and standard deviation of the relative salinity differences depicting the mean and the standard deviation through a fat line and slightly transparent area, respectively. Especially the variation of  $\Delta z$  shows large influence on the approximation in terms of global diffusion. Also  $\Delta x$  has quite an influence on global diffusion and shows a peak in the beginning because of probable measurement errors. Finally spurious oscillations appear sensitive to temporal parameters.

ence of approximately 0.25 ppt on the global diffusion. Lastly, on spurious oscillations with a maximum amplitude of approximately 0.6 ppt are most sensitive to  $\Delta t$ , but some sensitivity to  $Courant_{max}$  can also be observed. It makes sense that oscillations (which are a sign of instability) disappear with a decreasing  $\Delta t$  since they are typical for explicit schemes which become a lot more accurate as they approach the exact integral. This could be confirmed by varying the  $\theta$  (the implicitness parameter) and look at the effects of different  $\Delta t$ .

Different values of  $\Delta z$  can have a major influence on the shape of the high density front and the boundary layer over time, translating to local and global diffusion errors respectively. For both fronts depicted in figures 3.10 and 3.11 this is clearly visible. Generally, causing a mean sensitivity range of approximately 2 ppt. in terms of global diffusion. Further, for all other parameters, at both fronts the sensitivity of global diffusion errors are between 0.5 and 1.0 ppt. Besides, only  $\Delta x$  also strongly influences the high density front with a mean range of approximately 2 ppt. and all differences seem to decrease over time. Lastly, clear sensitivity of spurious oscillations to  $\Delta t$  and  $Courant_{max}$  can be seen for the low density front, with an amplitude of approximately 0.5 ppt. Therewith it seems especially the low density front is sensitive to dispersive errors possibly due to the implicitness of the time integration.

For  $\Delta z$  the sensitivity range of global diffusion errors at the low density front (figure 3.10) are of approximately 2-4 ppt. In this figure, the peak indicating local diffusion is misleadingly caused by a backlog of the front for  $\Delta z = 2m$ , which is partly undone through the normalization in figure 3.12, but remains around 5 ppt. whereas inspection of figure 3.7 shows that the front does not change shape for  $\Delta z \leq 0.91$  and all relative differences can be dedicated to a global diffusive type of error.

The  $\Delta x$  parameter does have this type of local influence on the salinity profile at the high density front (see 3.11). A good example of the origin of this influence is figure A.7 in which the shape of the front changes only a little over the different values for  $\Delta x$  yet the relative differences are in the range of 3 - 5 ppt. The reason for the sensitivity of this local diffusion to changes in  $\Delta x$  can be explained by the Courant number; as the  $\Delta x$  increases to 100m the Courant number decreases drastically (given a  $\Delta t$  of 10s and average flow velocity of approximately 0.5 m/s). Next, because the velocity gradients are largest at the fronts the decrease in domain of influence causes most diffusive here. Finally, since during the variations of  $\Delta x$  the time step size was already sufficiently small, the diffusion does not persist till after the steep salinity gradient has passed but remains local.

Additionally over-/undershoot is mostly observed at the high density front for  $\Delta t$  and  $Courant_{max}$  yet occurs for all parameters. Resulting in small spikes in the standard deviation which can be seen in

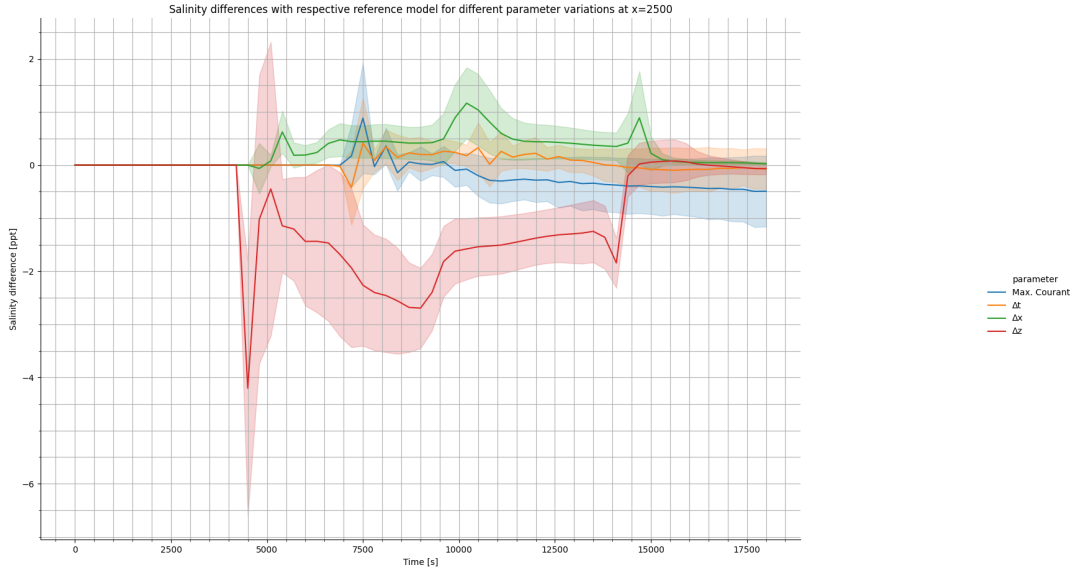


Figure 3.10: Relative differences depicting the mean and the standard deviation through a fat line and slightly transparent area, respectively. Global diffusion at the low density front appears to be most sensitive to  $\Delta z$ . Oscillations as the front has passed appear to be sensitive to  $\Delta t$  and  $Courant_{max}$ .

figure 3.11. Therewith, in the same figure, for  $\Delta t$  and  $Courant_{max}$  the global diffusion error increases over time of which the origin lies in the large Courant numbers, this can be seen in figures A.2 and A.5.

Finally spurious oscillations are observed to be sensitive to  $\Delta t$  and  $Courant_{max}$  for the low density front (see figure 3.10, probably caused by the implicitness of the time-integration. However, it can also be seen in the same figure that the oscillations endure till some time after the front has passed which could either indicate the presence of spurious oscillations in between the fronts or could be a result of a flow model error such as internal waves or artificial viscosity.

In figure 3.12 the sensitivity of the model's accuracy to the different parameters are quantified.

Global diffusion are most sensitive to  $\Delta z$  and generally have a range of influence of 2 ppt. Local diffusion is mostly sensitive to  $\Delta z$  and  $\Delta x$  and can change salinity values up to 5 ppt. at the fronts. Over-/undershoot is most sensitive to the  $Courant_{max}$  parameter but occurs very little and only up to 1 ppt. Finally, as established, both parameters  $\Delta t$  and  $Courant_{max}$  have a significant influence on the dispersive oscillatory type of error. Although the origin of these oscillations could not solely be dedicated to numerical dispersion, they are nonetheless quantified as follows; for the middle of the domain spurious oscillations are sensitive to  $\Delta t$  up to a value of 1 ppt. For the low density front both  $\Delta t$  and  $Courant_{max}$  can influence salinity values up to 2 ppt.

Lastly, the limits of the model are not observed for  $Courant_{max} \leq 2.0$  but show clearly for estimated Courant numbers between 0.7 and 1.5 in the horizontal. Whereas the model only fails at Courant numbers of 10 in the vertical (see section A.5). As shows from table A.1; With  $\Delta x = 100m$  and a maximum velocity of 0.58 m/s at  $\Delta t = 250s$ , this gives a Courant number of 1.8, at  $\Delta t \geq 300s$  the model fails. With  $\Delta t = 10s$  and a maximum velocity of 0.75 m/s at  $\Delta x = 16m$  gives a Courant number of 0.47, at  $\Delta x \leq 10m$  the model fails. With  $\Delta t = 10s$  and a maximum vertical velocity of 0.1 m/s at  $\Delta z = 0.59m$  gives a Courant number in the vertical of 10, at  $\Delta z \leq 0.5$  the model fails.

On the contrary in figure A.14 a model is presented that showed almost no signs of being limited by a flux limiter. Under the assumption that the contour lines of 15 and 25 ppt. away from the travelling fronts that do not contain values significantly outside the physical limits of the salinity ([15, 25], which would be indicated by red or blue dots) are indications of the approximation being limited by the flux limiter. This coincides with the fact that as  $\Delta t$  decreases the time integration approaches the actual integral. Therewith, because of the implicitness of D-Flow FM the model hardly has to be limited. This could be tested by running a model with the same  $\Delta t$  but with a fully explicit time integration scheme (i.e. setting  $\theta = 0$ ).

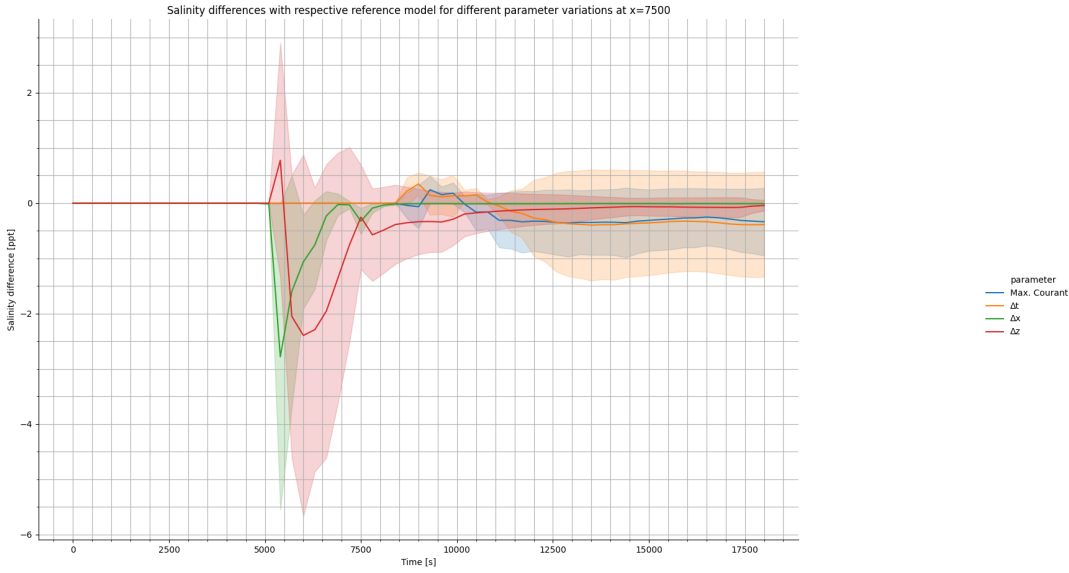


Figure 3.11: Normalized relative differences depicting the mean and the standard deviation through a fat line and slightly transparent area, respectively. Both  $\Delta x$  and  $\Delta t$  are observed to have a large influence on the shape of the front, defined as local diffusion. For these parameters global diffusion drastically decreases over time. For  $\Delta t$  and  $Courant_{max}$  minor over and undershoot can be observed and increased global diffusion over time is caused by large Courant numbers.

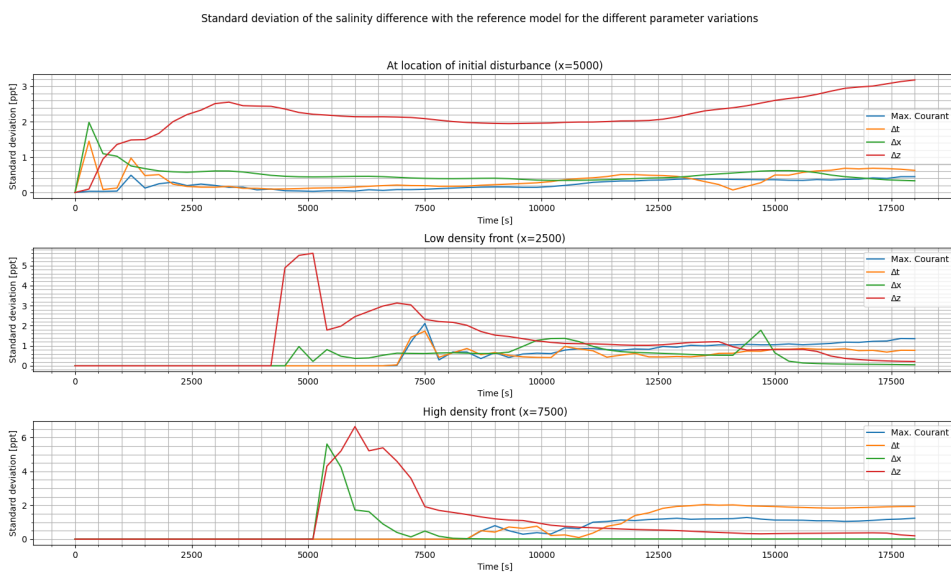


Figure 3.12: Normalized standard deviation of the relative salinity differences. In terms of global diffusion,  $\Delta z$  can influence salinity values up to 2 ppt. Salinity values at the front are highly sensitive by  $\Delta x$  and  $\Delta z$  up to 5 ppt. as a result of local diffusion. Both parameters  $\Delta t$  and  $Courant_{max}$  have a significant influence on the dispersive oscillatory type of error.



# 4

## Discussion and conclusion

Since, for the reference model in chapter 3.1 results were obtained that coincide with the expected physics and both numerical diffusion and dispersion can be identified from the presented plots, the baseline for the sensitivity analysis was sufficiently validated. However, to obtain better insight in what causes the observed phenomena and how these relate to the numerical accuracy of the model different ranges of  $Courant_{max}$ ,  $\Delta t$ ,  $\Delta x$  and  $\Delta z$  were modelled and the errors produced by the model were analyzed. The errors were defined as the relative difference of the salinity profile with the most recent version of the reference model at a specific location and depth over the whole time domain.

As expected the D-Flow FM shows spurious oscillations for large values of Max. Courant, nonetheless this only starts occurring at values higher than 1.6 (figure A.3). At values between 1.0 and 1.6 and values lower than 0.1 only minor over- and undershoot was observed. Next, at very large  $\Delta t$  clear oscillations are observed which have an amplitude of approximately 2 ppt. Both at the location of the initial disturbance and at the low density front (see figures 3.5 and A.4). And only for  $\Delta t \leq 50s$ , which gives an approximate Courant number of 0.25, the amplitude of these oscillations drops below 0.5.

With respect to the numerical diffusion produced by the model a plain observation is that it reduces especially if a constant time step size is set. This can be inferred from figure 3.8 which shows very little diffusion for the simulations that maintained  $\Delta t = 10s$ . Similarly 3.9 shows a large influence of  $\Delta z$  on the relative salinity differences across the whole domain, which is classified as global diffusion. This makes sense since oscillations, which are a sign of instability, are typical for explicit schemes which is why they require artificial damping [Zijlema, 2015]. This could be confirmed by varying the  $\theta$  (the implicitness parameter) and look at the effects of different  $\Delta t$ .

Further no direct relation between the Courant number at the front and the global diffusive character of the simulation could be found. Although  $\Delta z$  seems an exception, this is shown not necessarily to be the case. Nonetheless, it is clear that when the  $\Delta t$  and  $\Delta x$  are sufficiently small diffusion across the domain can very effectively be minimized by decreasing  $\Delta z$ . Further research studying the variations of  $\Delta z$  in the range 1.0-2.0 meter and at different  $\Delta t$  and  $\Delta x$  in this context would have to show for what range of values of  $\Delta z$ ,  $\Delta x$  and  $\Delta t$  such global diffusion can best be tackled.

The origin of the errors observed in the variations of  $\Delta x$  appear to be of a diffusive kind (figure 3.6), which explains the fact that at smaller values of  $\Delta x$  the front arrives earlier. The fact that the model is mainly diffusive might be explained by the fact that the time step size is chosen to be quite small ( $\Delta t = 10s$ ) which, for larger  $\Delta x$  causes the Courant number to decrease significantly. Since the domain of influence then becomes much larger than the modelled gradient the approximation is overly damped.

The resolution in z-direction shows a high mean relative difference throughout the sensitivity analysis, although at the high density front (figure 3.11) the least. Moreover the high amount of standard deviation of the relative differences over the range of  $\Delta z$  values indicates a large influence on the model's accuracy. Therefore it seems that when the limiting values of  $\Delta x$  and  $\Delta t$  are known  $\Delta z$  can serve to fit the model to produce as little diffusion as possible.

Further is should be noted that dispersion was observed as the model reached its limits in terms of Courant numbers and vertical velocities. Such a limit of the Courant number is beautifully visualized by a seemingly lack of viscosity. Lastly, the limits of the model are not observed for  $Courant_{max} \leq 2.0$  but show clearly for estimated Courant numbers between 0.7 and 1.5 in the horizontal. Whereas the

model only fails at Courant numbers of 10 in the vertical (see section A.5). The observed limits are visible in table A.1 in terms of maximum flow velocities and are plotted and visualized in section A.5.

Based on these results it is recommended to start modelling with either a varying  $\Delta x$  or  $\Delta t$ , depending on which is considered limiting (start with the limiting parameter). Increase the resolution of the parameter until the results show similar diffusion as in a model using an automatic time step setting with  $Courant_{max} = 0.7$ . Hereafter possibly reduce the diffusivity of the model by increasing the resolution in z-direction until computation times become unacceptable. Additionally it is assumed that all observed oscillations in models that could reasonable be considered were not significant or could not clearly be classified as numerical errors. Some of the discussion that brought this uncertainty is presented below.

Finally, the sensitivity of the model's most important type of errors to different parameters were quantified in terms of global diffusion, local diffusion, over-/undershoot and spurious oscillations. Global diffusion are most sensitive to  $\Delta z$  and generally have a range of influence of 2 ppt. Local diffusion is mostly sensitive to  $\Delta z$  and  $\Delta x$  and can change salinity values up to 5 ppt. at the fronts. Over-/undershoot is most sensitive to the  $Courant_{max}$  parameter but occurs very little and only up to 1 ppt. Finally both parameters  $\Delta t$  and  $Courant_{max}$  have a significant influence on the dispersive oscillatory type of error; for the middle of the domain spurious oscillations are sensitive to  $\Delta t$  up to a value of 1 ppt. For the low density front both  $\Delta t$  and  $Courant_{max}$  can influence salinity values up to 2 ppt. In general, it seems that as  $\Delta t$  is set smaller the model becomes more sensitive to spatial parameters. However, another option is that the model is more sensitive to  $\Delta x$  and  $\Delta z$  by design.

## 4.1. Discussion

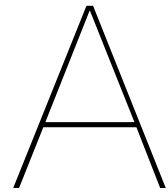
The errors in salinity profiles that show spurious oscillations could possibly be a result of the hydrostatic assumption or of the artificial viscosity of the model, a process imposed to mimic energy loss due to heat transfer which results in a transfer of kinetic energy in the form of waves. Moreover, they could also be a result of the internal waves formed due to friction at the interface of the two density currents. Because in this mixing layer turbulence is likely to occur the model could show oscillations in the salinity profiles to compensate for the vertical velocity gradients associated with turbulence. Further research on the relation between the Courant number and oscillations near the interface of the two currents, while using the absolute velocity difference between two vertically adjacent cells as the propagation speed of the disturbance, could possibly show the origin of these oscillations.

The influence of  $\Delta z$  and  $\Delta x$  on the global diffusion error can be because of a measurement error since the locations where data is taken depend on  $\Delta z$  (the middle of a cell at approximately a depth of 2.5, 4.5 or 6.5) and the initial location of the salinity delta depends on  $\Delta x$  (approximately at  $x = 5000$ ). The water level was not constraint, heat transfer and energy loss was not accounted for in the flow model thus artificial viscosity may be the origin of some of the oscillating errors. The order of parameters while converging to an accurate model might define the type of error observed per parameter just because in the first stages in general dispersive errors (oscillations and over-/undershoot) occur and in later stages only the diffusivity plays an important role in the model's accuracy. Given a large  $\Delta x$  then the semi-implicit time integration requires the domain of influence to be more diffused Zijlema [2015, Chapter 3] and thus requires a smaller time step size. Along this line the results in figure 3.8 also imply that at an earlier stage in the conversion process of the model (for  $\Delta t$  and  $Courant_{max}$  as  $\Delta x$  was still quite large), the model is more diffusive since the diffusion rates are all around 0.6.

# Bibliography

- C Adduce, G Sciortino, and S Proietti. Gravity currents produced by lock exchanges: experiments and simulations with a two-layer shallow-water model with entrainment. *Journal of Hydraulic Engineering*, 138(2):111–121, 2012.
- C Cenedese, R Nokes, and J Hyatt. Lock-exchange gravity currents over rough bottoms. *Environmental Fluid Mechanics*, 18(1):59–73, 2018.
- Deltas. *Technical Reference Manual D-Flow FM*. Deltas systems, version 1.1.0 - svn revision 66571 edition, April 2020.
- Y Friocourt, K Kuijper, and N Leung. Salt intrusion. *Deltafacts*, 2014.
- George G. O'Brien, Morton A. Hyman, and Sidney Kaplan. A Study of the Numerical Solution of Partial Differential Equations. *Journal of Mathematics and Physics*, 29(1-4):223–251, 1950. ISSN 1467-9590. doi: 10.1002/sapm1950291223. URL <https://onlinelibrary.wiley.com/doi/abs/10.1002/sapm1950291223>.
- Julie Pietrzak. The use of TVD limiters for forward-in-time upstream-biased advection schemes in ocean modeling. *Monthly Weather Review*, 126(3):812–830, mar 1998. doi: 10.1175/1520-0493(1998)126<0812:tuotlf>2.0.co;2.
- John P. Rafferty. Internal wave | hydrology. URL <https://www.britannica.com/science/internal-wave>.
- JO Shin, SB Dalziel, and PF Linden. Gravity currents produced by lock exchange. *Journal of Fluid Mechanics*, 521:1–34, 2004.
- John E. Simpson and Michael Manga. Gravity currents in the environment and the laboratory. 51: 70–72, 1998. ISSN 0031-9228. doi: 10.1063/1.882214.
- Bram Van Leer. Towards the ultimate conservative difference scheme. IV. a new approach to numerical convection. *Journal of Computational Physics*, 23(3):276–299, mar 1977. doi: 10.1016/0021-9991(77)90095-x.
- M. Zijlema. Computational Modelling of Flow and Transport. *Collegedictaat CIE4340*, 2015. URL <https://repository.tudelft.nl/islandora/object/uuid%3A5e7dac47-0159-4af3-b1d8-32d37d2a8406>.





# Simulation results

## A.1. Courant numbers reference model



Figure A.1: Depth maximized Courant number over time. The observed Courant numbers do not exceed 0.4 and are at their maximum at  $t = 2.5h$ .

## A.2. Relative salinity differences per parameter

### A.2.1. Max. Courant

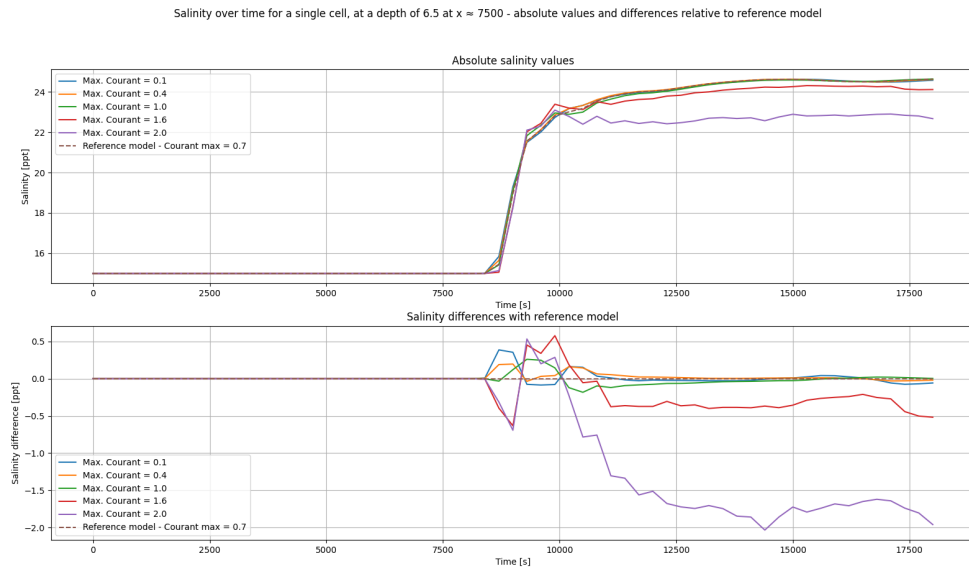


Figure A.2: Salinity of a single cell at  $d = 6.5m$  showing the high density front passing.

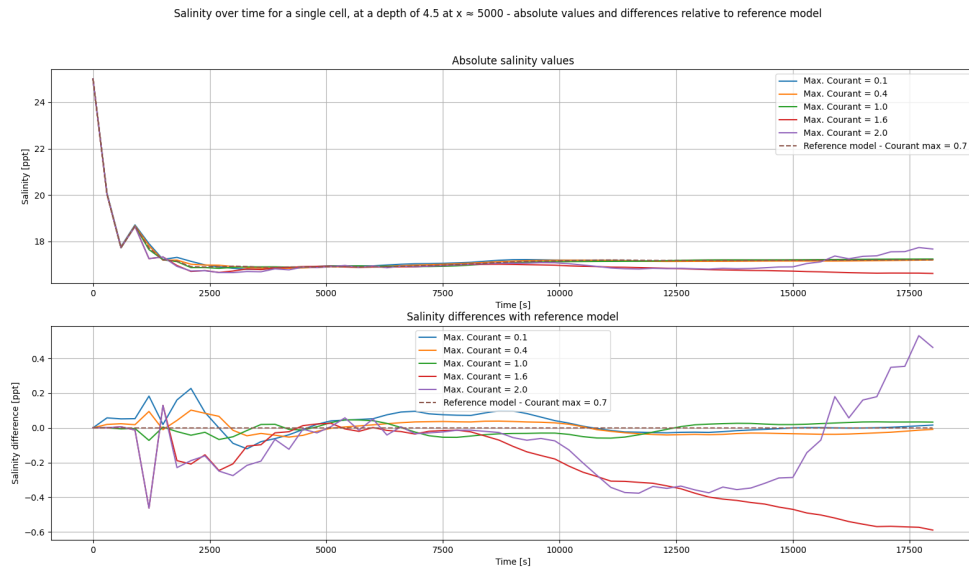


Figure A.3: Salinity of a single cell at  $d = 4.5m$  at the location of the initial salinity difference. A steep spike at  $t = 800$  can be observed (also seen in figure 3.2) which is probably due to a lack of resolution.

### A.2.2. Time step size

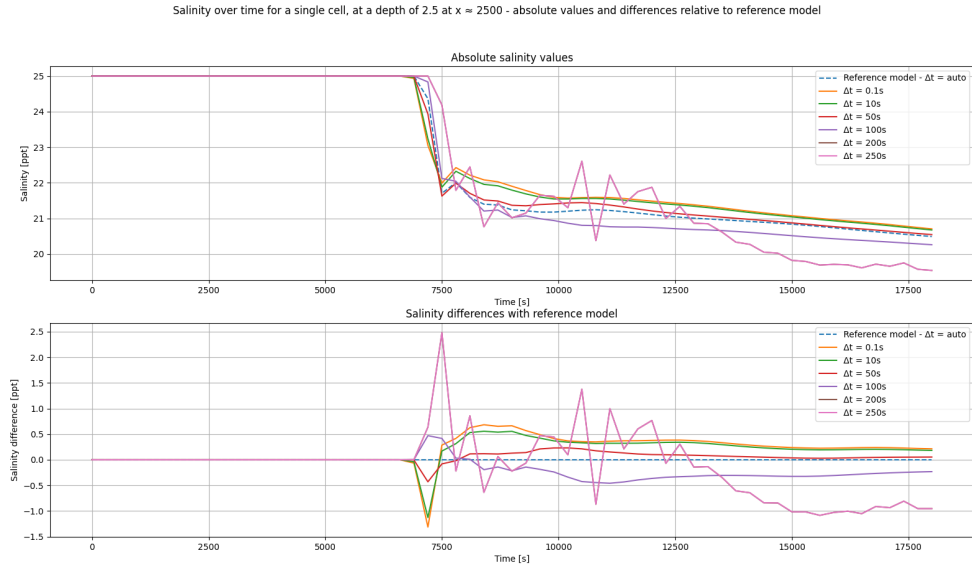


Figure A.4: Salinity of a single cell at  $d = 2.5\text{m}$  showing the low density front passing. Diffusion of the front at  $\Delta t = 250\text{s}$  can be observed as a backlog of the front. Over and undershoot can be observed for  $\Delta t \leq 100\text{s}$  and oscillations develop for  $\Delta t = 250\text{s}$ .

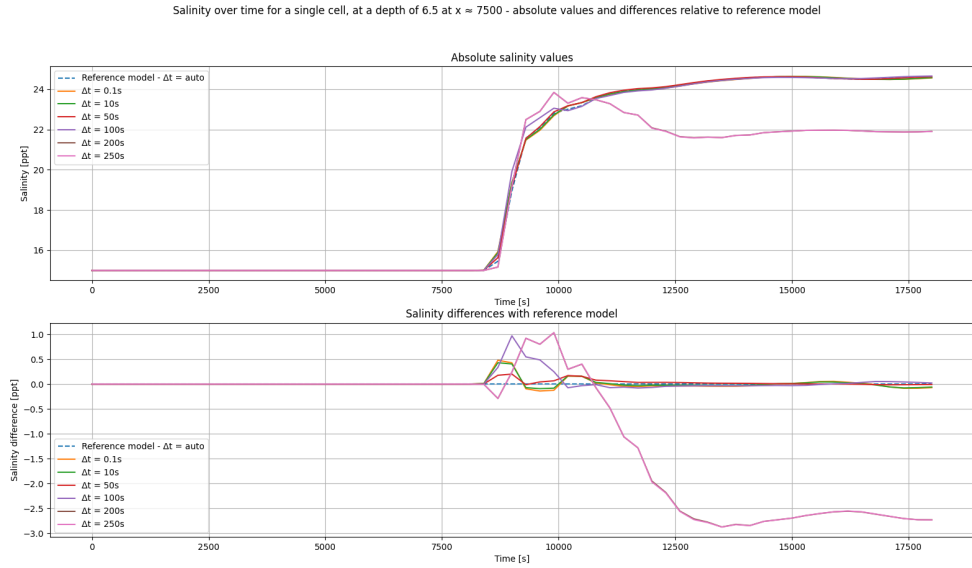


Figure A.5: Salinity of a single cell at  $d = 6.5\text{m}$  showing the high density front passing. A choppy top of the front can be observed for  $\Delta t = 250\text{s}$ , this was also the case for a high Courant number during the variations of  $Courant_{max}$ .

### A.2.3. Resolution x-direction

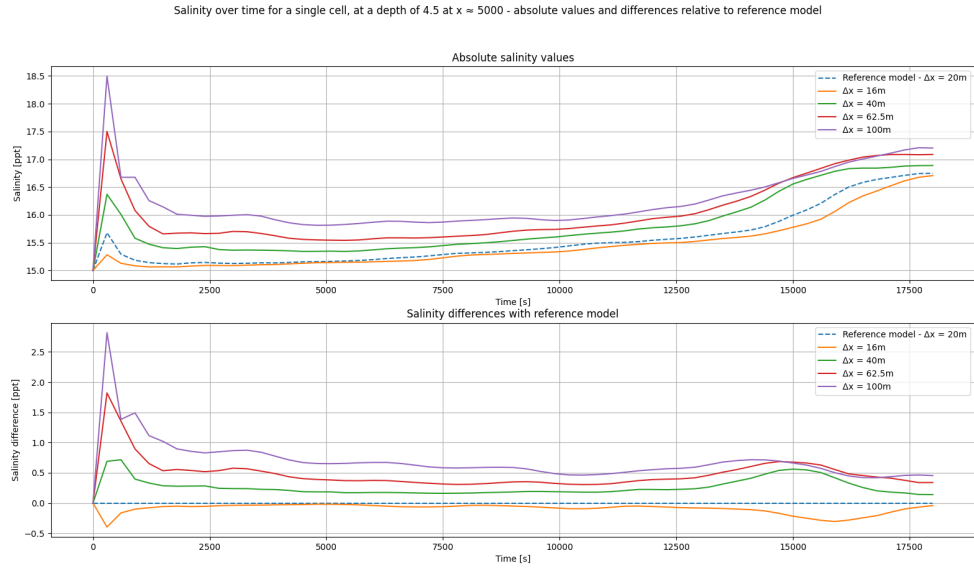


Figure A.6: Salinity of a single cell at  $d = 4.5\text{m}$  at the location of the initial salinity difference. It seems the shape and or location of the mixing layer changes with an increasing  $\Delta x$ , since the salinities do not convert to the same value even after the steep salinity gradient has passed. Although, it could also indicate an error in placement of the measurement location.

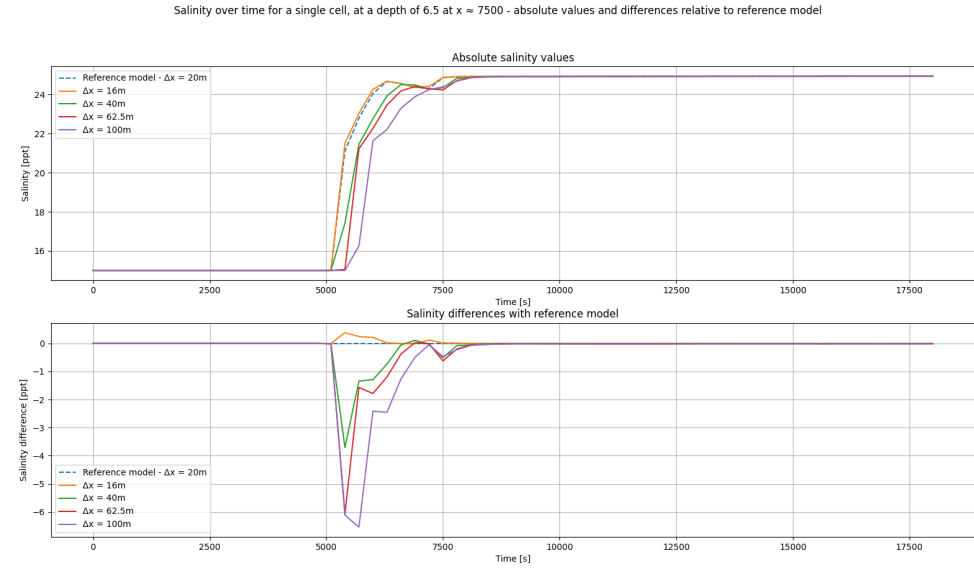


Figure A.7: Salinity of a single cell at  $d = 6.5\text{m}$  showing the high density front passing. A clear backlog of approximations with a larger  $\Delta x$  can be observed, causing a peek in the relative difference.

### A.2.4. Resolution z-direction

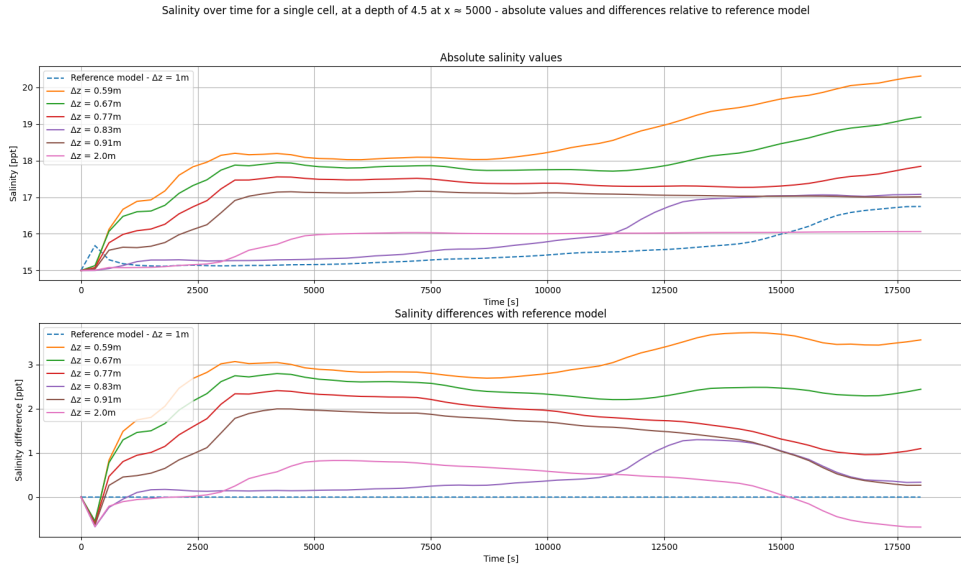


Figure A.8: Salinity of a single cell at  $d = 4.5\text{m}$  at the location of the initial salinity difference. The salinity at a depth of 4.5 meters increases as  $\Delta z$  decreases, this happens because the vertical location of the boundary layer moves upward possibly due to better modelling of vertical velocities. However, also a small measurement error has it's effect.

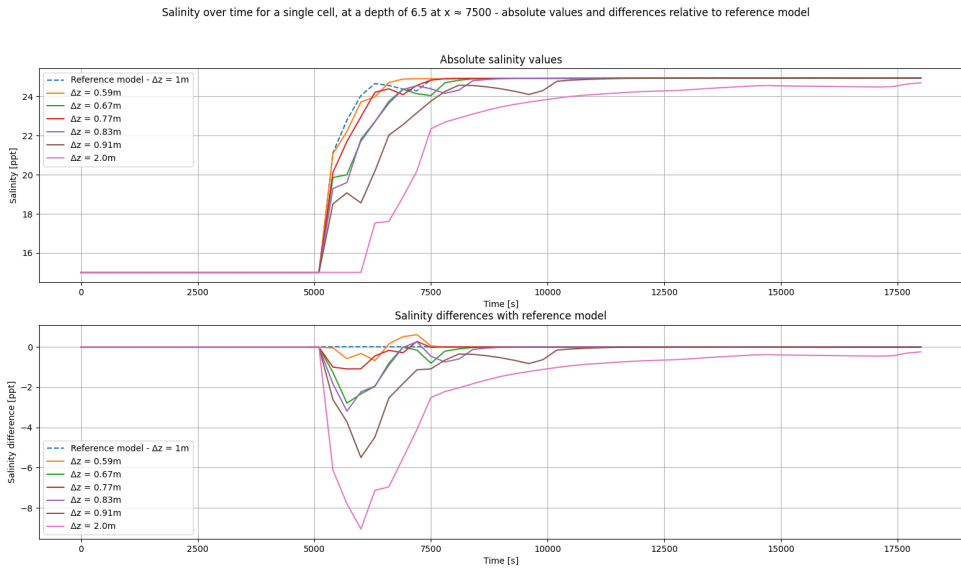


Figure A.9: Salinity of a single cell at  $d = 6.5\text{m}$  showing the high density front passing. The diffusion of the fronts are not proportionally spread to  $\Delta z$ , also the shape of the front changes for all values of  $\Delta z$  which causes peaks in the relative differences. With the exception of the approximation where  $\Delta z = 2\text{m}$ , here the cause is diffusion of the frontal propagation speed.

### A.3. Table of simulations

Table depicting most relevant data per parameter, where:

- *Run ID*: the unique id of the simulation
- *fps low*: the frontal propagation speed of the low density front,
- *fps high*: the frontal propagation speed of the high density front,
- *ldf diff rate*: the diffusion rate of the low density front,
- *hdf diff rate*: the diffusion rate of the high density front,
- *ldf courant*: the computed courant number of the low density front,
- *hdf courant*: the computed courant number of the high density front,
- *max courant lim*: the maximum times a cell was courant limiting,
- *string id*: characteristic parameter setting of the simulation,
- *parameter*: the parameter variation the simulation was part of,
- *max velocity x*: maximum velocity in the x-direction,
- *max velocity z*: maximum velocity in the z-direction.

A.3. Table of simulations

index	fps		fps		ldf		hdf		ldf		hdf		max		string		parameter		max		max	
	low	high	high	rate	diff	rate	courant	lim	courant	rate	courant	lim	courant	id	id	velocity	x	velocity	z	velocity	x	velocity
run <b>2605 1</b>	0.577	0.46	0.65	0.598	0.288	0.226	11.0	Ref. - Courant max = 0.7	Reference model	0.504	0.016											
run <b>0206 1</b>	0.577	0.46	0.659	0.598	0.197	0.179	12.0	Ref. - 3min output	Reference model	0.504	0.014											
run <b>1006 4</b>	0.577	0.46	0.954	1.006	0.385	0.325	0.0	Ref. - $\Delta x = 20m$	Reference model	0.754	0.099											
run <b>1106 2</b>	0.577	0.46	0.983	0.97	0.385	0.325	0.0	Ref. - $\Delta z = 1.0m$	Reference model	0.754	0.099											
run <b>0606 1</b>	0.577	0.46	0.659	0.598	0.054	0.038	0.0	$\Delta t = 10s$	Time step size	0.508	0.016											
run <b>0606 2</b>	0.577	0.46	0.659	0.598	0.105	0.076	0.0	$\Delta t = 20s$	Time step size	0.507	0.016											
run <b>0606 3</b>	0.577	0.46	0.659	0.598	0.153	0.114	0.0	$\Delta t = 30s$	Time step size	0.505	0.015											
run <b>0606 4</b>	0.577	0.46	0.659	0.598	0.186	0.142	0.0	$\Delta t = 40s$	Time step size	0.504	0.016											
run <b>0606 5</b>	0.577	0.46	0.659	0.598	0.234	0.192	0.0	$\Delta t = 50s$	Time step size	0.503	0.016											
run <b>0606 6</b>	0.577	0.46	0.659	0.598	0.265	0.239	0.0	$\Delta t = 60s$	Time step size	0.502	0.016											
run <b>0606 7</b>	0.577	0.46	0.659	0.598	0.265	0.239	0.0	$\Delta t = 70s$	Time step size	0.504	0.017											
run <b>0606 8</b>	0.577	0.46	0.63	0.598	0.403	0.308	0.0	$\Delta t = 80s$	Time step size	0.504	0.017											
run <b>0606 9</b>	0.577	0.46	0.63	0.598	0.403	0.308	0.0	$\Delta t = 90s$	Time step size	0.504	0.017											
run <b>0606 10</b>	0.577	0.46	0.63	0.598	0.513	0.42	0.0	$\Delta t = 100s$	Time step size	0.517	0.018											
run <b>0606 11</b>	0.577	0.46	0.621	0.598	0.722	0.659	0.0	$\Delta t = 200s$	Time step size	0.576	0.02											
<b>run 0606 12</b>	<b>0.577</b>	<b>0.46</b>	<b>1.444</b>	<b>0.652</b>	<b>5.554</b>	<b>6.672</b>	<b>28.0</b>	<b><math>\Delta t = 500s</math></b>	<b>Time step size</b>	<b>152.601</b>	<b>2466.423</b>											

Time step size										A. Simulation results	
Δt = 1000s					Time step size					115.369	8469.205
<b>run 0606 13</b>	<b>0.577</b>	<b>0.46</b>	<b>1.752</b>	<b>1.329</b>	<b>0.687</b>	<b>2.183</b>	<b>13.0</b>	<b>Δt = 1000s</b>	Time step size	0.509	0.015
<b>run 0606 14</b>	<b>0.577</b>	<b>0.46</b>	<b>0.659</b>	<b>0.598</b>	<b>0.027</b>	<b>0.019</b>	<b>0.0</b>	<b>Δt = 5s</b>	Time step size	0.509	0.015
<b>run 0606 15</b>	<b>0.577</b>	<b>0.46</b>	<b>0.659</b>	<b>0.598</b>	<b>0.006</b>	<b>0.004</b>	<b>0.0</b>	<b>Δt = 1s</b>	Time step size	0.509	0.016
<b>run 0606 16</b>	<b>0.577</b>	<b>0.46</b>	<b>0.659</b>	<b>0.598</b>	<b>0.0</b>	<b>0.0</b>	<b>0.0</b>	<b>Δt = 0.1s</b>	Time step size	0.509	0.016
<b>run 0606 17</b>	<b>0.577</b>	<b>0.46</b>	<b>0.621</b>	<b>0.598</b>	<b>0.722</b>	<b>0.659</b>	<b>0.0</b>	<b>Δt = 250s</b>	Time step size	0.576	0.02
<b>run 0606 18</b>	<b>0.577</b>	<b>0.46</b>	<b>1.444</b>	<b>0.701</b>	<b>14.935</b>	<b>6.453</b>	<b>11.0</b>	<b>Δt = 300s</b>	Time step size	116.374	4964.051
<b>run 0606 19</b>	<b>0.577</b>	<b>0.46</b>	<b>1.906</b>	<b>1.716</b>	<b>0.117</b>	<b>0.204</b>	<b>11.0</b>	<b>Δt = 350s</b>	Time step size	246.67	1580.379
<b>run 0606 20</b>	<b>0.577</b>	<b>0.46</b>	<b>1.198</b>	<b>0.888</b>	<b>8.674</b>	<b>10.817</b>	<b>12.0</b>	<b>Δt = 400s</b>	Time step size	177.126	1397.693
<b>run 0606 21</b>	<b>0.577</b>	<b>0.46</b>	<b>1.906</b>	<b>2.247</b>	<b>0.0</b>	<b>0.0</b>	<b>5.0</b>	<b>Δt = 120s</b>	Time step size	350.809	4435.914
<b>run 0606 22</b>	<b>0.577</b>	<b>0.46</b>	<b>1.906</b>	<b>2.247</b>	<b>2.245</b>	<b>1.608</b>	<b>14.0</b>	<b>Δt = 140s</b>	Time step size	170.575	25517.104
<b>run 0606 23</b>	<b>0.577</b>	<b>0.46</b>	<b>1.906</b>	<b>2.247</b>	<b>4.697</b>	<b>0.368</b>	<b>14.0</b>	<b>Δt = 160s</b>	Time step size	157.309	1008.179
<b>run 0606 24</b>	<b>0.577</b>	<b>0.46</b>					<b>10.0</b>	<b>Δt = 180s</b>	Time step size	201.342	3250.988
<b>run 0106 1</b>	<b>0.577</b>	<b>0.46</b>	<b>0.659</b>	<b>0.598</b>	<b>0.238</b>	<b>0.199</b>	<b>13.0</b>	<b>Max. Courant = 0.5</b>	Max. Courant	0.505	0.016
<b>run 0106 2</b>	<b>0.577</b>	<b>0.46</b>	<b>0.659</b>	<b>0.598</b>	<b>0.22</b>	<b>0.198</b>	<b>11.0</b>	<b>Max. Courant = 0.6</b>	Max. Courant	0.504	0.016
<b>run 0106 3</b>	<b>0.577</b>	<b>0.46</b>	<b>0.63</b>	<b>0.598</b>	<b>0.401</b>	<b>0.306</b>	<b>10.0</b>	<b>Max. Courant = 0.8</b>	Max. Courant	0.503	0.016
<b>run 0106 4</b>	<b>0.577</b>	<b>0.46</b>	<b>0.63</b>	<b>0.598</b>	<b>0.462</b>	<b>0.355</b>	<b>10.0</b>	<b>Max. Courant = 0.9</b>	Max. Courant	0.503	0.016
<b>run 0106 5</b>	<b>0.577</b>	<b>0.46</b>	<b>0.63</b>	<b>0.598</b>	<b>0.518</b>	<b>0.413</b>	<b>9.0</b>	<b>Max. Courant = 1.0</b>	Max. Courant	0.503	0.016
<b>run 0106 6</b>	<b>0.577</b>	<b>0.46</b>	<b>0.63</b>	<b>0.598</b>	<b>0.505</b>	<b>0.419</b>	<b>8.0</b>	<b>Max. Courant = 1.1</b>	Max. Courant	0.504	0.016
<b>run 0106 7</b>	<b>0.577</b>	<b>0.46</b>	<b>0.63</b>	<b>0.598</b>	<b>0.503</b>	<b>0.42</b>	<b>8.0</b>	<b>Max. Courant = 1.2</b>	Max. Courant	0.504	0.016

### A.3. Table of simulations

run 0106 8	0.577	0.46	0.659	0.598	0.066	0.047	40.0	Max. Courant = 0.1		Max. Courant		0.508	0.016						
run 0106 9	0.577	0.46	0.659	0.598	0.124	0.091	27.0	Max. Courant = 0.2		Max. Courant		0.507	0.016						
run 0106 10	0.577	0.46	0.659	0.598	0.175	0.132	18.0	Max. Courant = 0.3		Max. Courant		0.506	0.016						
run 0106 11	0.577	0.46	0.659	0.598	0.209	0.163	15.0	Max. Courant = 0.4		Max. Courant		0.506	0.016						
run 0106 12	0.577	0.46	0.63	0.598	0.5	0.42	9.0	Max. Courant = 1.3		Max. Courant		0.504	0.016						
run 0106 13	0.577	0.46	0.63	0.598	0.496	0.417	9.0	Max. Courant = 1.4		Max. Courant		0.504	0.016						
run 0106 14	0.577	0.46	0.621	0.598	0.653	0.523	9.0	Max. Courant = 1.5		Max. Courant		0.504	0.016						
run 0106 15	0.577	0.46	0.621	0.598	0.741	0.637	9.0	Max. Courant = 1.6		Max. Courant		0.504	0.016						
run 0106 16	0.577	0.46	0.621	0.598	0.71	0.646	11.0	Max. Courant = 1.7		Max. Courant		0.504	0.016						
run 0106 17	0.577	0.46	0.621	0.598	0.594	0.538	18.0	Max. Courant = 1.8		Max. Courant		0.504	0.016						
run 0106 18	0.577	0.46	0.621	0.598	0.594	0.538	12.0	Max. Courant = 1.9		Max. Courant		0.504	0.016						
run 0106 19	0.577	0.46	0.621	0.598	0.594	0.538	10.0	Max. Courant = 2.0		Max. Courant		0.504	0.016						
run 1006 1	0.577	0.46						23.0	Δx = 5m		Resolution x-direction	145.151	59642.768						
run 1006 2	0.577	0.46						18.0	Δx = 10m		Resolution x-direction	76.866	18237.859						
run 1006 3	0.577	0.46	0.954	1.01	0.472	0.402	0.0	Δx = 16m		Resolution x-direction	0.754	0.153							
run 1006 5	0.577	0.46	0.954	0.998	0.312	0.259	0.0	Δx = 25m		Resolution x-direction	0.753	0.079							
run 1006 6	0.577	0.46	0.957	0.993	0.256	0.205	0.0	Δx = 31.25m		Resolution x-direction	0.752	0.07							
run 1006 7	0.577	0.46	0.958	0.98	0.222	0.175	0.0	Δx = 36.5m		Resolution x-direction	0.751	0.074							
run 1006 8	0.577	0.46	0.955	0.976	0.202	0.158	0.0	Δx = 40m		Resolution x-direction	0.747	0.064							

Table A.1: Table depicting most relevant data per parameter: Run ID: the unique id of the simulation, fps low: the frontal propagation speed of the low density front, fps high: the frontal propagation speed of the high density front, ldf diff rate: the diffusion rate of the low density front, ldf courant: the computed courant number of the low density front, hdf diff rate: the diffusion rate of the high density front, hdf courant: the computed courant number of the high density front, max courant lim: the maximum times a cell was courant limiting, string id: characteristic parameter setting of the simulation, parameter: the parameter variation the simulation was part of, max velocity x: maximum velocity in the x-direction, max velocity z: maximum velocity in the z-direction.

## A.4. Example explorative model

The below salinity profile is referred to yet was only part of the explorative modelling, therefore not included in the salinity profile.

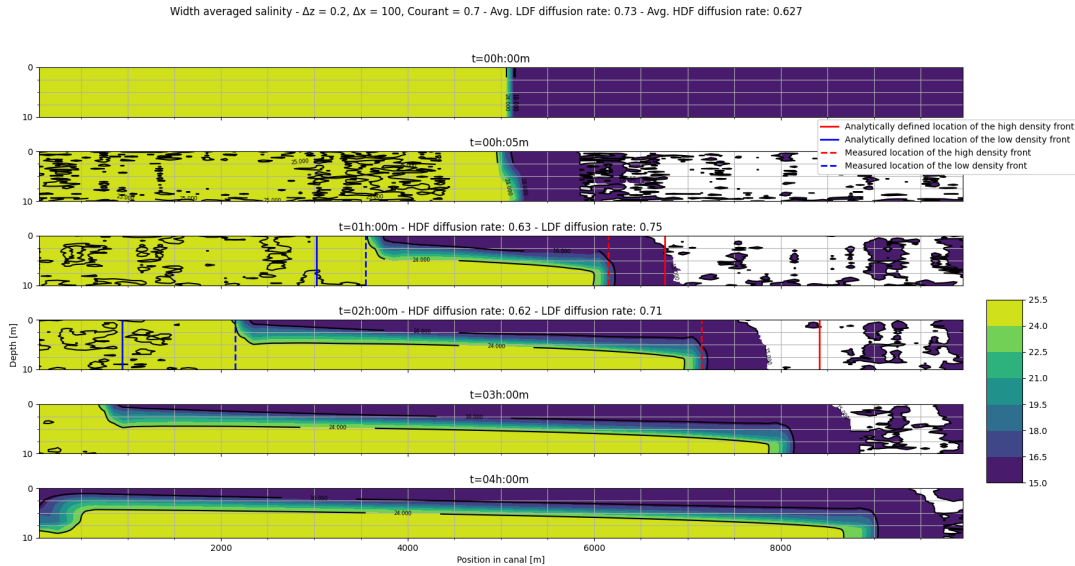


Figure A.10: Salinity contour of a explorative simulation where  $\Delta z = 0.2\text{m}$ ,  $\Delta x = 100\text{m}$  and  $\Delta t = \text{automatic}$ . This shows that not all simulations where  $\Delta z$  is small enough global diffusion can be minimized.

## A.5. Limits of D-Flow FM

Below the salinity contour plots of the simulations that failed to produce reasonable results are depicted.

### A.5.1. Limits of time step size

The simulations where  $\Delta t$  was varied clearly showed the limits of the model for minimal and maximum Courant numbers. Given  $\Delta x = 100\text{m}$  and an estimated average velocity of 0.5 m/s the model stopped producing reasonable results for  $\Delta t \geq 300\text{s}$  which gives a Courant number of 1.5. It almost did not show indications for a salinity transport flux limiter anymore for  $\Delta t \leq 0.1\text{s}$  which gives a Courant number of 0.0005.

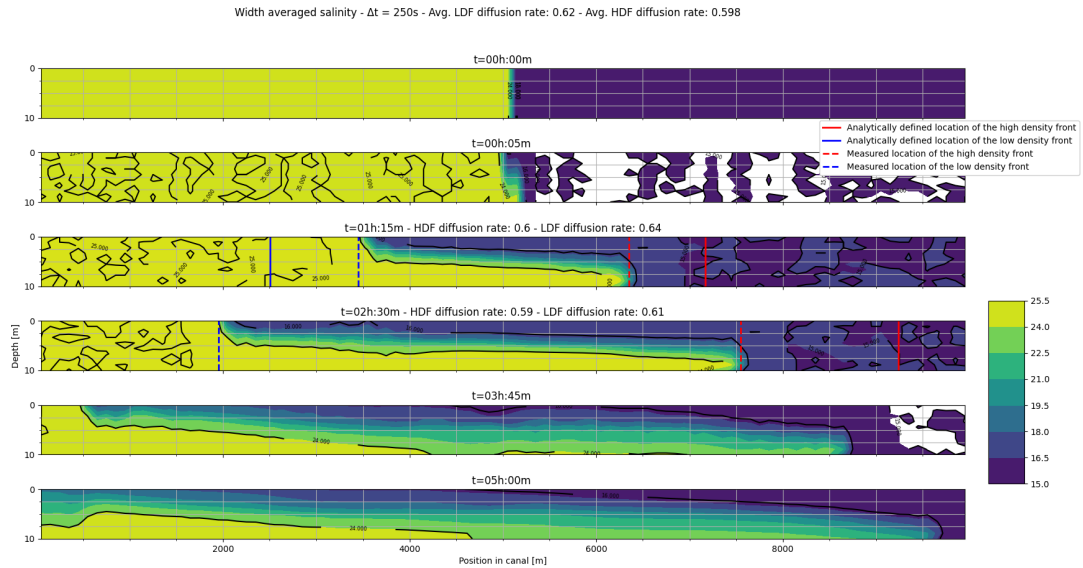


Figure A.11: A salinity profile for the whole domain that is close to the limits of the boundary, dispersion around the mixing layer starts develop and an extremely low artificial viscosity is introduced causing the mixing layer to grow to extremes.

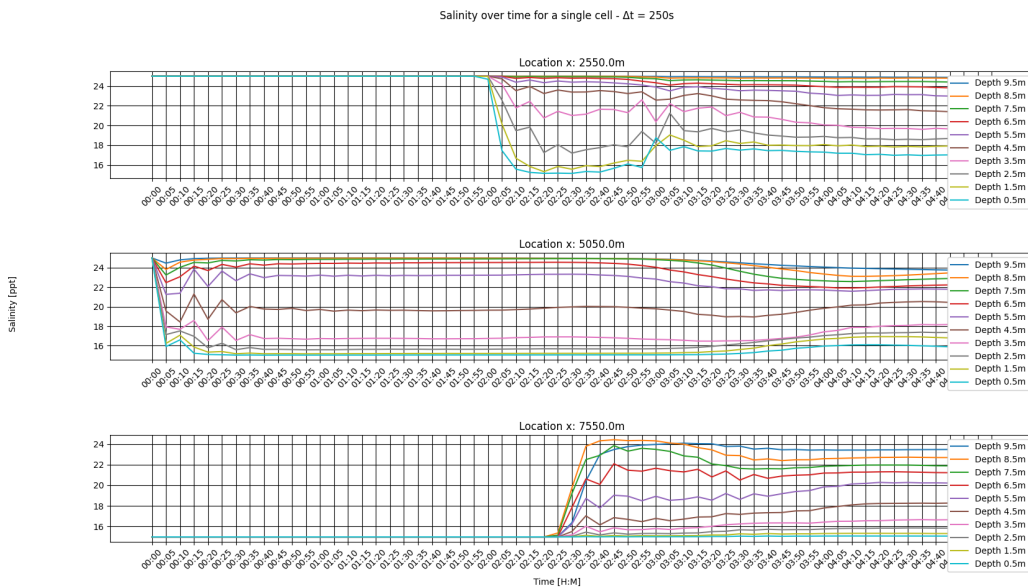


Figure A.12: Salinity profile at different depths for a model that is on the edge of failing where clear oscillations can be observed, indicating numerical dispersion.

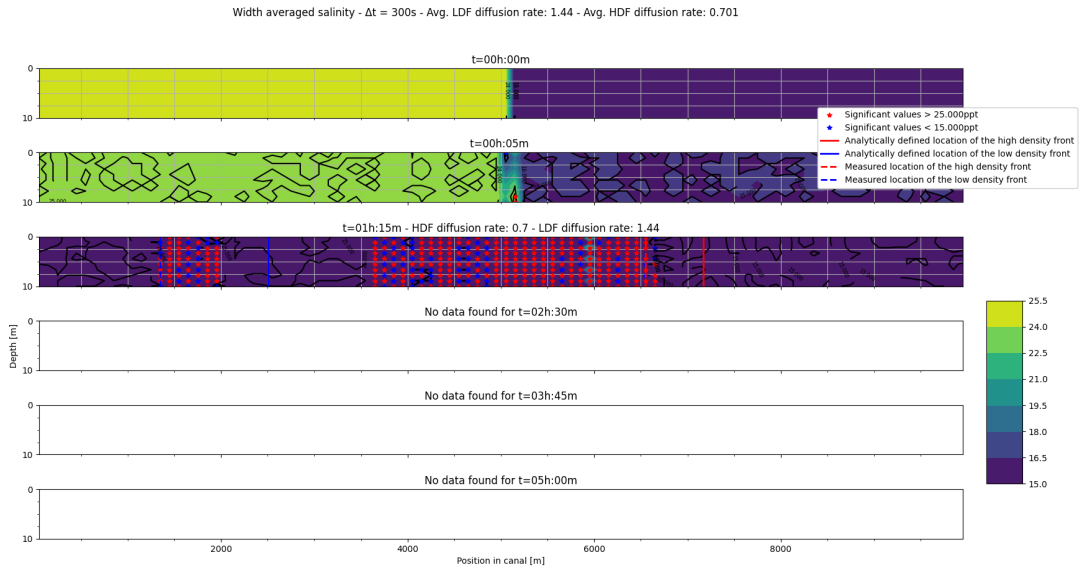


Figure A.13: Salinity profile of a model that failed because of a too high Courant number, depicting unrealistic extreme values (i.e. values where the *Salinity*  $\notin [15, 25]$ ) which are a result of numerical dispersion.

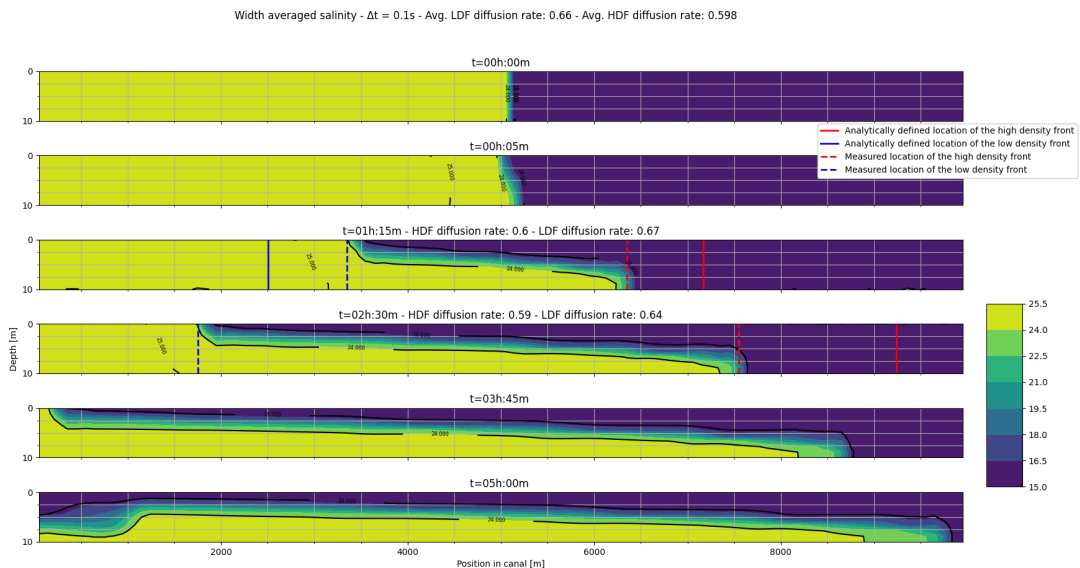
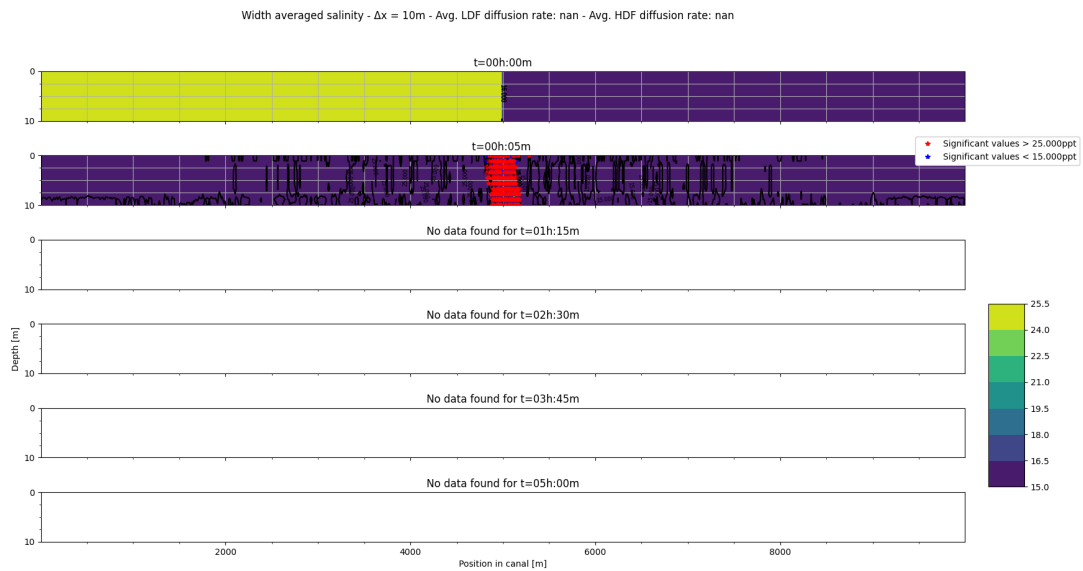
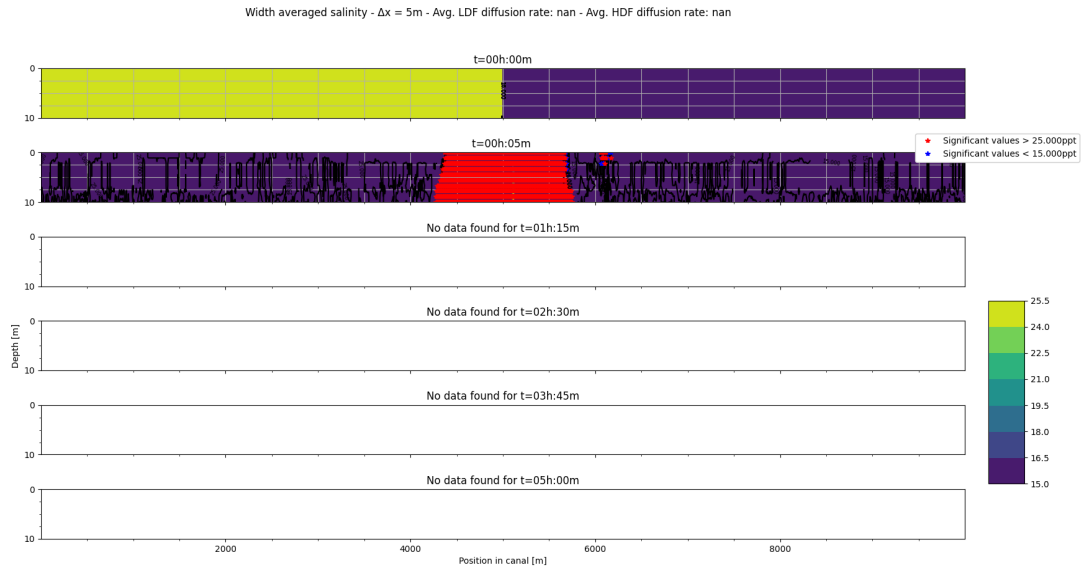


Figure A.14: Salinity profile of a model that showed almost no signs of being limited by a flux limiter. Under the assumption that the contour lines of 15 and 25 ppt. away from the travelling fronts that do not contain values significantly outside the physical limits of the salinity ( $[15, 25]$ , which would be indicated by red or blue dots) are indications of the approximation being limited by the flux limiter.

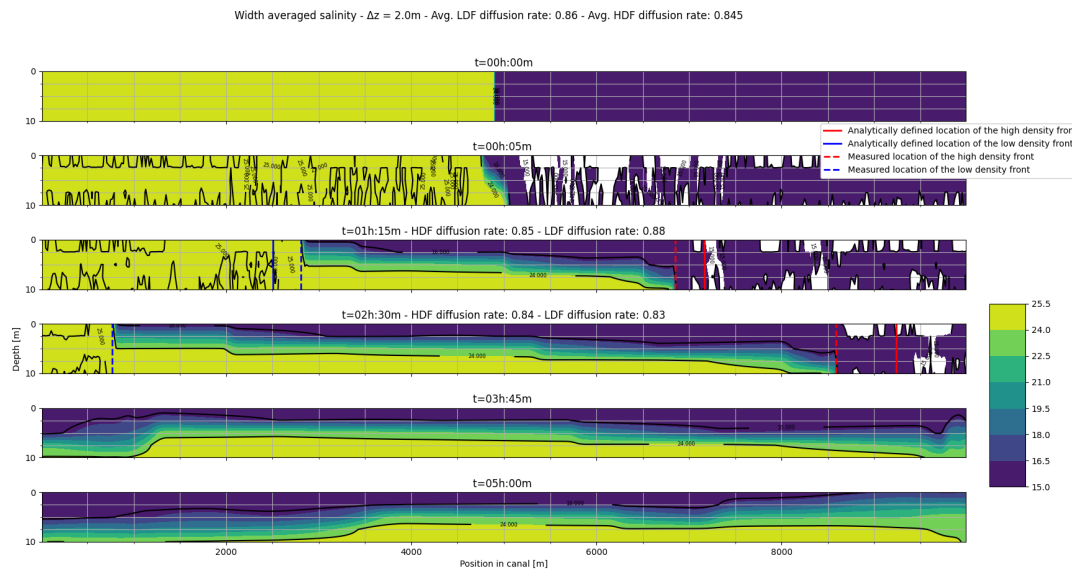
### A.5.2. Limits of resolution x-direction

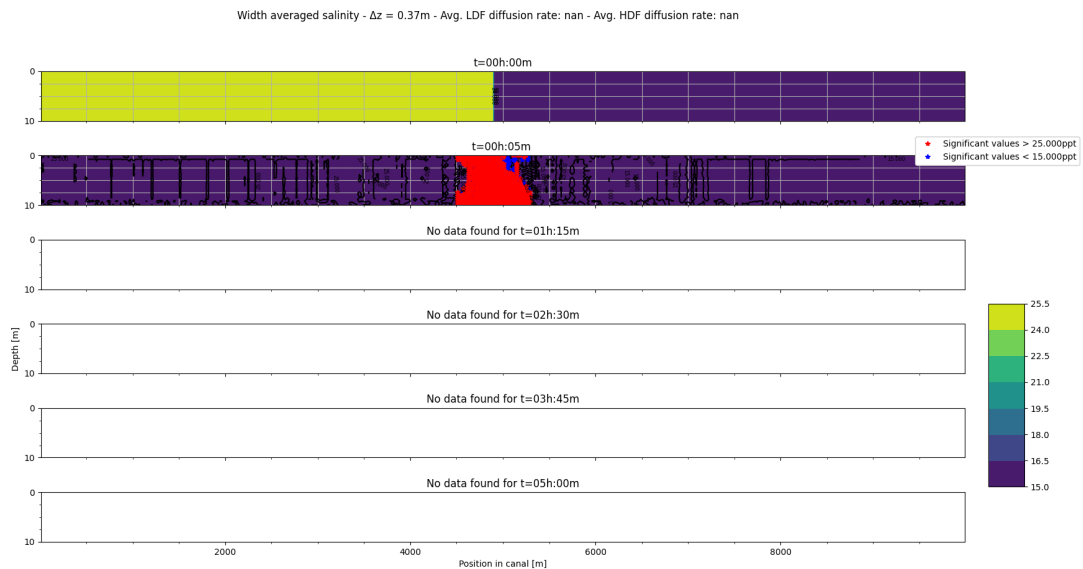
The limits of  $\Delta x$  were observed for  $\Delta x \geq 5\text{m}$ , given  $\Delta t = 10\text{s}$  and an estimated average velocity of 0.7 m/s this gives a Courant number of 1.4.



### A.5.3. Limits of resolution z-direction

The limits of the  $\Delta z$  become visible for  $\Delta z \leq 0.5m$  which corresponds with a Courant number of 2.0, given  $\Delta t = 10s$  and an estimated vertical velocity of 0.1 m/s.

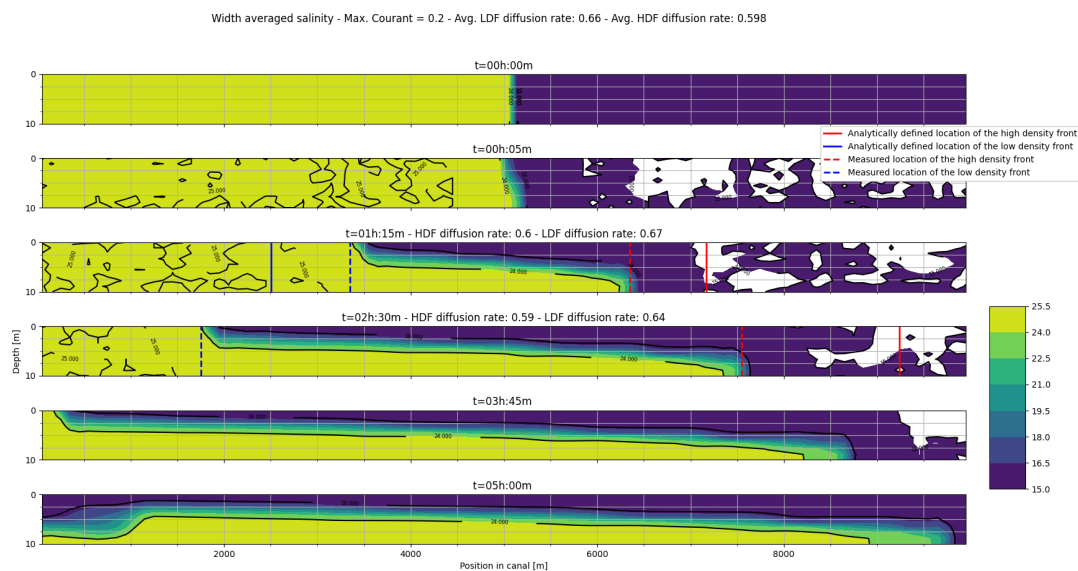
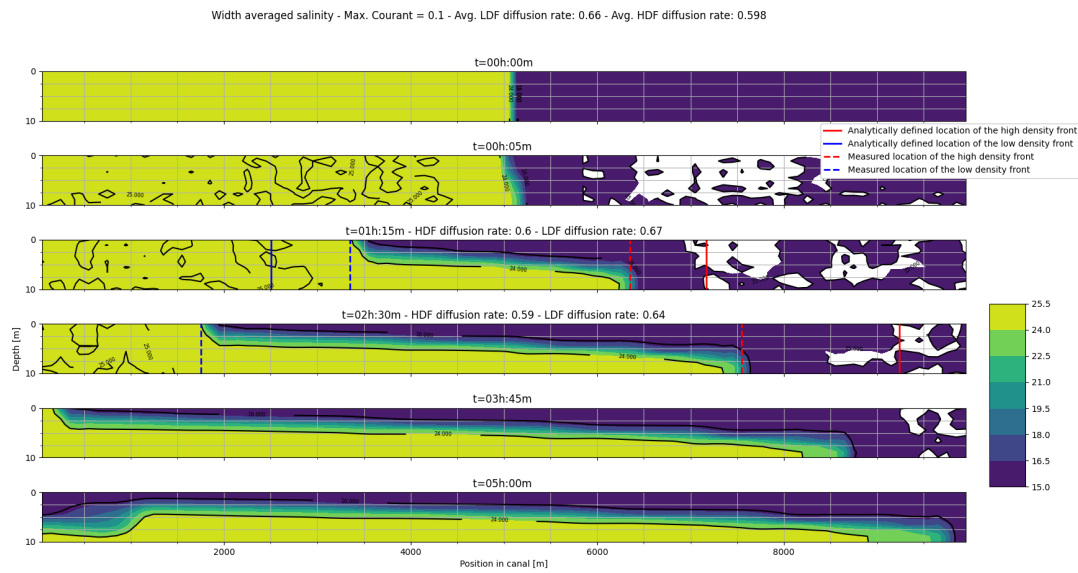


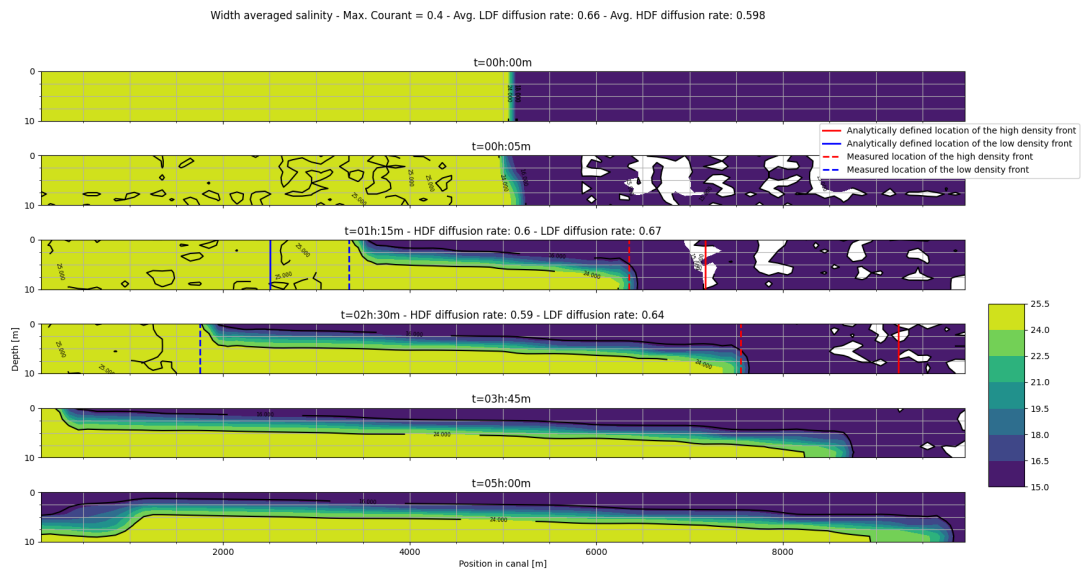
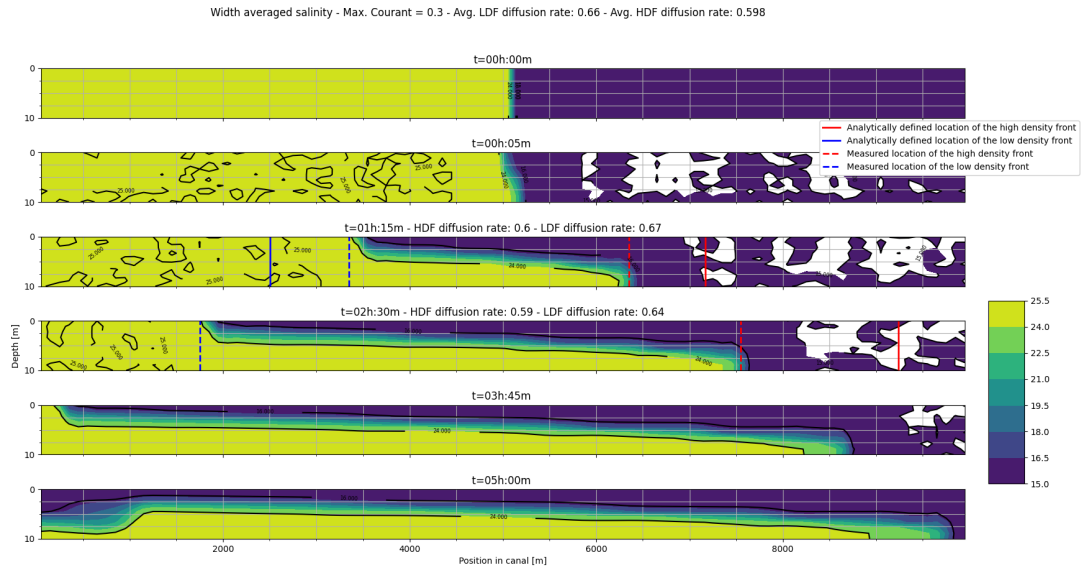


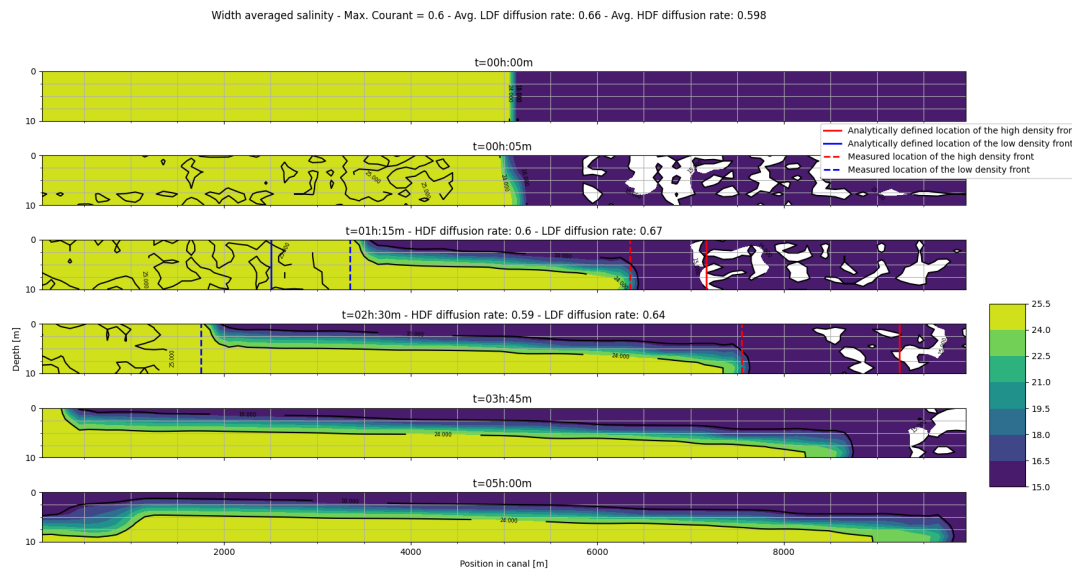
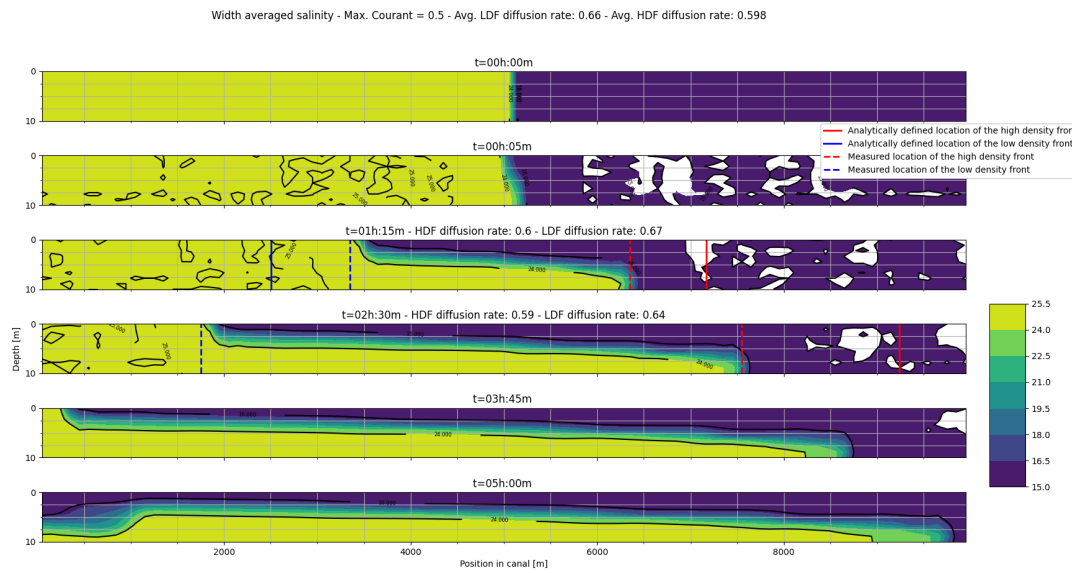
## A.6. Salinity contour plots of simulations used for analysis

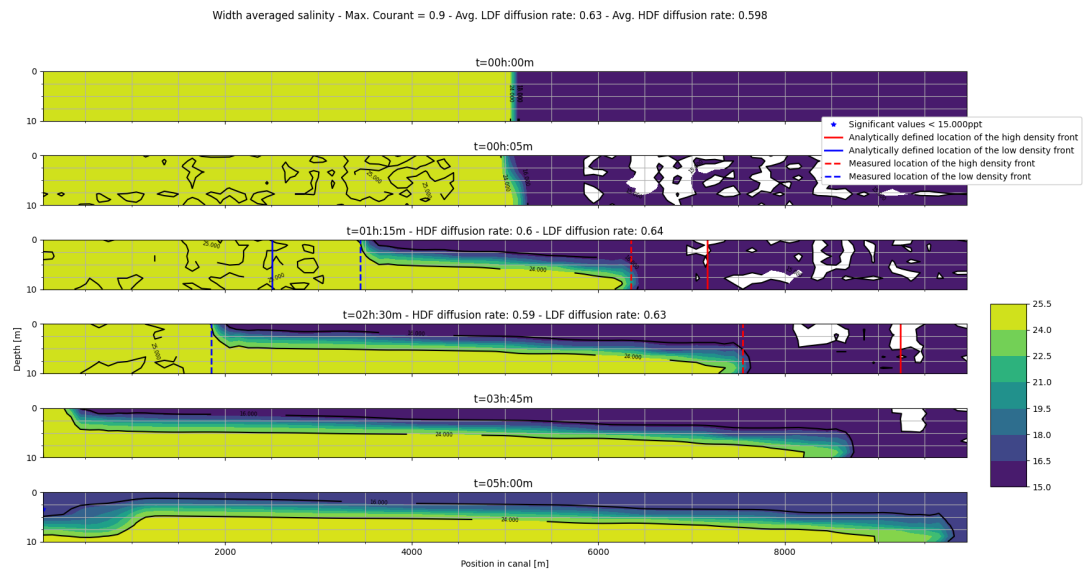
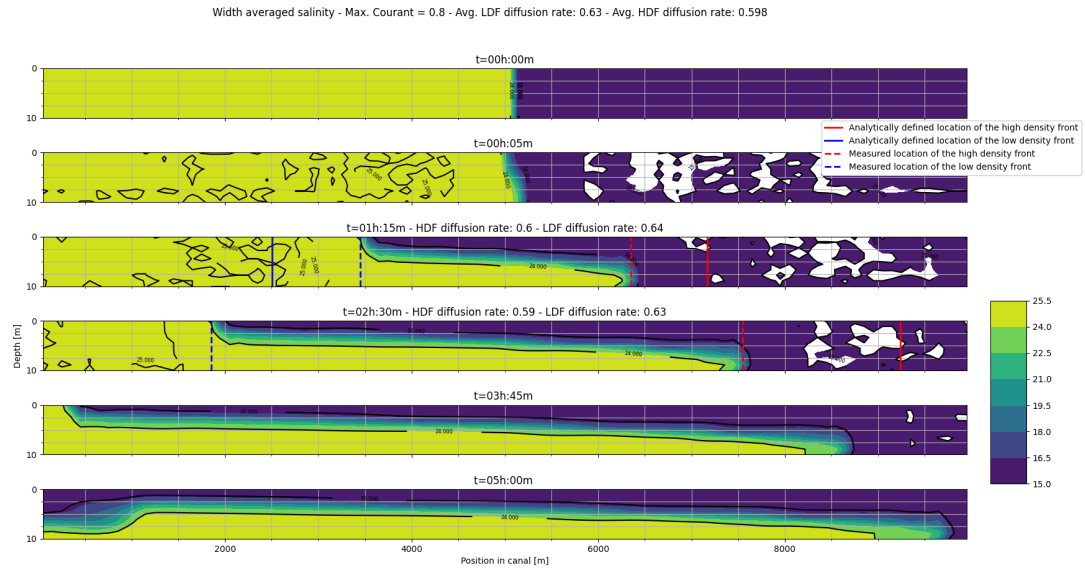
Below the salinity contour plots of all simulations that were reasonably interpretable and thus used in the sensitivity analysis are presented. All information is in the figure title.

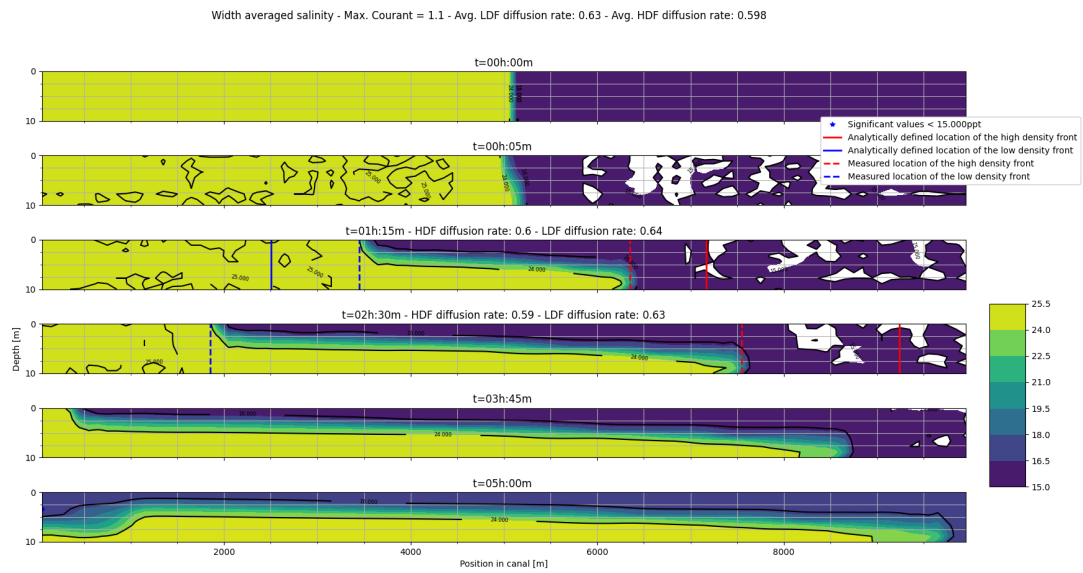
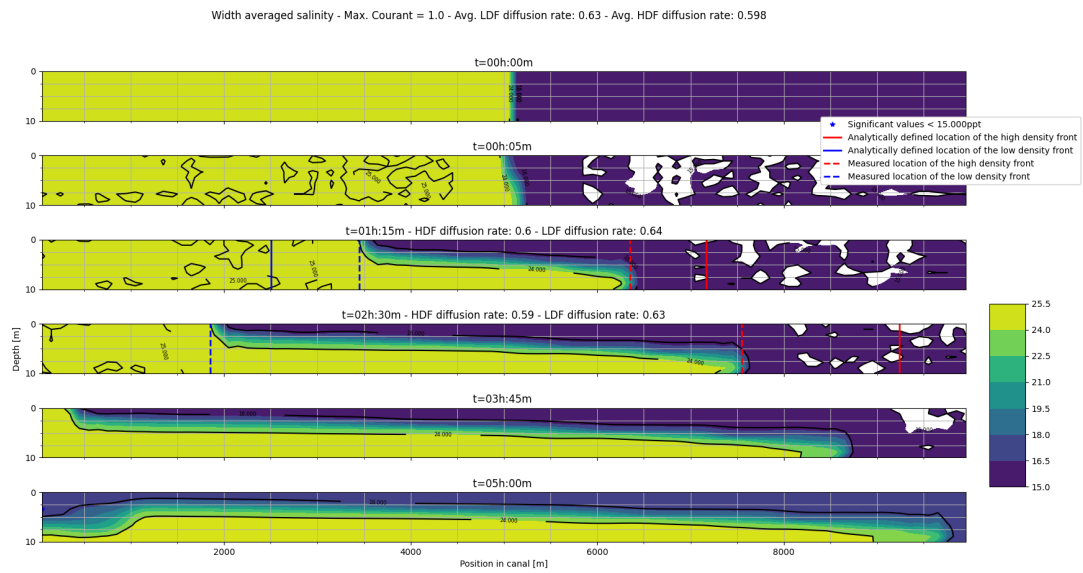
### A.6.1. Max. Courant

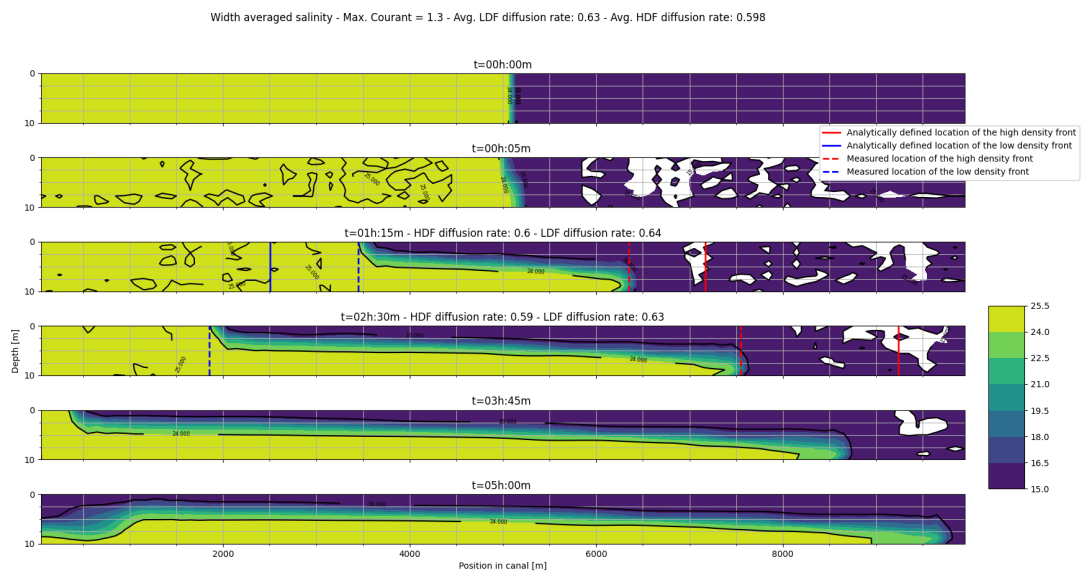
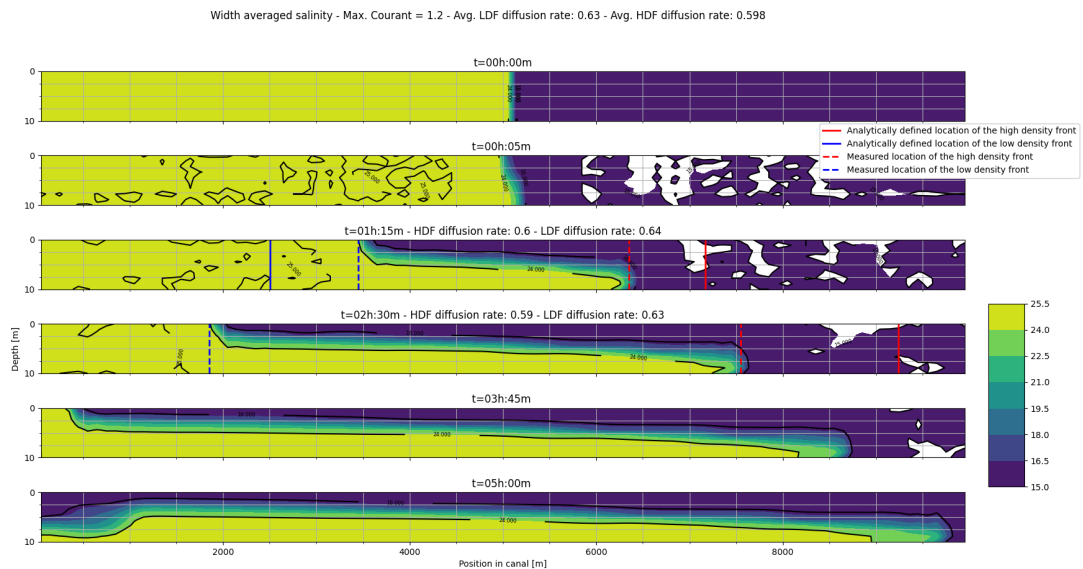


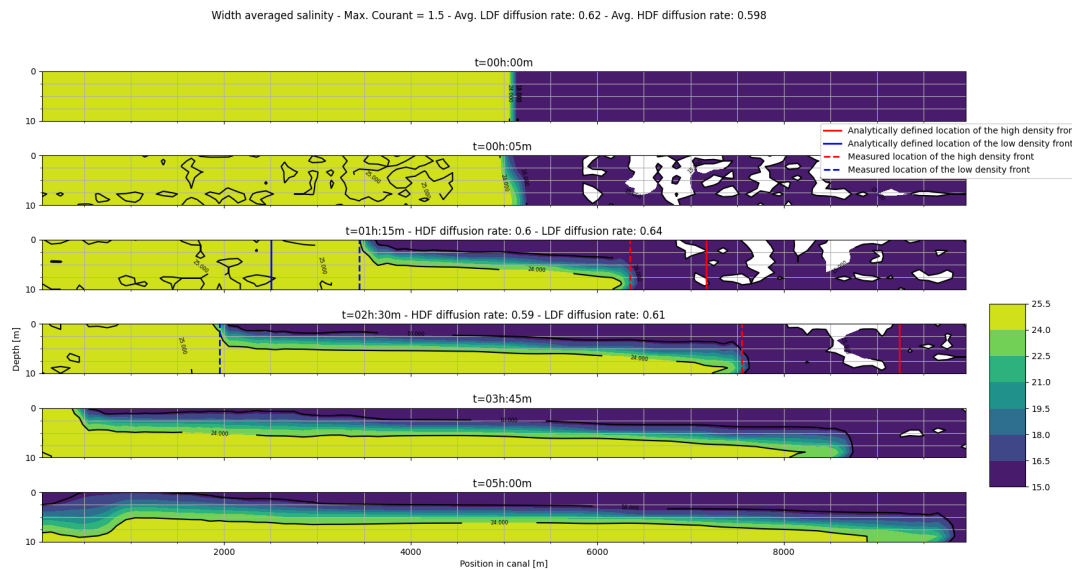
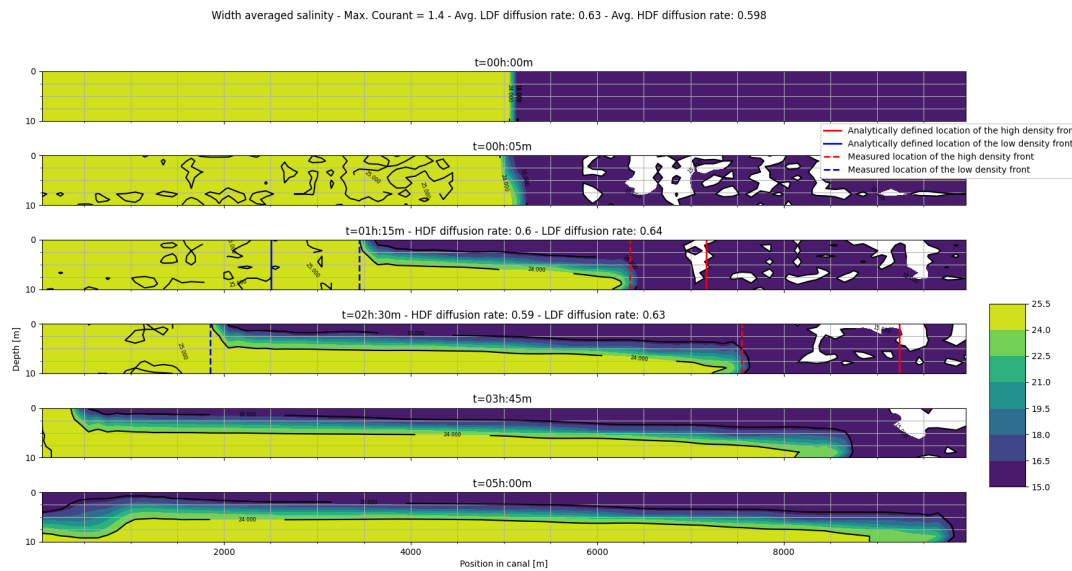


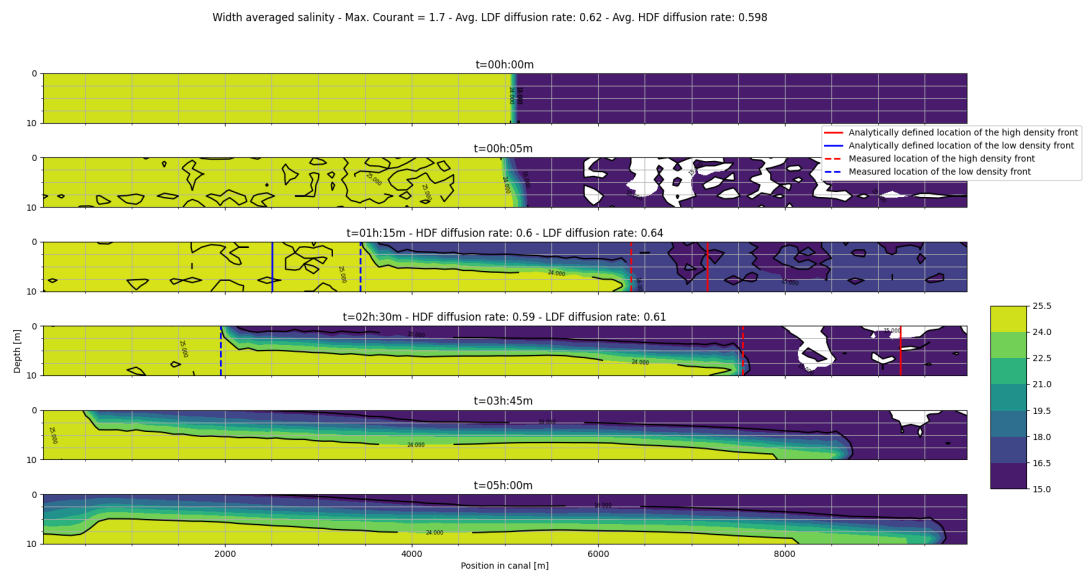
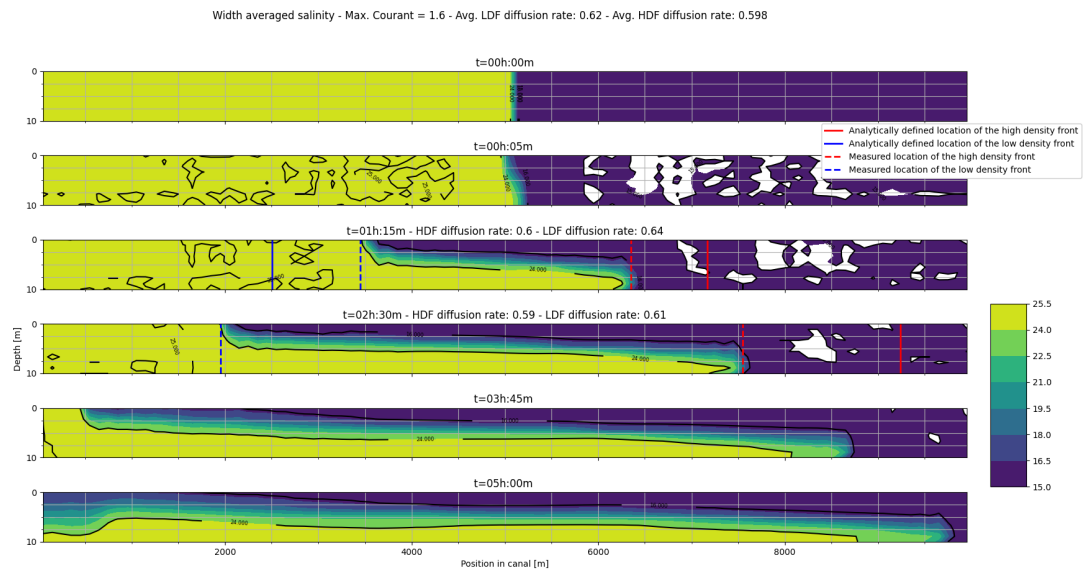


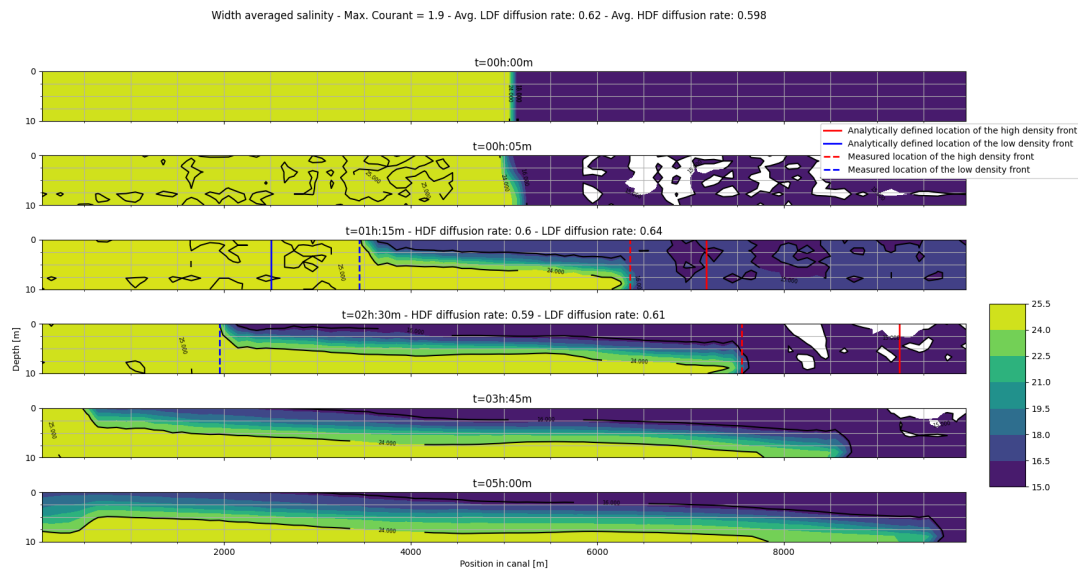
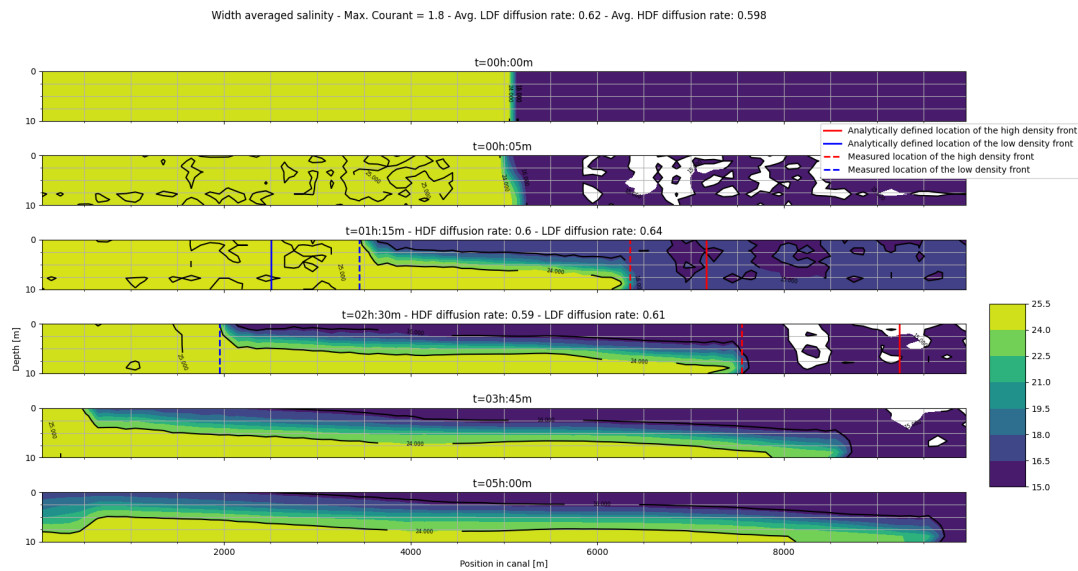


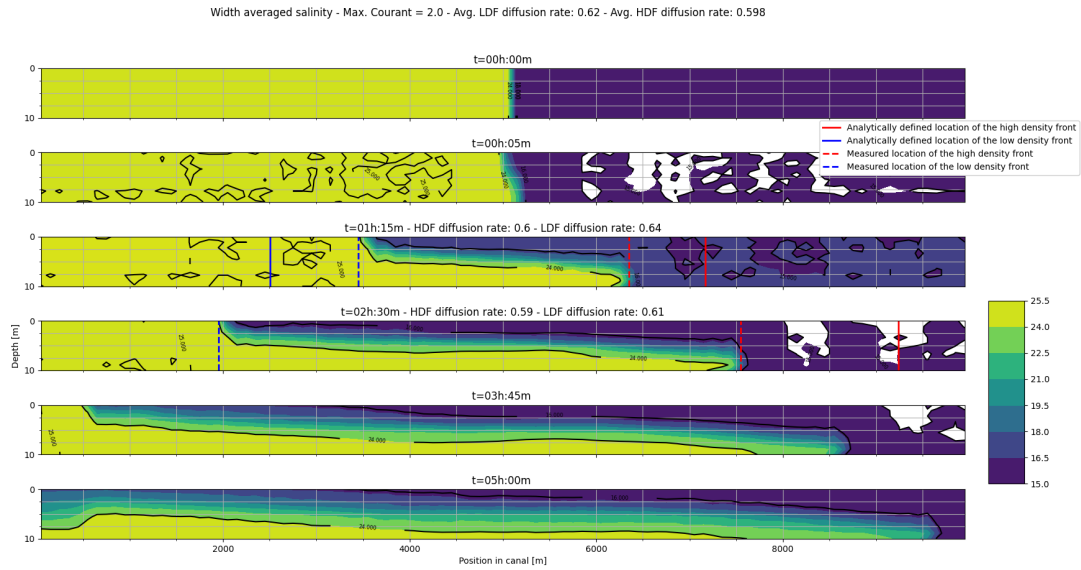




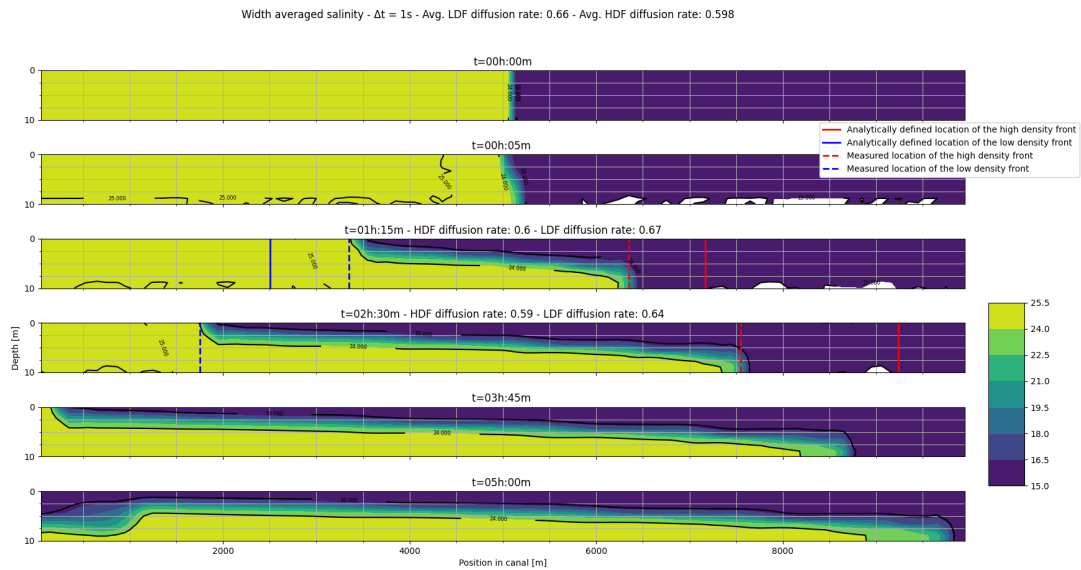


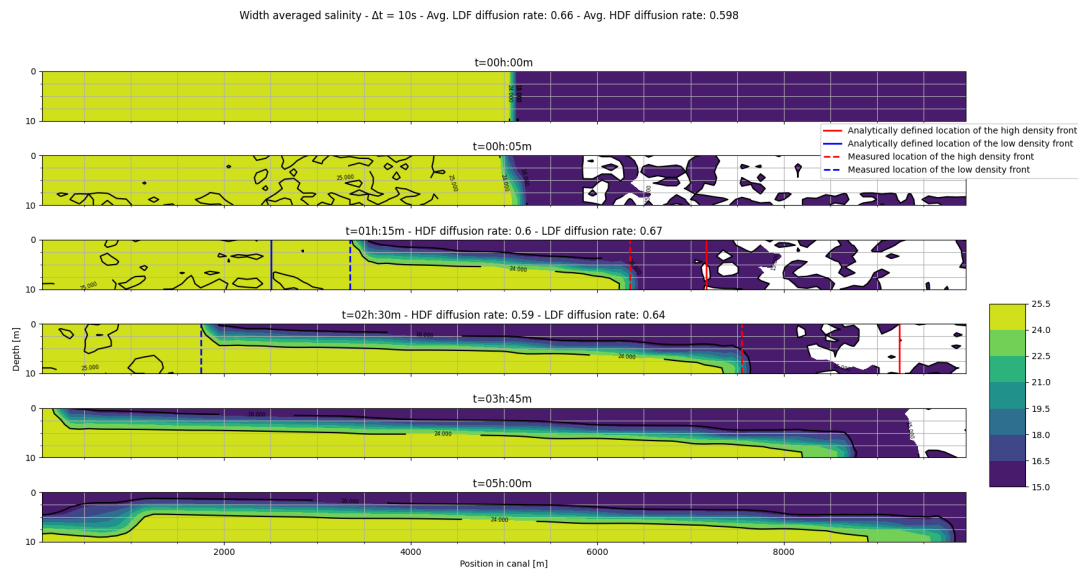
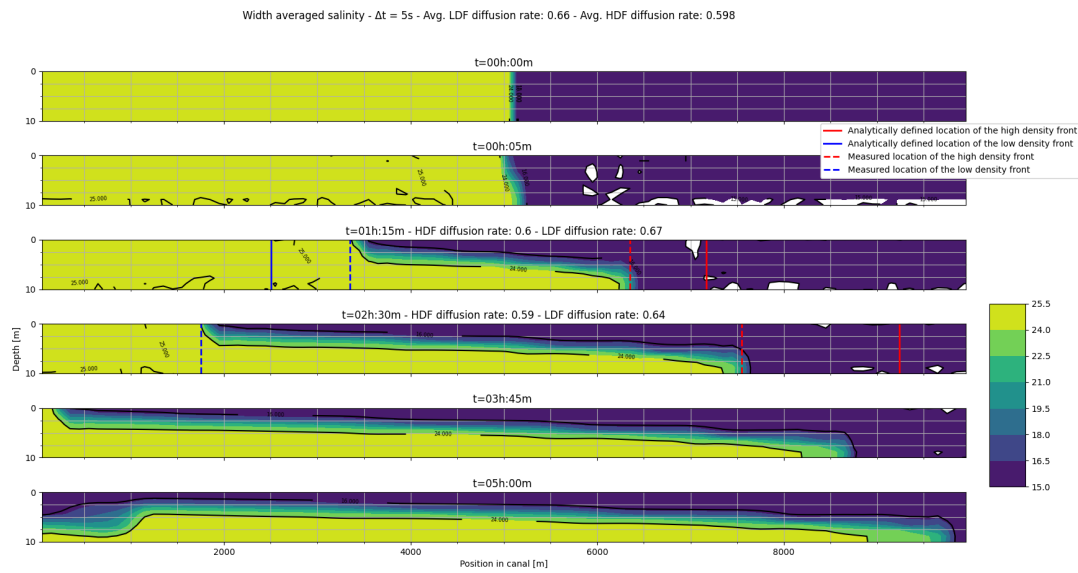


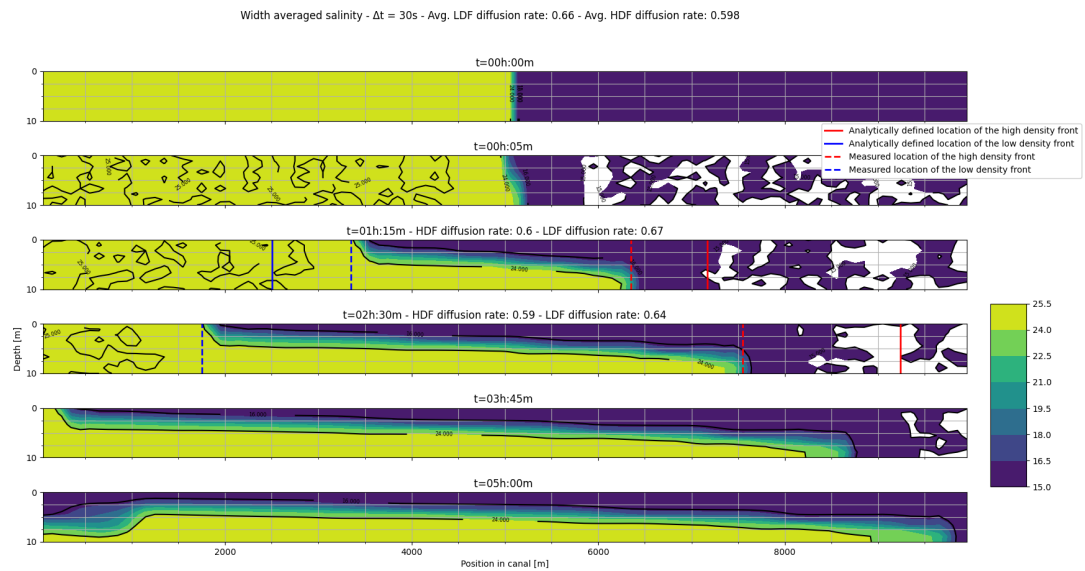
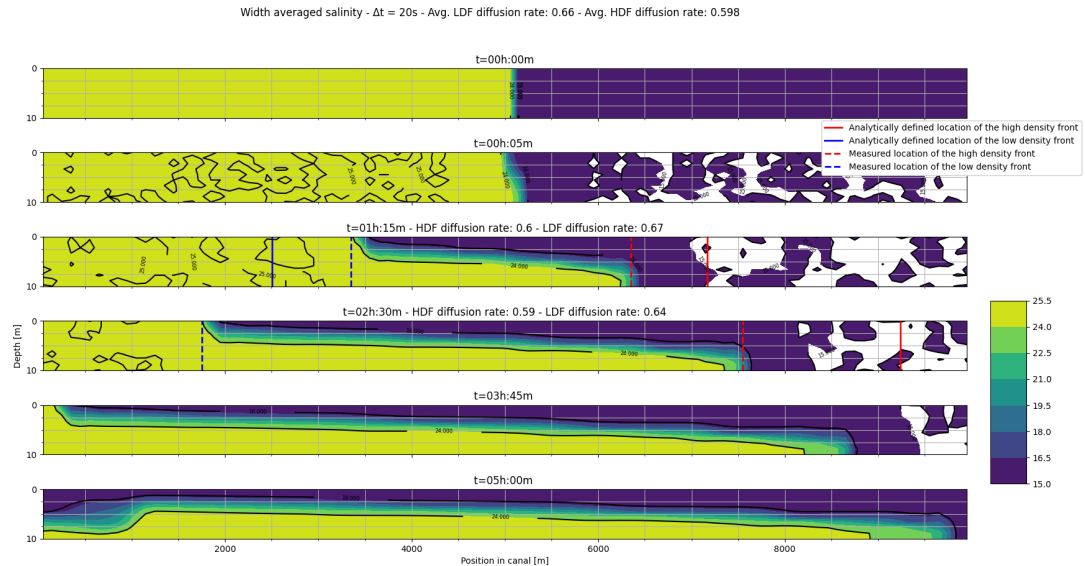


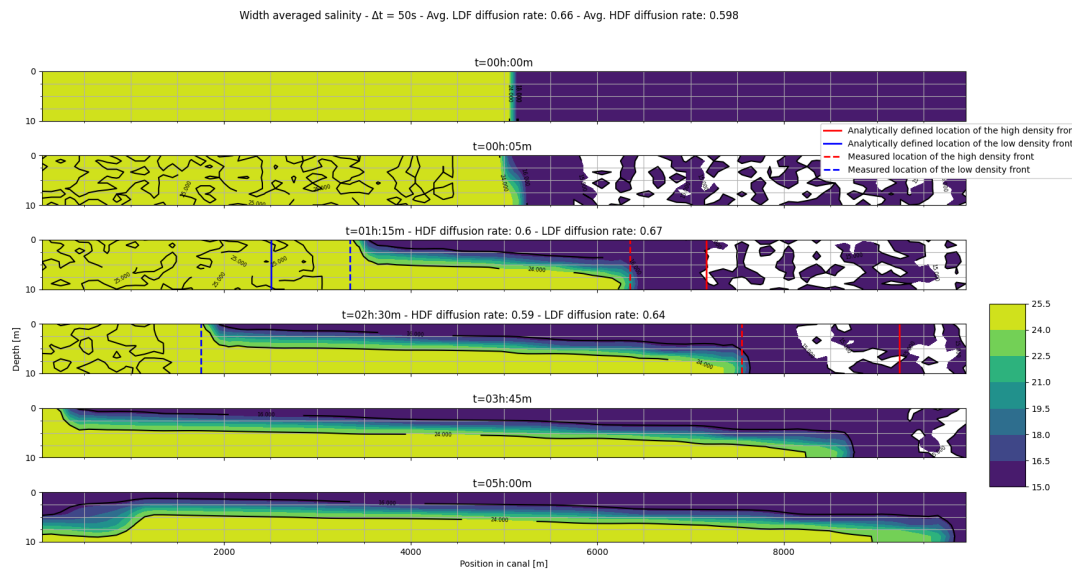
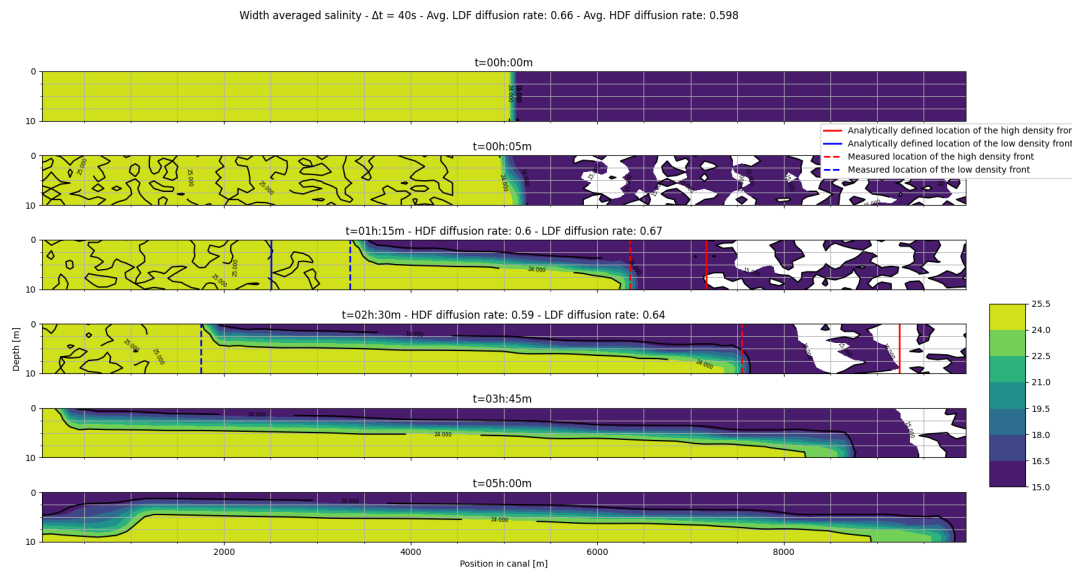


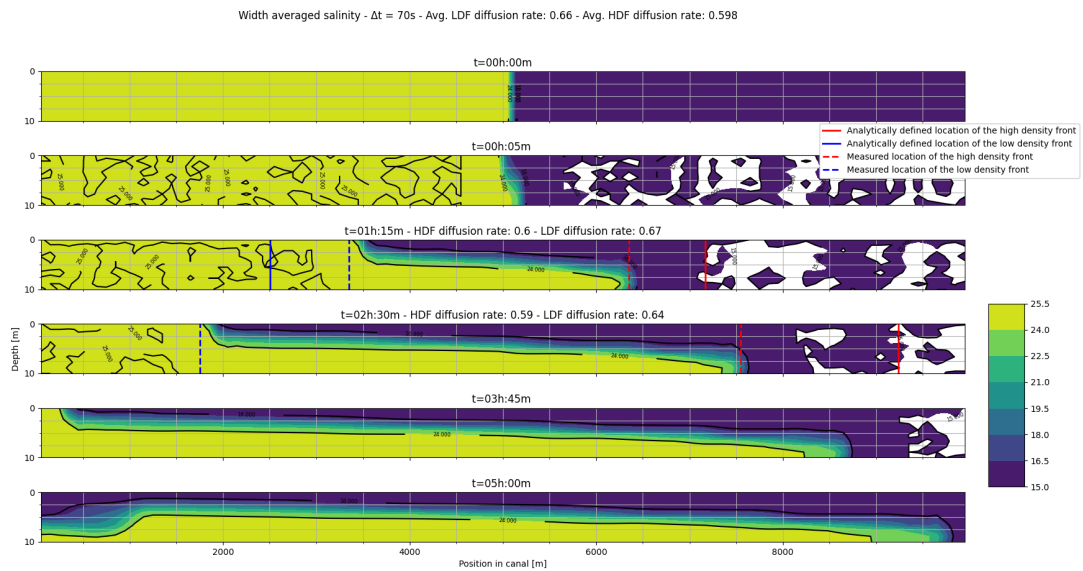
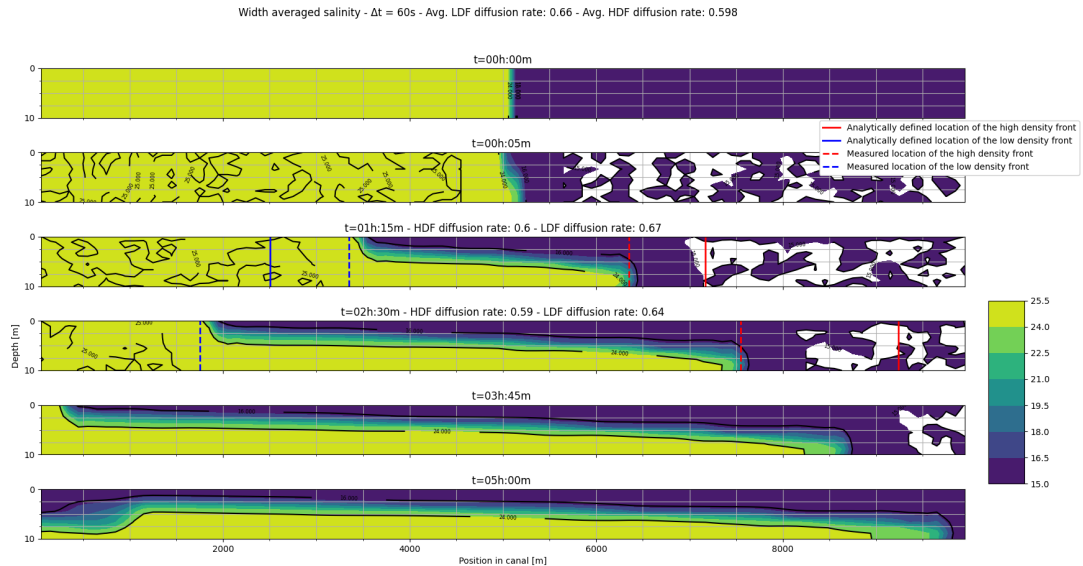
### A.6.2. Time step size

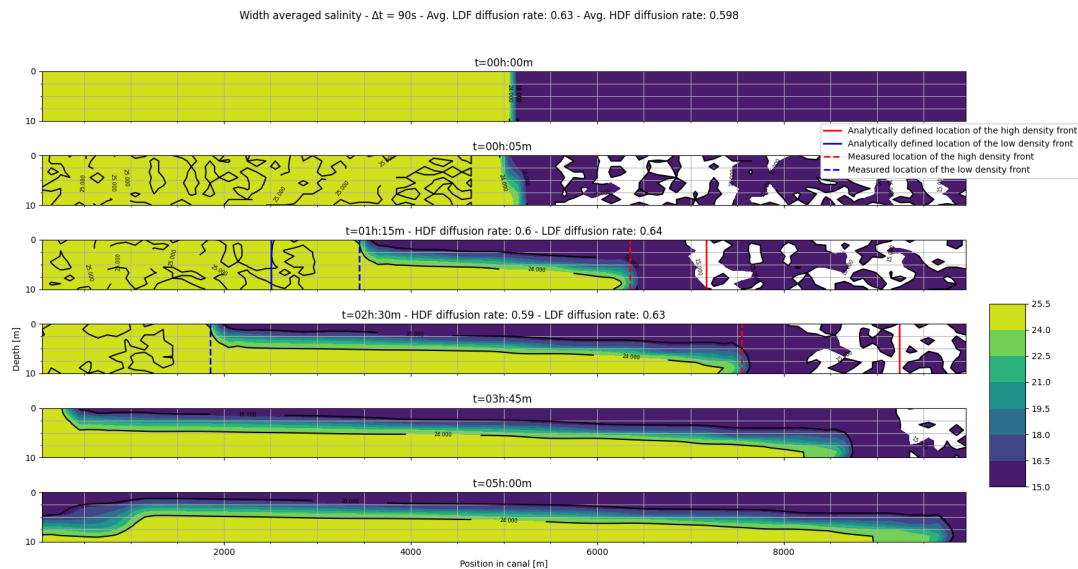
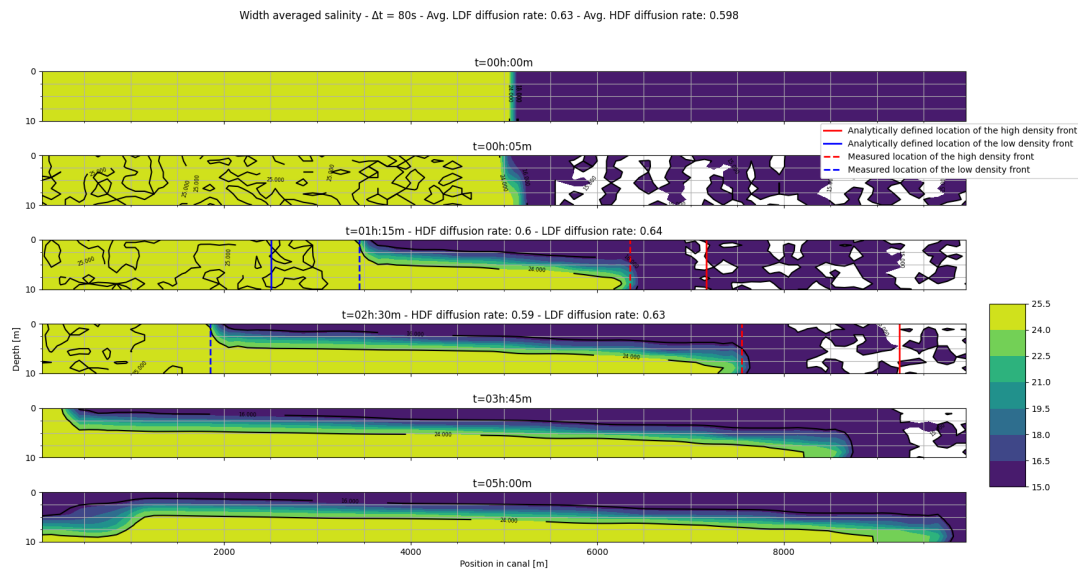


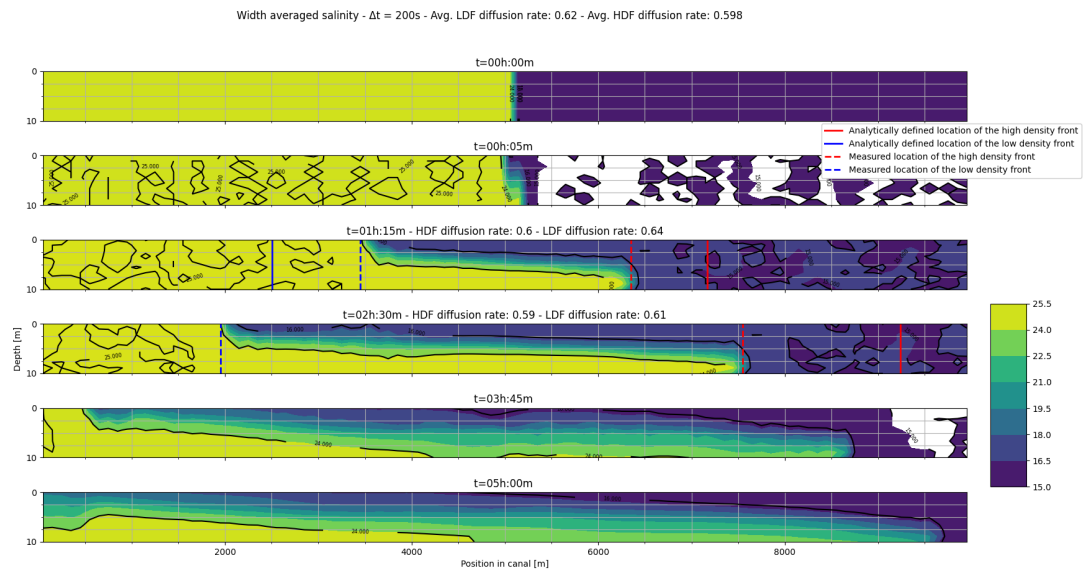
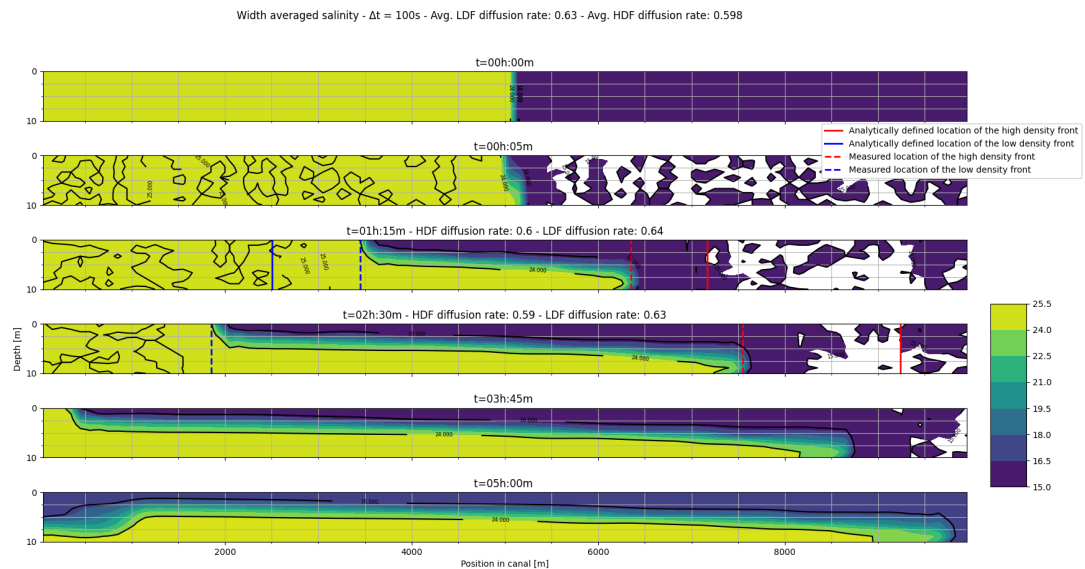




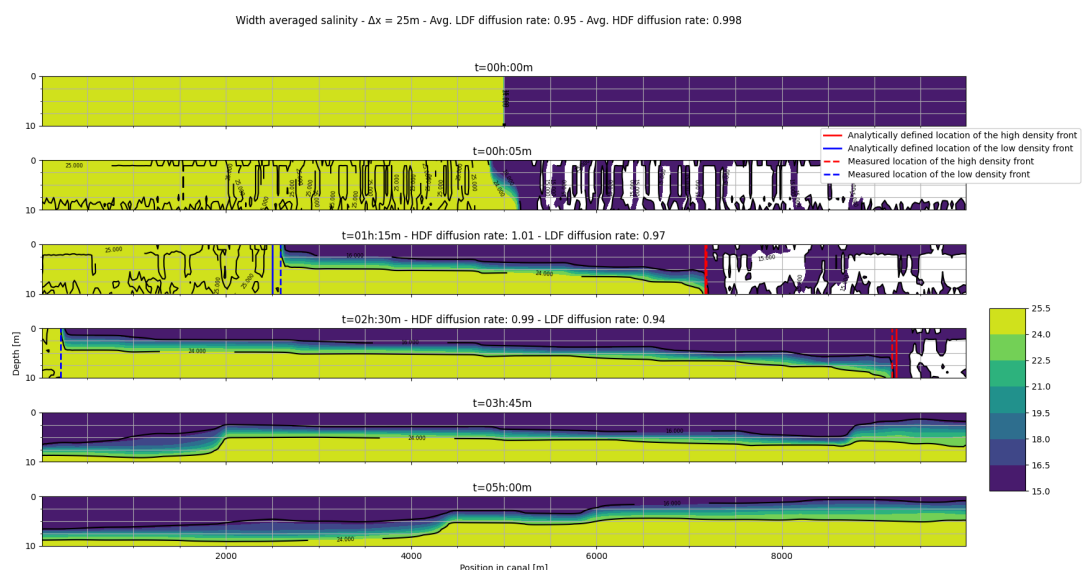
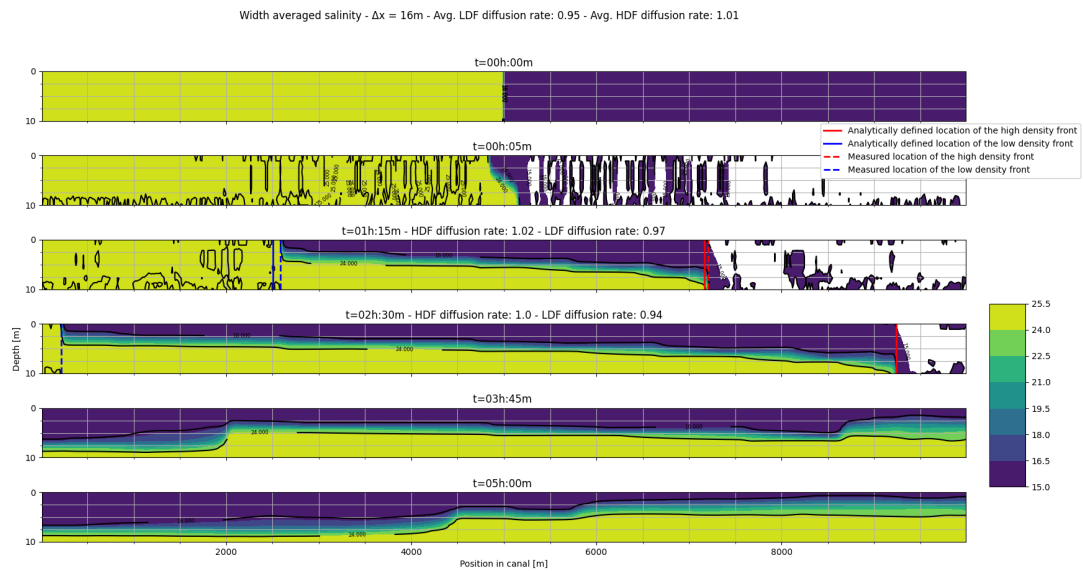


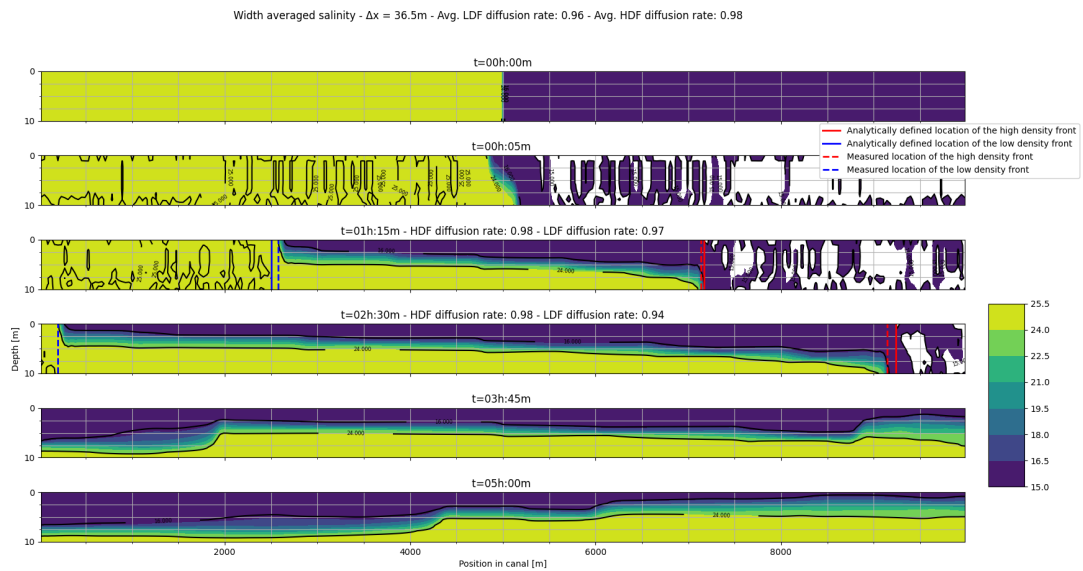
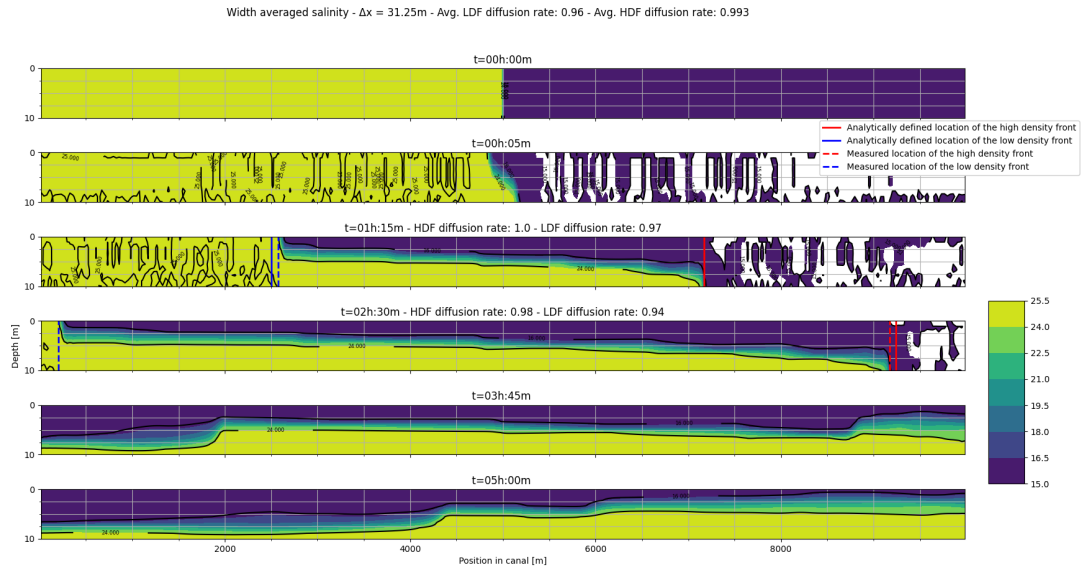


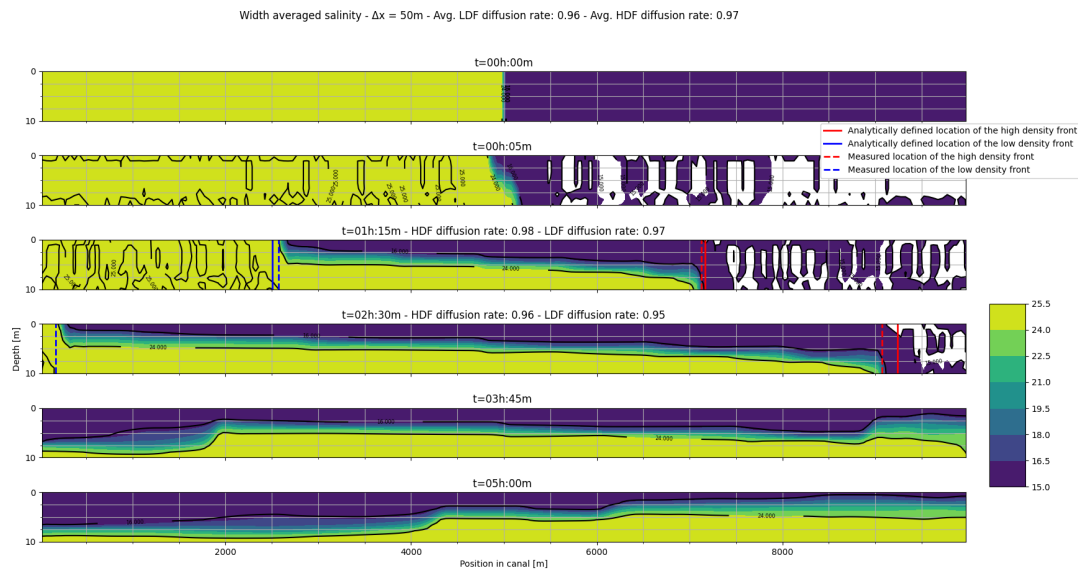
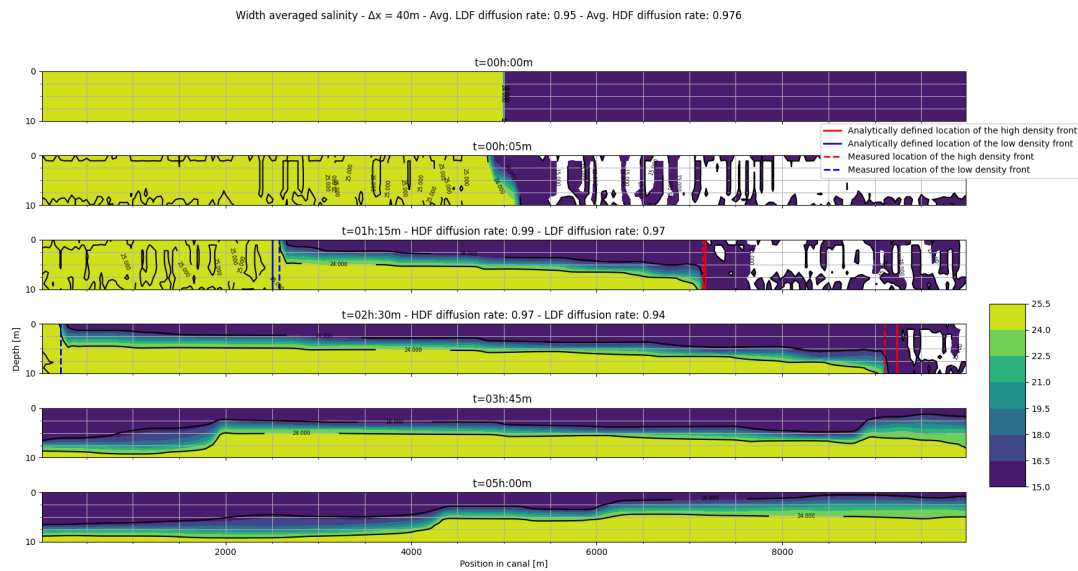


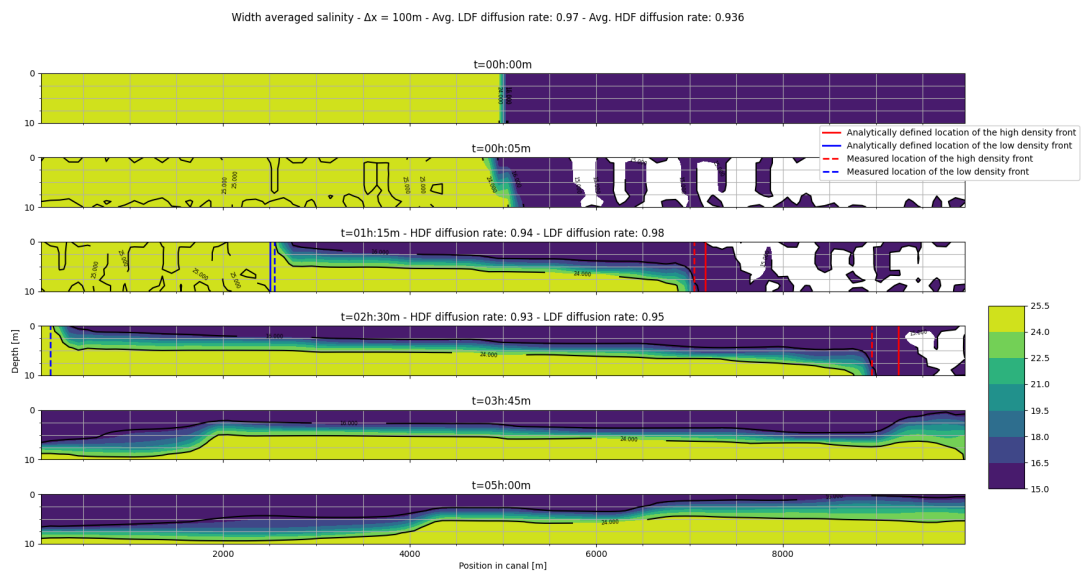
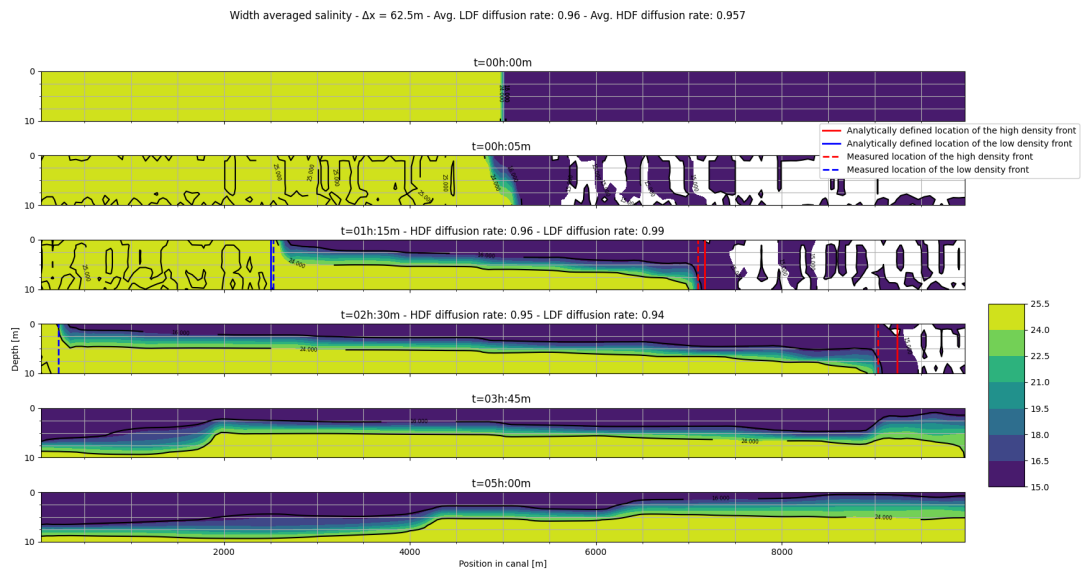


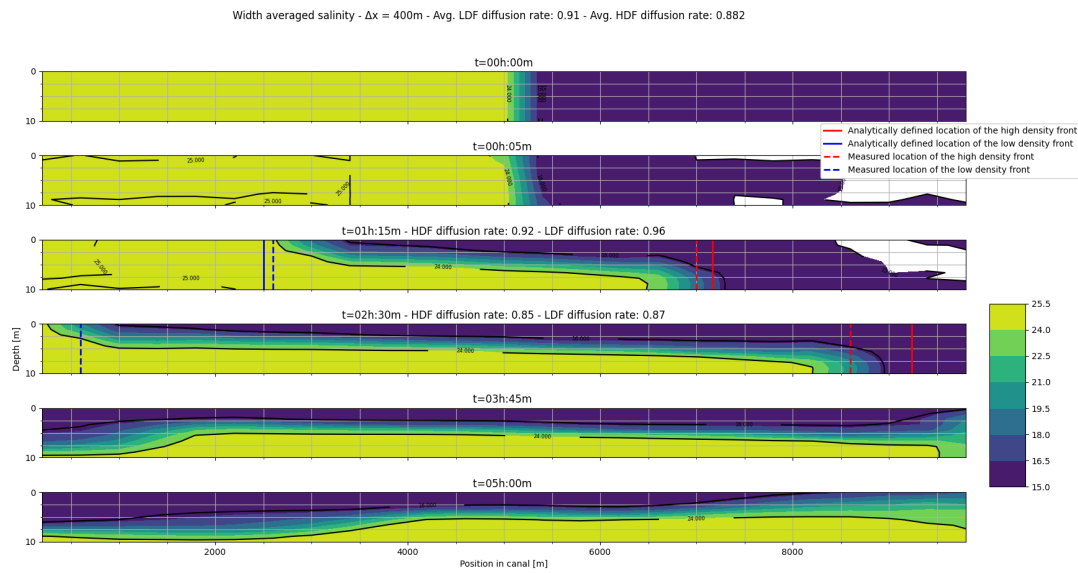
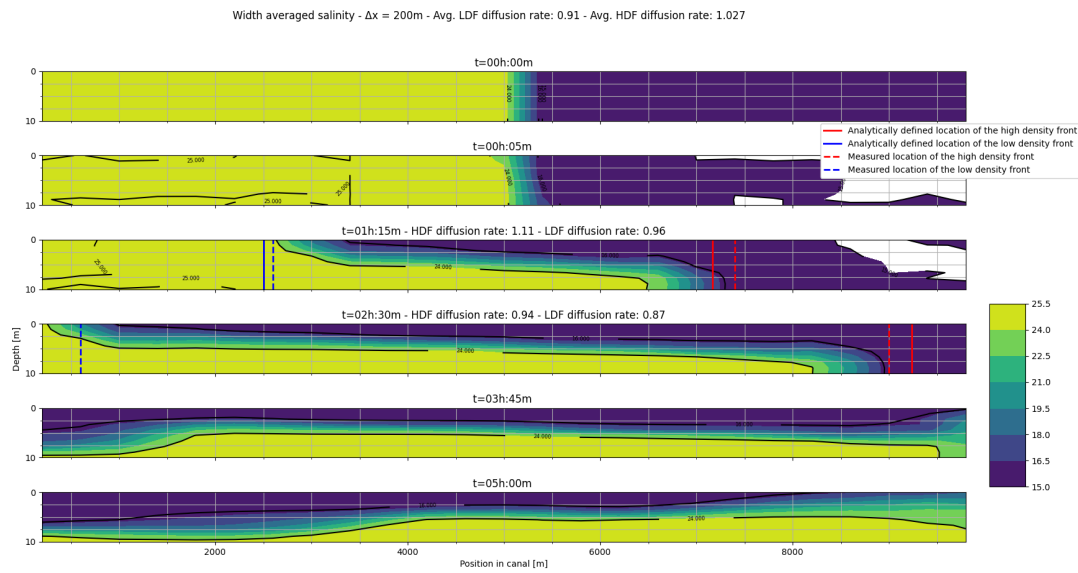
### A.6.3. Resolution x-direction











#### A.6.4. Resolution z-direction

